DISSERTATION

submitted to the

Combined Faculties for the Natural Sciences and for Mathematics

of the Ruperto-Carola University of Heidelberg, Germany

for the degree of

Doctor of Natural Sciences

presented by

Diplom-Biol. Jennifer Hüllein

born in Bad Soden, Germany

Oral examination: …….

Identification of Burkitt lymphoma vulnerabilities using RNAi

Referees:

Professor Dr. Christof von Kalle

Professor Dr. Stefan Wiemann

Summary

Oncogenic activation of MYC drives cell proliferation in Burkitt lymphoma (BL), but also evokes stress signals that have to be counterbalanced to escape apoptosis. Pro-survival signals from tonic B cell receptor and PI3K signaling are essential, but additional mutations are required for malignant transformation.

TP53 mutations were identified in 43% of BL patients. Mutations in the conserved *MYC* box I that abrogate activation of pro-apoptotic Bcl2-family member Bim were present in 17% of BL patients. Notably, *MYC* box I and *TP53* mutations occurred independently and accounted for 54% of cases, suggesting that alternative failsafe mechanisms may be inactivated in BL. To study alternative mechanisms of transformation in the absence of *TP53* mutations, we analyzed the pattern of recurrent genetic aberrations in BL for associations with *TP53* status. We observed an overrepresentation of chromosome 1q gains in *TP53* wild-type BL patients, which was not observed in diffuse large B cell lymphoma (DLBCL) patients. Minimally gained regions comprised 1q21-q23 and 1q32 and amplified regions displayed a gene dosage effect as shown by gene expression analysis.

To identify genes essential for p53 wild-type BL cells we performed a RNAi loss-of-function screen in a panel of genetically defined cell lines. We used a pooled shRNA library targeting 5,000 genes in key signaling pathways across the genome. Our data was probed against published RNAi screens across cancer entities and showed a high overlap of common essential and non-essential genes. p53 wild-type BL cell lines showed a strong and specific dependence on the p53 inhibitor MDM4. Depletion of MDM4 resulted in an upregulation of p53 target genes and induced cell cycle arrest. In a mouse xenograft model, MDM4 knock-down significantly reduced tumor growth. These effects were p53 dependent as confirmed in an isogenic p53 knock-out cell line. MDM4 is located within the minimally gained region 1q32 associated with p53 wild-type BL patients and might therefore contribute to BL pathogenesis by inactivation of the p53 pathway. Our data suggest that reactivation of p53 in patients lacking *TP53* mutation, e.g. by specific MDM4 inhibition, is a promising therapeutic approach. Re-analysis of published RNAi screening data revealed p53-specific sensitivity of MDM4 knock-down across cancer cell lines, suggesting a broader application for MDM4 inhibitors.

Our data set on essential genes in Burkitt lymphoma proved to be a valuable resource for identification of genotype-specific vulnerabilities. This analysis could be extended by integration of published RNAi screening data in non-lymphoid cell lines to identify interesting potential entity-specific vulnerabilities.

Keywords: Burkitt lymphoma, RNAi, MDM4

Zusammenfassung

Das Onkogen *MYC* ist überexprimiert im Burkitt Lymphom (BL) und fördert das Zellwachstum. Gleichzeitig löst *MYC* Stresssignale aus, die durch überlebensfördernde Signale kompensiert werden, um Apoptose vorzubeugen. Neben tonischer B-Zell-Rezeptor Aktivität und konstitutivem PI3K-Signalweg tragen genetische Mutationen zur malignen Transformation bei.

43% aller Patienten weisen Mutation im Tumorsuppressorgen *TP53* auf und 17% in der konservierten *MYC* Box I-Region. Beide Mutationen können die Aktivierung apoptotischer Programme verhindern. Nach unseren Beobachtungen treten diese Mutationen unabhängig voneinander auf und betreffen 54% aller Patienten. Dies lässt vermuten, dass es weitere Sicherheitsmechanismen gibt, die im BL deaktiviert sind.

Um Alternativen zu *TP53* Mutationen zu identifizieren, haben wir genetische Informationen aus Primärmaterial mit Daten aus einem funktionellen Screen in Zelllinienmodellen integriert. Ein Zugewinn auf dem q-Arm von Chromosom 1 war überrepräsentiert in BL Patienten mit *TP53* Wildtyp-Gen, aber unabhängig von p53 in Patienten mit diffus großzelligem B-Zell-Lymphom. Die Regionen minimalen Zugewinns umfassten 1q21-23 und 1q32 und korrelierten mit der Genexpression.

Um Gene zu identifizieren, die in Anwesenheit von Wildtyp p53 essentiell sind, wurde ein RNA-Interferenz (RNAi) Screen mit einem Pool aus short-hairpin RNAs (shRNAs), gerichtet gegen 5000 Gene in zentralen Signalwegen, in genetisch definierten Zelllinien durchgeführt. Gene, die basierend auf früheren RNAi Screens in verscheidenen Krebsentitäten als essentiell oder nicht-essentiell klassifiziert wurden, wiesen eine hohe Übereinstimmung mit unseren Daten auf. p53 Wildtyp Zelllinien zeigten zudem eine starke und spezifische Abhängigkeit vom p53 Inhibitor MDM4. Herunterregulation von MDM4 führte zur Aktivierung des p53 Signalweges und löste Zellzyklusarrest aus. Reduzierte MDM4 Expression unterdrückte darüber hinaus das Wachstum eines Heterotransplants in immunsuppremierten Mäusen. Wie an einem Zelllinienmodel mit genetisch inaktiviertem p53 gezeigt werden konnte, waren alle Effekte p53-abhängig.

MDM4 liegt auf 1q32. Chromosomaler Zugewinn dieser Region könnte zur Inaktivierung von p53 und somit zur Pathogenese von p53 Wildtyp BL Patienten beitragen. Unsere Daten lassen vermuten, dass Reaktivierung von p53, z.B. durch MDM4 Inhbitoren, in Patienten ohne *TP53* Mutation ein vielversprechender therapeutischer Ansatz ist. Durch Metaanalyse eines öffentlichen RNAi Screens wurde eine p53-spezifische Abhängigkeit von MDM4 in Zelllinien unterschiedlicher Entitäten beobachtet. Dies lässt vermuten, dass MDM4 Inhibitoren für eine breite Anwendung verwendet werden können.

Schlüsselwörter: Burkitt Lymphom, RNAi, MDM4

Index of contents

List of figures

List of tables

List of abbreviations

Abbreviation	Full name
7-AAD	7-aminoactinomycin
ABC DLBCL	activated B cell diffuse large B cell lymphoma
ALL	acute lymphoblastic leukemia
AML	acute myeloid leukemia
APC	allophycocyanin
ASHM	aberrant somatic hypermutation
ATP	adenosine triphosphate
BCA	bicinchoninic acid
BCR	B cell receptor
BL	Burkitt lymphoma
BM	bone marrow
B-NHL	B cell non-Hodgkin lymphoma
bp	base pairs
BrdU	bromodeoxyuridine
CCE	constitutive core essential (defined set of genes)
CGHa	comparative genome hybridization array
CHOP	combinatorial chemotherapeutic reagents (cyclophosphamide, doxorubicin, vincristine, prednisone)
chr	chromosome (indication of chromosomal location, e.g. chr1q32, consisting of chromosome number, arm and band)
CKI	cyclin dependent kinase inhibitor
CML	chronic myelogenous leukemia
CNA	copy number alteration
CNV	copy number variation
CR	clinical response rate
CRISPR	clustered regulatory interspaced short palindromic repeats
CSR	class switch recombination
DLBCL	diffuse large B cell lymphoma
DMSO	dimethylsulfoxid
DNA	deoxyribonucleic acid
DSB	double-strand break
dsRNA	double-stranded RNA
DZ	dark zone (substructure of germinal centers)
eBL	endemic Burkitt lymphoma
EBV	Epstein-Bar virus
ES	enrichment score
EtOH	ethanol
ETS	E26 transformation specific (class of transcription factors)
FACS	fluorescence-activated cell sorting
FBS	fetal bovine serum
FC	fold-change
FDC	follicular dendritic cells
FDG	fluordesoxyglucose
FDR	false discovery rate

Abbreviation	Full name
FISH	fluorescent in-situ hybridization
FITC	fluorescein
FL	follicular lymphoma
FSC	forward scatter
GADD	growth arrest and DNA-damage inducible (GADD) protein family
GC	germinal center
GPCF	genomics and proteomics core facility
GSEA	gene set enrichment analysis
HAT	histone acetyltransferase
HDR	homology-directed repair
HIV	human immunodeficiency virus
HPLC	high performance liquid chromatography
HPSF	high purity salt free
HSC	hematopoietic stem cell
Ig	immunoglobulin
IgH	heavy chain of immunoglobulin proteins
IgV	variable region of immunoglobulins
indels	insertions and deletions
INF	interferon
kd	knock-down
ko	knock-out
KS	Kolmogorov-Smirnov (statistical method)
LB	Luria Broth (bacterial cell culture medium)
LDH	lactate dehydrogenase
log2FC	logarithmic transformation of fold-change values
LZ	light zone (substructure of germinal centers)
mBL	molecular Burkitt lymphoma (disease classification based on molecular gene expression signature)
MeOH	methanol
MGR	minimally gained region
MHC	major histocompatibility complex
MMML	Molecular Mechanisms of Malignant Lymphoma (German consortium)
mRNA	messenger RNA
mut	mutant
NE	non-essential (defined set of genes)
NF-κB	nuclear factor kappa-light-chain-enhancer of activated B cells
NGS	next-generation sequencing
NHEJ	non-homologous end joining
NHL	non-Hodgkin lymphoma
nt	nucleotides
OS	overall survival
PAM	protospacer-adjacent motif
pBL	pediatric BL
PBS	phosphate-buffered saline
PCR	polymerase chain reaction
PET	positron emission tomography
PFA	paraformaldehyde
PMAD	peak median absolute deviation

Abbreviation	Full name
RISC	RNA-induced silencing complex
RIGER	RNAi Gene Enrichment Ranking (name of a bioinformatics algorithm)
RNA	ribonucleic acid
RNAi	RNA interference
RT	room temperature
RT-qPCR	reverse transcriptase quantitative polymerase chain reaction
sBL	sporadic Burkitt lymphoma
SDS	sodium dodecyl sulfate
sgRNA	single-guide RNA
SHM	somatic hypermutation
shNT	non-targeting shRNA
shRNA	short hairpin RNA
siRNA	short interfering RNA
SMRV	Squirrel Monkey Retrovirus
SNPa	single-nucleotide polymorphism array
SSC	sideward scatter
SWI/SNF	SWItch/Sucrose Non-Fermentable (name of a nucleosome remodeling complex)
T-ALL	acute T cell leukemia
e.g. t(8;14)	translocation between chromosome 8 and 14
TRC	The RNAi Consortium
VDJ	gene segments of immunoglobulins: V (variable), D (diversity), J (joining)
WHO	Word Health Organization
wt	wild-type
wZ	weighted z-score

List of gene names

Ensembl Gene ID	HGNC	Description	Species	Chr	Band
ENSG00000108846	*ABCC3*	ATP-binding cassette, sub-family C (CFTR/MRP), member 3	Homo sapiens	17	q21.33
ENSG00000111732	*AICDA*/ AID	activation-induced cytidine deaminase	Homo sapiens	12	p13.31
protein family	*Akt*	V-akt murine thymoma viral oncogene homolog	Homo sapiens		
ENSG00000151360	*ALLC*	allantoicase	Homo sapiens	2	p25.3
ENSG00000145020	*AMT*	aminomethyltransferase	Homo sapiens	3	p21.31
ENSG00000110244	*APOA4*	apolipoprotein A-IV	Homo sapiens	11	q23.3
ENSG00000117713	*ARID1A*	AT rich interactive domain 1A	Homo sapiens	1	p36.11
ENSG00000049618	*ARID1B*	AT rich interactive domain 1B	Homo sapiens	6	q25.3
ENSG00000128524	*ATP6V1F*	ATPase, H+ transporting, lysosomal 14kDa, V1 subunit F	Homo sapiens	7	q32.1
ENSG00000002330	*BAD*	BCL2-associated agonist of cell death	Homo sapiens	11	q13.1
ENSG00000087088	*BAX*	BCL2-associated X protein	Homo sapiens	19	q13.33
ENSG00000105327	*BBC3*/ PUMA	BCL2 binding component 3	Homo sapiens	19	q13.32
ENSG00000171791	*BCL2*	B-cell CLL/lymphoma 2	Homo sapiens	18	q21.33
ENSG00000153094	*BCL2L11*/ Bim	BCL2-like 11 (apoptosis facilitator)	Homo sapiens	2	q13
ENSG00000113916	*BCL6*	B-cell CLL/lymphoma 6	Homo sapiens	3	q27.3
ENSG00000116128	*BCL9*	B-cell CLL/lymphoma 9	Homo sapiens	1	q21.2
ENSG00000132840	*BHMT2*	betaine--homocysteine S-methyltransferase 2	Homo sapiens	5	q14.1
ENSG00000157764	*BRAF*	B-Raf proto-oncogene, serine/threonine kinase	Homo sapiens	7	q34
ENSG00000111678	*C12orf57*	chromosome 12 open reading frame 57 (encoding C10)	Homo sapiens	12	p13.31
NA	*Cas9*	CRISPR associated	Strepptococcus pyogenes		
ENSG00000110092	*CCND1*	cyclin D1	Homo sapiens	11	q13.3
ENSG00000112576	*CCND3*	cyclin D3	Homo sapiens	6	p21.1
ENSG00000105173	*CCNE1*	cyclin E1	Homo sapiens	19	q12
ENSG00000113328	*CCNG1*	cyclin G1	Homo sapiens	5	q34
ENSG00000177455	*CD19*	CD19 molecule	Homo sapiens	16	p11.2
ENSG00000164045	*CDC25A*	cell division cycle 25A	Homo sapiens	3	p21.31
ENSG00000170312	*CDK1*	cyclin-dependent kinase 1	Homo sapiens	10	q21.2
ENSG00000123374	*CDK2*	cyclin-dependent kinase 2	Homo sapiens	12	q13.2
ENSG00000135446	*CDK4*	cyclin-dependent kinase 4	Homo sapiens	12	q14.1
ENSG00000124762	*CDKN1A*	cyclin-dependent kinase inhibitor 1A (p21, Cip1)	Homo sapiens	6	p21.2
ENSG00000147889	*CDKN2A*	cyclin-dependent kinase inhibitor 2A	Homo sapiens	9	p21.3
ENSG00000100526	*CDKN3*	cyclin-dependent kinase inhibitor 3	Homo sapiens	14	q22.2
ENSG00000149554	*CHEK1*	checkpoint kinase 1	Homo sapiens	11	q24.2
ENSG00000173207	*CKS1B*	CDC28 protein kinase regulatory subunit 1B	Homo sapiens	1	q21.3

Ensembl Gene ID	HGNC	Description	Species	Chr	Band
ENSG00000146233	*CYP39A1*	cytochrome P450, family 39, subfamily A, polypeptide 1	Homo sapiens	6	p12.3
ENSG00000134574	*DDB2*	damage-specific DNA binding protein 2, 48kDa	Homo sapiens	11	p11.2
ENSG00000100697	*DICER1*	dicer 1, ribonuclease type III	Homo sapiens	14	q32.13
ENSG00000101412	*E2F1*	E2F transcription factor 1	Homo sapiens	20	q11.22
ENSG00000182944	*EWSR1*	EWS RNA-binding protein 1	Homo sapiens	22	q12.2
ENSG00000117560	*FASLG*	Fas ligand (TNF superfamily, member 6)	Homo sapiens	1	q24.3
ENSG00000161513	*FDXR*	ferredoxin reductase	Homo sapiens	17	q25.1
ENSG00000151702	*FLI1*	Fli-1 proto-oncogene, ETS transcription factor	Homo sapiens	11	q24.3
ENSG00000150907	*FOXO1*	forkhead box O1	Homo sapiens	13	q14.11
ENSG00000111640	*GAPDH*	glyceraldehyde-3-phosphate dehydrogenase	Homo sapiens	12	p13.31
ENSG00000171766	*GATM*	glycine amidinotransferase	Homo sapiens	15	q21.1
NA	*GFP*	green fluorescent protein	Aequorea victoria		
ENSG00000168148	*HIST3H3*	histone cluster 3, H3	Homo sapiens	1	q42.13
ENSG00000143621	*ILF2*	interleukin enhancer binding factor 2	Homo sapiens	1	q21.3
ENSG00000184216	*IRAK1*	interleukin-1 receptor-associated kinase 1	Homo sapiens	X	q28
ENSG00000133703	*KRAS*	Kirsten rat sarcoma viral oncogene homolog	Homo sapiens	12	p12.1
ENSG00000125952	*MAX*	MYC associated factor X	Homo sapiens	14	q23.3
ENSG00000065328	*MCM10*	minichromosome maintenance 10 replication initiation factor	Homo sapiens	10	p13
ENSG00000076003	*MCM6*	minichromosome maintenance complex component 6	Homo sapiens	2	q21.3
ENSG00000166508	*MCM7*	minichromosome maintenance complex component 7	Homo sapiens	7	q22.1
ENSG00000135679	*MDM2*	MDM2 proto-oncogene, E3 ubiquitin protein ligase	Homo sapiens	12	q15
ENSG00000198625	*MDM4*	MDM4, p53 regulator	Homo sapiens	1	q32.1
ENSG00000215417	*MIR17HG*	MiR-17-92 cluster host gene	Homo sapiens	13	q31.3
ENSG00000270499	*MKI67P1*	marker of proliferation Ki-67 pseudogene 1	Homo sapiens	X	p11.3
ENSG00000157227	*MMP14*	matrix metallopeptidase 14 (membrane-inserted)	Homo sapiens	14	q11.2
ENSG00000156738	*MS4A1*/ CD20	membrane-spanning 4-domains, subfamily A, member 1	Homo sapiens	11	q12.2
ENSG00000198793	*MTOR*	mechanistic target of rapamycin (serine/threonine kinase)	Homo sapiens	1	p36.22
ENSG00000185499	*MUC1*	mucin 1, cell surface associated	Homo sapiens	1	q22
ENSG00000059728	*MXD1*/ MAD1	MAX dimerization protein 1	Homo sapiens	2	p13.3
ENSG00000136997	*MYC*	v-myc avian myelocytomatosis viral oncogene homolog	Homo sapiens	8	q24.21
ENSG00000172936	*MYD88*	myeloid differentiation primary response 88	Homo sapiens	3	p22.2
ENSG00000134250	*NOTCH2*	notch 2	Homo sapiens	1	p12
ENSG00000143799	*PARP1*	poly (ADP-ribose) polymerase 1	Homo sapiens	1	q42.12
ENSG00000196092	*PAX5*	paired box 5	Homo sapiens	9	p13.2

Ensembl Gene ID	HGNC	Description	Species	Chr	Band
protein family	*PI3K*	Phosphoinositide-3-kinase	Homo sapiens		
ENSG00000137193	*PIM1*	Pim-1 proto-oncogene, serine/threonine kinase	Homo sapiens	6	p21.2
ENSG00000057657	*PRDM1*	PR domain containing 1, with ZNF domain	Homo sapiens	6	q21
ENSG00000159377	*PSMB4*	proteasome subunit beta 4	Homo sapiens	1	q21.3
ENSG00000171862	*PTEN*	phosphatase and tensin homolog	Homo sapiens	10	q23.31
ENSG00000183010	*PYCR1*	pyrroline-5-carboxylate reductase 1	Homo sapiens	17	q25.3
ENSG00000166349	*RAG1*	recombination activating gene 1	Homo sapiens	11	p12
ENSG00000175097	*RAG2*	recombination activating gene 2	Homo sapiens	11	p12
ENSG00000139687	*RB1*	retinoblastoma 1	Homo sapiens	13	q14.2
NA	*RFP*	red fluorescent protein	Entacmaea quadricolor		
ENSG00000176393	*RNPEP*	arginyl aminopeptidase	Homo sapiens	1	q32.1
ENSG00000156482	*RPL30*	ribosomal protein L30	Homo sapiens	8	q22.2
ENSG00000185088	*RPS27L*	ribosomal protein S27-like	Homo sapiens	15	q22.2
ENSG00000048392	*RRM2B*	ribonucleotide reductase M2 B (TP53 inducible)	Homo sapiens	8	q22.3
ENSG00000071564	*TCF3*	transcription factor 3	Homo sapiens	19	p13.3
ENSG00000163513	*TGFBR2*	transforming growth factor, beta receptor II	Homo sapiens	3	p24.1
ENSG00000112742	*TKK/MSP1*	TTK protein kinase	Homo sapiens	6	q14.1
ENSG00000120889	*TNFRSF10B*	tumor necrosis factor receptor superfamily, member 10b	Homo sapiens	8	p21.3
ENSG00000141510	*TP53*	tumor protein p53	Homo sapiens	17	p13.1
ENSG00000132274	*TRIM22*	tripartite motif containing 22	Homo sapiens	11	p15.4
ENSG00000265972	*TXNIP*	thioredoxin interacting protein	Homo sapiens	1	q21.1
ENSG00000187555	*USP7*/ HAUSP	ubiquitin specific peptidase 7 (herpes virus-associated)	Homo sapiens	16	p13.2
14-3-2 protein family	*YWHA*	Tyrosine 3-monooxygenase/ tryptophan 5-monooxygenase activation	Homo sapiens		
ENSG00000116809	*ZBTB17* MIZ-1	zinc finger and BTB domain containing 17	Homo sapiens	1	p36.13

1 Introduction

1.1 B-cell development and maturation

B cells belong to the lymphoid lineage and derive from hematopoietic stem cells (HSC) in the bone marrow. They are part of the humoral and cellular adaptive immune system and recognize antigens through immunoglobulin (Ig) proteins, that are either bound to the cell membrane (as part of the B-cell receptor; BCR) or secreted as antibodies. Ig proteins are highly diverse and can be tailored in regard to antigen specificity and immune effector function (Figure 1). In early B-cell development the recombination activating genes (*RAG1* and *RAG2*) randomly re-arrange segments of the *IG* gene (variable region, *IGV*) in a process called V(D)J recombination to create various antigen-binding sites[1]. During maturation, the activation-induced cytidine deaminase (AID) enzyme mediates class-switch recombination (CSR) and somatic hyper-mutation (SHM)[2,3]. SHM introduces random mutations in the *IGV* and therefore further increases the repertoire of antigen recognition sites. CSR results into exchange of DNA fragments of the heavy chain of the *IG* gene (*IGH*) and isotype switch from the IgM subtype into IgD (as found in the BCR), IgG, IgA or IgD (as found in antibodies). The isotype determines the interaction with other immune effector cells.

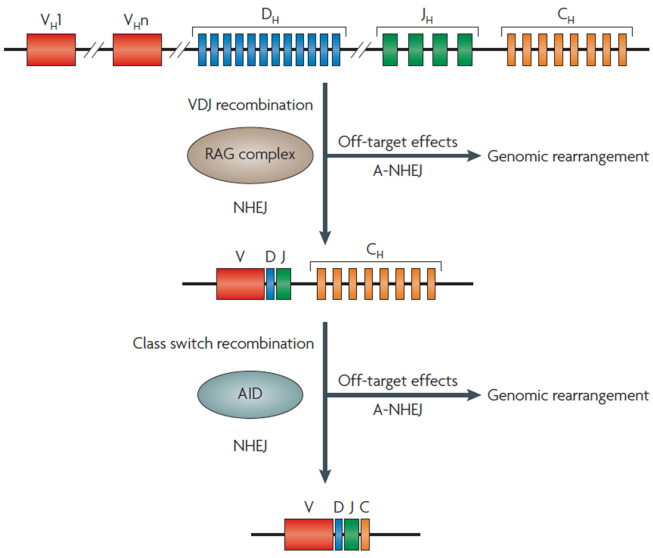

Figure 1: Genomic rearrangement of immunoglobulin proteins
Immunoglobulin (Ig) proteins mediate the diverse antigen binding capacity of B cells. They are encoded on several gene segments that are combined to a functional gene by two genomic rearrangement processes. During V(D)J recombination the RAG complex randomly combines V, D and J segments through non-homologous end-joining (NHEJ). The enzyme activation-induced cytidine deaminase (AID) adds the constant (C) region leading to class switch recombination (CSR). Aberrant NHEJ (A-NHEJ) causes genomic rearrangements (Mani & Chinnaiyan, 2010).

Upon T cell-mediated antigen stimulation immature B cells start to proliferate and form germinal centers (GC) in peripheral lymphoid organs that are the origin of antibody producing plasma cells and memory cells (Figure 2)[4,5]. GCs consist of two structural subunits: The dark zone (DZ), that is densely packed with B cells, and the light zone (LZ), that is additionally infiltrated by follicular dendritic cells (FDC), T cells and macrophages[4,6]. Activated B cells enter the DZ where they turn into fast proliferating centroblasts and undergo SHM to create a pool of immune cells with various antigen-binding capabilities. Centroblasts suppress cell cycle inhibitors and DNA damage response to allow rapid proliferation and mutagenesis, but also present with high apoptotic rates[5]. In addition, reactivated telomerase prevents senescence by reconstitution of chromosomal ends, allowing clonal B-cell expansion[7]. Steered by cytokines, centroblasts traffic into the LZ of the GC where they turn into smaller, non-dividing centrocytes[4]. Here, B cells carrying diverse mutations in their *IGV* gene are exposed to antigens and selected for high-affinity binding to pathogenic antigens. Selected B cells either differentiate into resting memory cells or undergo CSR to turn into antibody-secreting plasma cells. B cells reactive against self-antigens undergo apoptosis.

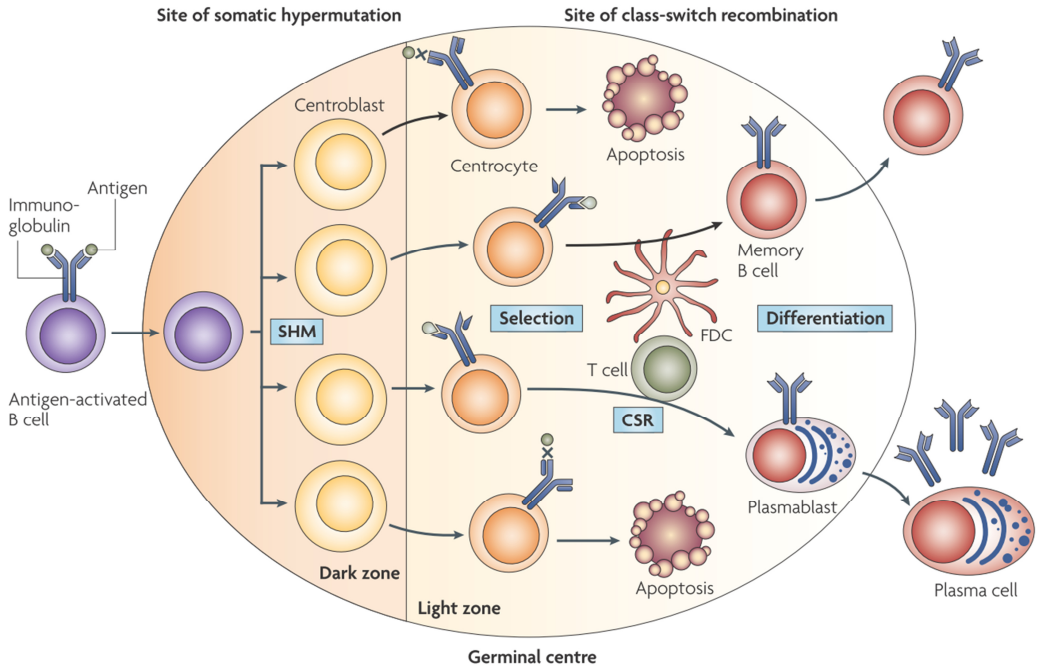

Figure 2: B-cell maturation in the germinal center
Antigen-activated immature B cells start to proliferate and form germinal centers (GC). Fast proliferating B cells, the centroblasts, form the dark zone of the GC. They are subjected to somatic hypermutation (SHM) introducing changes within the variable region of the immunoglobulin (*IGV*) gene to expand the B-cell repertoire. Stimulated by cytokines the cells traffic to the light zone of the GC and turn into small, non-dividing centrocytes. After antigen-affinity selection B cells either differentiate into resting memory B cells or turn into antibody-secreting plasma cells after class switch recombination (CSR) of their immunoglobulin *IGH* genes (Klein & Dalla-Favera, 2008).

1.2 Aggressive B-cell lymphomas

GC B cells are prone to malignant transformation. Proliferation, survival and impaired response to DNA damage are cancer hallmarks[8]. Lymphoma cells retain their natural differentiation profile[9], but errors during genomic modification circumvent failsafe mechanisms of the GC reaction[4,5]. Most B-cell non-Hodgkin lymphomas (B-NHL), including Burkitt lymphoma (BL), diffuse large B-cell lymphoma (DLBCL) and follicular lymphoma (FL), derive from GC or post-GC B cells[10,11]. Aberrant V(D)J recombination or CSR can activate oncogenes by chromosomal translocation to highly active promotor or enhancer regions of *IG*-loci[3,12]. Common oncogenes that are activated by this mechanism include the anti-apoptotic *BCL2* gene in FL[13], the cell cycle activator *CCND1* in mantle cell lymphoma[14] and the transcription factor *MYC* in virtually all BL[15] and about 10% of DLBCL[16]. Translocation of the transcriptional repressor *BCL6*, that blocks differentiation into plasma cells, is commonly seen in DLBCL[17]. Aberrant SHM of *MYC* and *PRDM1* occurs in 50% of DLBCL[18].

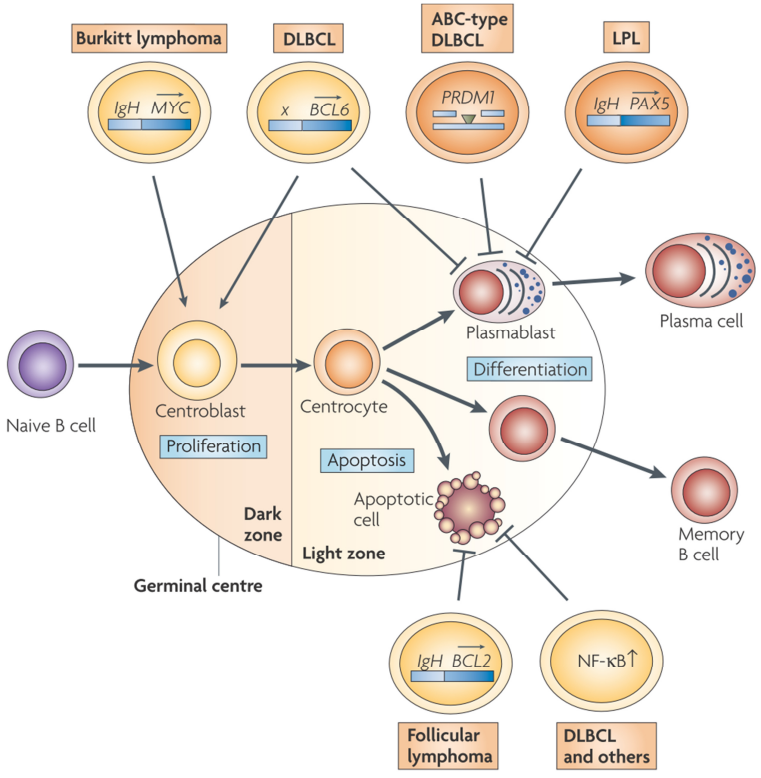

Figure 3: Development of aggressive B-cell lymphoma from the germinal center.
B-cell lymphomas arise at many stages of B-cell development and mostly display signs of GC reaction, including mutated IgV genes, chromosomal translocations and aberrant somatic hypermutation (ASHM) of cancer associated genes. Burkitt lymphoma (BL) develops from fast proliferating centroblasts and acquires *MYC*-translocations. Diffuse large B-cell lymphoma (DLBCL) describes a heterogeneous group of lymphomas. Common genetic aberrations include translocations of *BCL6* or ASHM of *PRMD1* impairing differentiation into plasma cells. NF-kB signaling is upregulated in subtypes of DLBCL. Follicular lymphoma (FL) is characterized by *BCL2* translocations (Klein & Dalla-Favera, 2008).

1.3 Burkitt lymphoma

BL is a mature aggressive B-NHL derived from GC B cells. The WHO classification distinguishes three subtypes: Endemic BL (eBL) is associated with Epstein-Barr virus (EBV) and mainly seen in malaria-prone regions in equatorial Africa[19]. Sporadic BL (sBL) mainly occurs in the Western World and closely resembles eBL although not linked to infection. A third variant is associated with human immunodeficiency virus (HIV-associated BL)[20,21]. BL is the fastest growing tumor with a proliferation index of nearly 100%. The aggressiveness of the disease is driven by oncogenic MYC activation and adoption of the transcriptional program of fast-proliferating centroblasts. In the last decade molecular and genetic findings greatly improved our understanding of BL pathogenesis and extended classical diagnostic criteria.

1.3.1 Historical review: A "stalking horse" of cancer research

BL was first described by the clinician Denis Burkitt in 1958 as a jaw tumor in children in Uganda[22]. It was later entitled as the "stalking horse" of cancer[23] as it was the first cancer with described contribution of viral infection and oncogene activation (by means of chromosomal translocation). EBV was first isolated from a BL patient[24] and initially thought to be the main cause of BL. However, it became apparent later, that EBV is present in 98% of all humans. EBV contributes to malignant transformation only in combination with malaria or HIV, when strong B-cell cytokine secretion provides pro-survival signals to the pre-malignant B cells[25,26]. Shortly after establishment of chromosomal banding techniques, translocations involving chromosomes 8 and 14 were detected in BL[27]. About 70-80% of cases acquire the translocation t(8;14)(q24;q32) which juxtaposes the *MYC* gene to an *IGH*-loci and is seen as the hallmark lesion in BL. Both variant translocations t(2;8)(p12;q24) and t(8;22)(q24;q11) involving the Ig kappa or lambda light chain, respectively, occur at a frequency of about 10%[28].

1.3.2 Epidemiology, clinical and molecular presentation

eBL mainly occurs in areas with holodemic malaria infection where it accounts for 50% of cancers and 90% of lymphomas in children with an incidence of 40-50/million/year (age <18 years) and a preference in boys[29]. It presents as swelling of the jaw or periorbital with abdominal involvement, but rarely bone marrow (BM) infiltration[30]. In developed countries sBL accounts for 1-5% of B-NHL in adults with an overall incidence of 2.5 cases/million/year and 30-40% of B-NHL in children with an incidence of 2/million/year[31] (Figure 4A). sBL occurs bimodal at an age of 3-12 years and in patients aged >60 years[32]. Childhood and adult sBL share a similar gene expression profile[33] and therefore seem to depend on the same oncogenic pathways although they are often studied separately. Clinical presentation includes rapid cell proliferation, BM infiltration (20%), abdominal involvement (60-80%), nodal (mostly in adults) and extra-nodal (mostly in children) disease[34]. Extensive BM infiltration can be a sign of development into a leukemic form of BL (acute lymphoblastic leukemia, ALL3). Morphologically the cells are medium sized and display with round uncleaved nuclei and

basophilic nucleoli and cytoplasm[34]. All cells are positive for the proliferation marker Ki-67 and show a diffuse growth pattern and high apoptotic rate (Figure 4B). Infiltrating macrophages engulf apoptotic cells and cause the typically "starry sky" appearance. Immunohistochemistry shows markers of B-cell lineage (CD19+, CD20+) and germinal center profile (CD10+, Bcl-6+, Bcl-2-) (Figure 4B) (reviewed in Molyneux 2012, Hochberg *et al.* 2009, Miles *et al.* 2012).

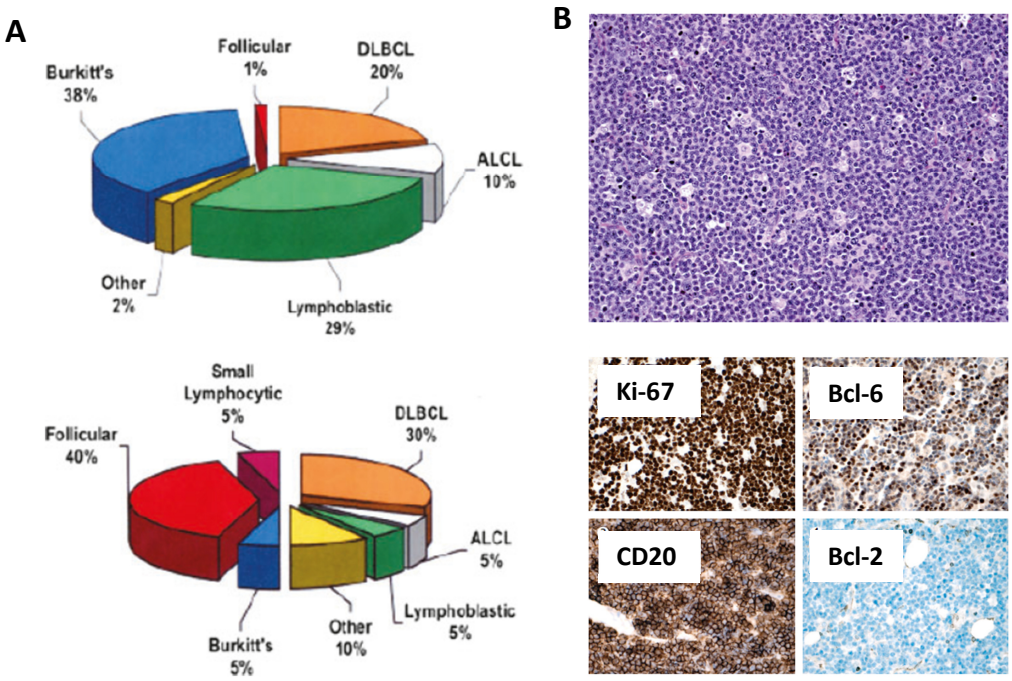

Figure 4: Incidence and molecular presentation of BL
(A) Frequency of B-NHL sub-types in children (age 0-14, top) and adults (age >20, bottom). BL accounts for about 40% of B-NHL in children and 5% in adults. However, due to the larger age span there are more adult BL patients compared to pediatric (modified from Hochberg *et al.*, 2009). **(B)** Immunohistochemical features of BL. *upper image:* The tissue section shows the "starry sky" appearance caused by infiltrating macrophages that ingest apoptotic cells. *lower images*: Clinical markers used for BL diagnosis. BL cells are all positive for the proliferation marker Ki-67 and express B cell as well as GC markers (CD20+, Bcl-6+, Bcl-2-) (modified from Molyneux 2012).

The aggressive growth of BL requires rapid treatment initiation after diagnosis. Treatment protocols are mostly based on the FAB LMB study[35,36] and include high-dose chemotherapy containing methotrexate and cytarabine[37]. Addition of the monoclonal antibody rituximab has greatly improved clinical response (CR) and overall survival (OS) rates[38]. Remission can be achieved in about 90% of children and 70% of adults, but no treatment options are available for relapsed patients. The staging of BL is based on the Ann Arbor system in adults and the Murphy/St Jude system in children[39,40]. Poor prognostic markers include age, high LDH levels, bone marrow and CNS involvement and failed CR 4-6 month after treatment initiation.

The diagnosis of BL is mainly based on morphological, cytogenetic and immunophenotypic characteristics that are distinctive, but also shared by DLBCL that accounts for 30% of B-NHL in adults. An independent review of >200 leukemia and lymphoma patients diagnosed by international hematologists showed poor overlap (42%) for patients with intermediate phenotype[41] that were classified over time as “non-BL”, “Burkitt-like”, “atypical BL” (WHO classification 2001) or “B-cell lymphomas unclassifiable with features intermediate between DLBCL and BL (BLU)” (WHO classification 2008)[19]. Distinct gene expression and mutation profiles might improve the diagnostic accuracy in the future[42-44].

1.3.3 Molecular characterization

Two microarray studies published at the same time distinguished BL and DLBCL based on their molecular gene expression signature (Figure 5)[42,43]. Both signatures confirmed the pathological diagnosis in a subset of “core” BL and re-classified patients displaying with mixed diagnostic criteria. Importantly, in the study of Dave *et al*. patients with a molecular BL (mBL) signature that were pathologically diagnosed as DLBCL and treated accordingly with a mixture of chemotherapeutic drugs (CHOP - cyclophosphamide, doxorubicin, vincristine, prednisone) had significantly inferior outcome. All patients with available data (7/9) died within two years whereas 80% of patients treated with intensive regiments, according to BL-specific guidelines, were still alive after 10 years of follow-up. Hummel *et al*. re-defined about 20% of patients independent of the *IGH-MYC* fusion, Bcl-6 or Bcl-2 expression, therefore expanding the conventional diagnostic criteria. Low genetic complexity and favorable clinical outcome were characteristics of molecular BL. *MYC* breakpoints in combination with complex karyotype and lack of mBL signature were markers for unfavorable clinical outcome.

The molecular signature also provided insights into pathogenic mechanisms. BL cells expressed high level of MYC-targets and typical GC markers, while major histocompatiblity complex (MHC) class I and NF-kB targets were low. As shown later, BL is an exception among B-cell malignancies as it resembles the transcriptional activation state of centroblasts from the DZ of the GC instead of LZ centrocytes[9].

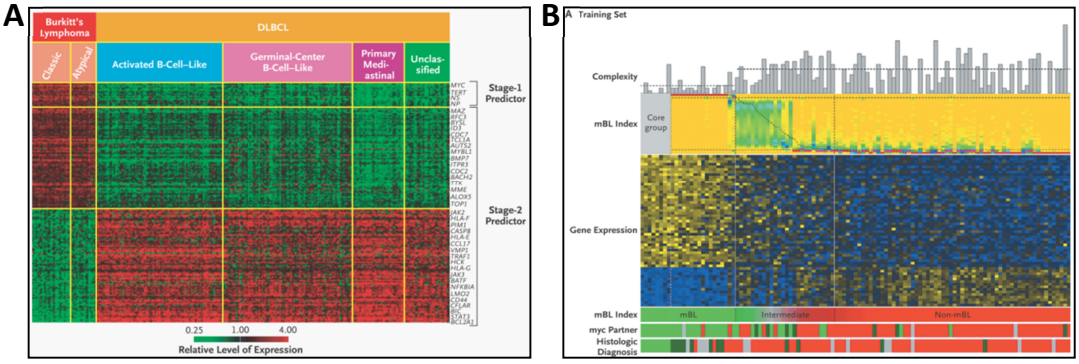

Figure 5: Gene expression signatures for molecular BL
For a molecular distinction of BL and DLBCL two independent studies derived gene expression signatures based on microarray data. **(A)** Molecular classification for BL from Dave *et al*., 2006 was based on high MYC-target gene expression (stage-1 predictor) and the statistically most significant differentially expressed genes compared to DLBCL (stage-2 predictor). **(B)** Signature for molecular BL (mBL) as defined by Hummel *et al*., 2006. The signature distinguishes mBL from DLBCL (non-mBL) and an intermediate group. Genetic complexity is lower in mBL compared to non-mBL or intermediates. The core mBL group fulfills all conventional diagnostic criteria.

1.3.4 Recurrent copy number alterations in BL

Translocation of the *MYC* gene on chr8q24 is a hallmark of BL. Several studies addressed the question if additional genetic aberrations contribute to the pathogenesis of this disease or classify subgroups. Copy number alterations (CNAs) in BL were studied with increasing resolution using conventional cytogenetics[45], fluorescent in-situ hybridization (FISH)[46], comparative genomic hybridization array (CGHa)[33,47,48] or single nucleotide polymorphism array (SNPa)[49-51]. About 70% of BL carry secondary structural aberrations and overall genetic complexity is lower compared to solid cancer or DLBCL[43,49]. Comparison of CNAs in pediatric and adult BL showed a similar profile, which is in line with the observation that the gene expression profile is indistinguishable[33,52] (Figure 6A). Discrepant BL and complex BL with *MYC* re-arrangements differ in their cytogenetic profile from mBL[33,53] and for comparison across cytogenetic studies we have to consider that different criteria were applied to classify the patients. Cell lines have in general a more complex karyotype than primary samples[47,54,55].

The most frequent CNAs are gains of chr1q (40%), and chr13q (10-20%) and loss of chr17p (20%) and CNAs were closely correlated to gene expression[33,48,49]. Despite of the high frequency of these aberrations, disease-associated genes often remain elusive. Description of candidates is mainly based on highly deregulated cancer consensus genes within minimally gained/lost regions. The gain of chr13q31 was linked to the miRNA-17-92 supercluster, a transcriptional target of MYC[56]. miRNAs from this locus prevent apoptosis by downregulation of *Bim*, *PTEN* or *TGFB2*[57-59]. Amplification and overexpression is found in solid cancer[60] and lymphomas where it has been shown to accelerate lymphomagenesis and cooperate with MYC in *in vivo* models[59]. In pediatric BL gain of chr13q is associated with poor prognosis[46,50,52].

Chromosome 1q gain is the most frequent CNA in BL and across cancer[61]. The gained regions affect many genes and prediction of cancer drivers is therefore difficult. Amplified segments that are consistently reported can be further delineated to 1q25.1 and 1q31.3. The study of Salaverria *et al.* described highly overexpressed cancer-associated genes such as *NOTCH2*, *BCL9*, *PSMB4, MUC1, TXNIP, CKIP-1, ILF2* and *CKS1B* in the 1cen-q22 region. Scholtysik *et al.* suggested a role for hsa-mir-181b-1 and -213 on chr1q31 and *FASL* on 1q25, but functional validation is needed.

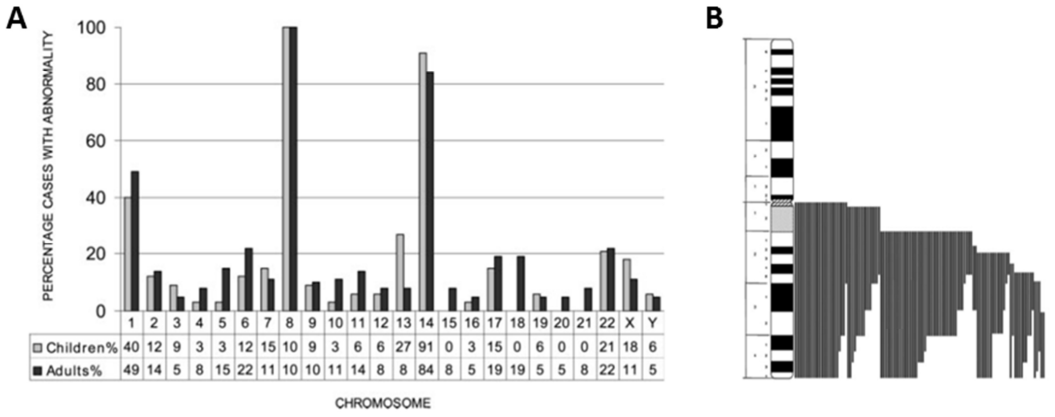

Figure 6: Recurrent copy number alterations in BL
(A) Profile of recurrent genomic alterations in adult and pediatric BL. Gains on chromosome 1 are the most frequent alteration apart from the translocation of *MYC* on chromosome 8 to the *IgH*-locus on chromosome 14 (Onciu *et al.*, 2006). **(B)** Gained regions on chromosome 1q reported in the Mitelman data base (modified from Davidsson *et al.*, 2007).

1.3.5 Oncogenesis

Pre-malignant B cells frequently adopt transcriptional features from their cell of origin. Additional genetic aberrations uncouple the cell from environmental survival and proliferation signals[10]. BL derives and closely resembles centroblasts from the DZ of the GC that are negative for MYC[62], raising the question at which stage BL cells acquire oncogenic MYC activation. MYC expression seems to be limited to a rare population of GC B cells in the LZ that interact with antigen-presenting T-helper cells for selection of high-affinity binding[63]. The translocation of *MYC* to the *IgH*-locus might be favored by AID-mediated CSR that takes place here[18]. Centrocytes from the LZ can return to the DZ for clonal expansion, a process that is favored by MYC expression[64]. Exposure of the *IgH-MYC* gene to SHM introduces multiple mutations, some of which have been shown to stabilize MYC protein level or to abrogate activation of pro-apoptotic Bcl2-family member Bim[65,66]. The GC phenotype and high proliferation rate of BL cells is retained by acquisition of activating mutations in the transcription factor E2A (encoded by the gene *TCF3*) or deleterious mutations in its negative inhibitor ID3[44,67,68]. E2A expression is higher in centroblasts compared to centrocytes[9] and was suggested to increase BCR surface expression and PI3K signaling[44]. E2A also transactivates the cell cycle promoting gene *CCND3*, a

gene that is again frequently targeted by activating mutations[44]. The tumor suppressor p53 (encoded by the gene *TP53*) senses DNA damage and oncogene activation, in part by MYC-mediated transactivation of *ARF*. Mutations in *TP53* occur in 30-40% of BL patients[69].

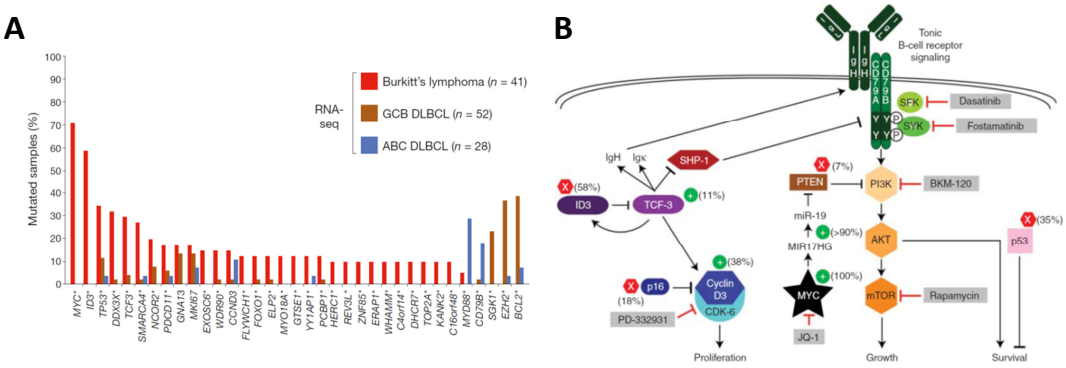

Figure 7: Recurrent mutations and oncogenic pathways in BL
(A) Recurrently mutated genes in BL, GCB DLBCL and ABC DLBCL. In the study of Schmitz *et al.* (2012) RNA sequencing was performed in 28 sporadic BL and 13 BL cell lines. The pattern of recurrent mutation was compared to publically available data on mutations in 52 GC DLBCL and 28 ABC DLBCL. **(B)** Schematic overview of key oncogenic signaling pathways in BL with indicated contribution of recurrent mutations (Schmitz *et al.*, 2014).

1.3.5.1 Physiological and oncogenic functions of MYC

The proto-oncogene *MYC* was first discovered in BL[15] and initially called *c-MYC* ('c' for 'cellular') as it closely resembled the myelocytomatosis viral oncogene, *v-MYC*[70]. The MYC family of nuclear transcription factors includes MYC, N-MYC and L-MYC, three basic helix-loop-helix (bHLH) leucine zipper proteins that control transcription of its target genes by binding to DNA enhancer box sequences (E-boxes) and recruitment of histone acetyltransferases (HATs). MYC functions as a transcriptional activator after heterodimerization with MYC-associated factor (MAX), and as a repressor of transcription upon binding to Miz-1. Physiologically, MYC controls protein biosynthesis, metabolism and cell cycle upon mitogenic signaling leading to an increase in cell size before division. MYC transactivates cyclins, cyclin-dependent kinase 4 (CDK4) and E2F transcription factor and simultaneously represses cyclin-dependent kinase inhibitors (CKI) of the Cip/Kip protein family (e.g. p27, p15, p21, p57) and DNA damage induced proteins of the GADD family (growth arrest and DNA-damage inducible). The protein MAD1 (mitotic arrest deficient 1) competes with MYC for the binding of MAX and therefore negatively regulates MYC. Under physiological conditions MYC is transcribed from the P2 promotor, one out of four alternative promotors, resulting into an instable, short-lived protein (based on reviews [71-73]).

Deregulated MYC is found across cancers. It is mainly associated with hematological malignancies, but also found in carcinomas of the lung, stomach, breast and cervix[73]. MYC functions as an oncogene by stimulatory effects on metabolism and protein synthesis[74]. The oncogenic function of MYC is studied in many cellular and transgenic mouse models. Mice

bearing a *MYC* gene under the highly active *IGH* enhancer (Eμ-MYC-mice) develop lymphomas from both immature and mature B cells[75]. Simultaneous activation of PI3K and MYC results into BL-like tumors displaying a gene expression signature of GC B cells[76]. BL is commonly used as a model to study the pathogenesis of MYC-driven diseases. The translocation of MYC to an Ig-locus leads to constitutive transcription from the P1 promotor producing a more stable protein that accumulates at high levels in the malignant cell. In addition, MYC is subjected to SHM and mutated in 70% of BL. Mutated MYC is a more potent oncogene, although the mechanism has only been resolved for selected hotspots within the conserved MYC box I and II regions. Tumors arising from MYC-overexpression in Rat1a fibroblasts showed lower apoptotic rates when the P138C mutation (box II) was introduced[77]. Mutations within the conserved MYC box I region, mostly on Thr58, stabilize the protein from proteasomal degradation[66,78,79]. In addition, these transactivation domain deficient mutants fail to induce pro-apoptotic Bcl2-family member Bim and were found to be exclusive to *TP53* mutations in one study[65].

1.3.5.2 Importance of p53 pathway in BL

Oncogenic MYC activation triggers p53-dependent apoptosis and senescence as an intrinsic safety mechanism[80]. The transcription factor p53 is a potent tumor suppressor entitled "guardian of the genome"[81]. Upon cellular stress such as DNA damage, hypoxia and oncogene activation p53 activates proteins and miRNAs that halt the cell cycle or induces intrinsic apoptotic programs. p53 is constitutively expressed, but protein levels are tightly regulated. In unstressed cells, the p53 inhibitor MDM2 associates with p53, blocks its transactivation domain and targets p53 for proteasomal degradation via its E3 ubiqutin-ligase activity[82,83]. MDM2 itself is a transcriptional target of p53 and activation of p53 therefore induces a negative feedback loop. A close homologue of MDM2, MDM4, also blocks the transactivation domain of p53, but lacks E3 ubiquitin-ligase activity[84]. Both proteins are needed for p53 inactivation. MDM2 forms a heterodimer with MDM4 that is more potent in ubiquitination and degradation of p53. However, the E3-ubiquitin ligase activity of MDM2 can be redirected from p53 towards MDM4 and self-degradation, based on post-translational protein modifications. DNA damage or oncogenic MYC signaling, e.g., activate the p53 pathway by induction of the kinase $p14^{ARF}$ (encoded on the *CDKN2A* locus), that subjects MDM2 for self-degradation[85].

p53 is mutated in 50% of cancers and can be deactivated by alternative mechanisms, such as *CDKN2A* inactivation or MDM2/MDM4 overexpression[86]. Transgenic Eμ-MYC mice develop clonal tumors with delayed onset and high *TP53* mutation rate, indicating that secondary genetic events, presumably in the p53 pathway, are needed for malignant transformation. In fact, *TP53* is mutated in 30-40% of BL patients[87-89] and 80% of cell lines[90,91]. Most mutations are missense mutations in the core DNA binding domain including the hotspot codons R213, R248 and less frequently R273[88]. In contrast to other cancer entities, deletion of the *TP53* locus on 17p13.1 is rare and most *TP53* mutations are heterozygous. Mutant p53 exerts a dominant negative effect on the wild-type form[92]. Therefore, monoallelic inactivation leads to a loss of

the tumor suppressor function of p53[93] and confers radio- and chemoresistance[92,94] as shown in cell line models. Little is known about the clinical implications of *TP53* mutations in BL, although the standard therapy is based on chemotherapeutic regiments. In the study of Preudhomme *et al*. (1995) *TP53* mutation status did not impact overall survival of 48 BL and ALL3 patients. A separate analysis of BL and its leukemic form was not performed.

Alternative mechanisms to p53 mutations may exist, which inactivate p53 function. Loss of *CDKN2A* in Eμ-MYC mice abrogates apoptosis and accelerates lymphomagenesis[95], but rarely occurs in BL patients. In some cases promotor methylation was reported for the *INK4a* transcript, but not for *ARF* [96,97]. Mutations of *FOXO1* that occur in ~10% of BL patients might abrogate the activation of *ARF*[44]. MDM2 overexpression, while common in some cancers, is absent in BL. In pediatric BL, Leventaki et al. (2014) did not observe MDM2 upregulation, however MDM4 mRNA level were elevated in 4 p53 wild-type patients with chromosome 1q32 gain, including the *MDM4* locus. Although an exclusive pattern of *CDKN2A* deletion, MDM2 overexpression and *TP53* mutations was observed in cell lines[98] p53 deactivating mechanisms in BL patients are still poorly understood.

1.4 RNAi screens

Genetic perturbation screens are widely used to understand cellular processes[99,100]. Two naturally occurring mechanisms were exploited as tools to modulate or edit genes of interest: RNAi (RNA interference) and CRISPR sequences (clustered regulatory interspaced short palindromic repeats). Applications include generation of genetically modified cells or organisms and genome-wide positive and negative selection screens for a desired phenotype.

RNAi is mediated by short interfering RNAs (siRNA) that target complementary mRNA for degradation and therefore lead to post-transcriptional gene silencing[101]. The first silencing triggers were long double-stranded RNA (dsRNA) precursors that were introduced into the target cell from *C. elegans* and *D. melanogaster*[102,103]. The RNase Dicer cleaves the precursors into siRNAs of 21-23 nucleotides (nt) with 2nt 3'-overhang. Upon binding of siRNAs to argonaute proteins of the degradation complex RISC (RNA-induced silencing complex) the sense strand is degraded and the antisense strand serves as a template to recruit the target mRNA[104,105]. This application was hampered in mammalian organisms by induction of interferon (INF) response. Therefore, techniques were developed for direct transfer of synthetic siRNAs into mammalian cells leading to transient gene knock-down[106]. Establishment of vector-expressed short-hairpin RNAs (shRNA) that integrate into the genome allowed stable gene knock-down[107,108]. shRNAs are expressed from a RNA polymerase III promoter as ~70nt precursors that are processed by Dicer. Initially, retroviral vectors limited the application of shRNAs to dividing cells. This was overcome by lentiviral vectors that also integrate into non-dividing cells[109].

Establishment of lentiviral, genome-wide shRNA libraries for murine and human genes[110,111] provided a powerful new resource for functional genomics studies. Functional screens are performed either in arrayed or pooled format. In arrayed screens cultured cells are seeded out on a multi-well plate that contains different silencing triggers in each well. Different techniques, including fluorescence, luminescence and imaging can be used as a read-out of knock-down phenotypes. With decreasing costs of next-generation sequencing (NGS) pooled RNAi screen became an alternative for non-imaging based screens with libraries that integrate into the genome. In pooled RNAi screens all silencing triggers are delivered to the cells in one flask and genomic DNA is extracted from the cells before and after positive or negative selection of the desired phenotype. The abundance of RNA reagents is determined by amplification and sequencing of the RNA itself or sequence-optimized vector barcodes.

In cancer research, RNAi screens were applied to identify pathogenic signaling pathways, resistance mechanisms and novel drug targets. The Broad Institute performed a genome-wide loss-of-function screen in 216 cell lines across cancer entities with available genetic data and identified cancer- and genotype-specific vulnerabilities by loss of shRNAs during cultivation[112,113].

RNAi screens are restricted by certain limitations, such as incomplete gene knock-down and sequence-specific off-target effects leading to a high false-discovery rate[114,115]. In a huge effort, the RNAi consortium (TRC) from the Broad Institute created a resource of genome-wide shRNA libraries for human and murine genes that contains at least two shRNAs with validated on-target effect[111]. However, off-target effects are still unpredictable.

Sequence-guided endonucleases emerged as a novel technology for genetic perturbation screens and targeted genomic engineering[116]. The system exploits the microbial adaptive immune system in response to viral infection[117-119] and endogenous DNA repair mechanisms of eukaryotic cells[120,121]. Endonucleases directed against a target sequence introduce double-strand breaks (DSB). In the presence of an exogenous DNA template DSBs are repaired precisely by homology-directed repair (HDR)[122]. This mechanism can be exploited to repair mutations in malignant cell or to intentionally introduce mutations in model organisms to study their pathogenic function[123]. In the absence of DNA template DSBs are repaired by the error-prone non-homologous end joining (NHEJ) resulting into random insertions and deletions (indels) and therefore disrupts the gene[124]. A common system from *Streptococcus pyrogenes* involves endonuclease Cas9 which is directed to a target sequence by 20bp single guide RNAs (sgRNAs) that pair with a complementary sequence in the DNA followed by a 3bp PAM (protospacer-adjacent motif) sequence[125]. Genome-wide sgRNA libraries are already in use for *in vitro* and *in vivo* screens and might be potential therapeutic tools for gene therapy[126,127].

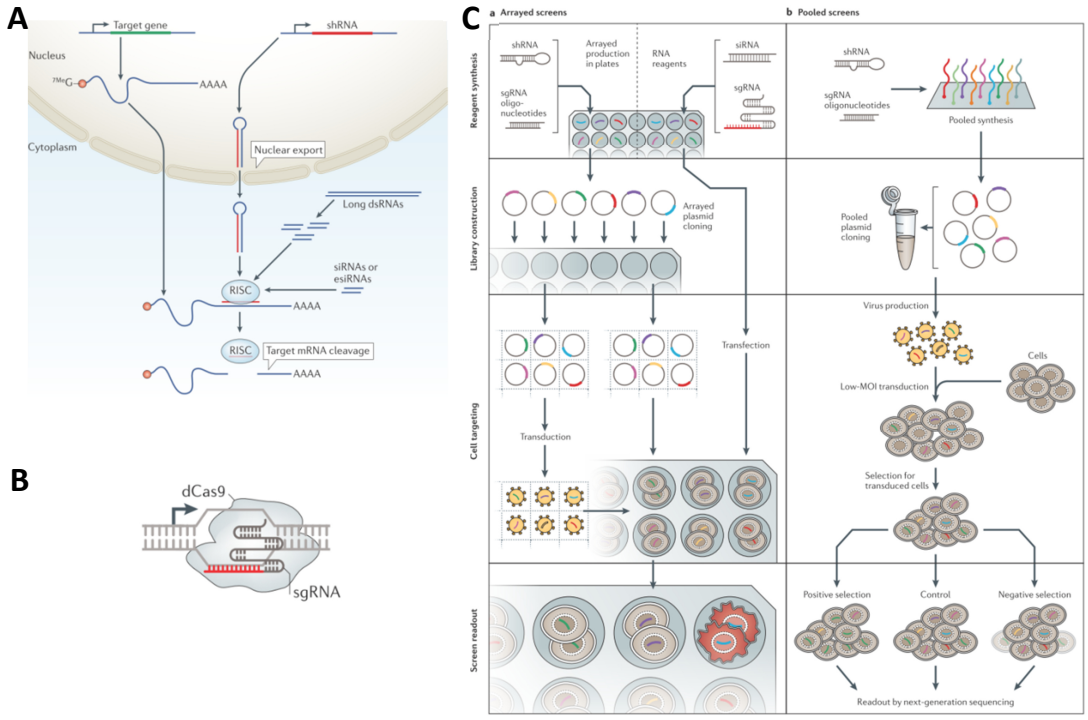

Figure 8: Functional genomics approaches

(A) Schematic overview of RNA interference (RNAi). Sequence complementary short hairpin RNAs (shRNAs), small interfering RNAs (siRNAs) or long double-stranded RNAs (dsRNAs) are introduced into the cell to target specific mRNA for degradation. shRNAs stable integrate into the genome while siRNAs and long dsRNAs are introduced transiently. After binding to the RNA-induced silencing complex (RISC) the sense strand is degraded and the antisense strand binds with complementary mRNA sequences and induces cleavage. **(B)** Genomic engineering and perturbation using the CRISPR/Cas9 technology. Directed by a guide RNA the bacterial endonuclease Cas9 unwinds the DNA strand next to the protospacer-adjacent motif (PAM) and induces double strand breaks. Error-prone non-homologous end-joining induces deletions and insertions leading to impaired gene function. **(C)** Schematic overview of arrayed (left) and pooled (right) genetic perturbation screens. In arrayed screens, RNA reagents are delivered to cells in single well format either by transduction (shRNAs) or by transfection (siRNAs). In pooled screens, RNA reagents are mixed in one tube, packaged in lentiviral particles and delivered to the bulk of cells at low infection rates to avoid infection with multiple vectors. The pool of cells is separated into different treatment branches and barcodes are read out by next-generation sequencing (modified from Shalem *et al.*, 2015).

2 Scientific Aims

Burkitt lymphoma (BL) is a highly proliferative B-cell lymphoma that arises from the germinal center during B-cell maturation. Oncogenic activation of MYC drives cell proliferation, but also evokes failsafe mechanisms that have to be counterbalanced. Mutations in the tumor suppressor gene *TP53* convey resistance towards MYC-induced stress signals, but alternative mechanisms of evading apoptotic programs are unknown.

Aim of this study was to identify alternative mechanisms of p53 inactivation in BL retaining a functional *TP53* gene. We addressed the following points:

1. Pattern of recurrent mutations in BL
   We analyzed the pattern of frequent mutations and copy number alterations for co-occurrence and exclusivity with *TP53* mutations to see if we can identify divergent mechanisms to deregulate this pathway.

2. Genetic vulnerabilities in BL cell lines
   To identify genes essential in the presence of functional p53, we explored the robustness and sensitivity of a RNAi loss-of-functionl screen in genetically defined cell line models.

3. Functional mechanisms underlying genotype-specific vulnerabilities
   To explore the molecular mechanisms of genotype-specific toxicities observed in the RNAi screen, we characterized downstream effects following shRNA-mediated knock-down of genes essential in p53 wild-type BL cell lines using cell cycle profiling, immunoblot analysis and micro-array based gene expression profiling.

4. Potential of p53 reactivating therapies
   To test if genes that were found to be essential specifically in p53 wild-type BL are potential therapeutic targets, we measured the effect of target gene knock-down on p53 reactivation, cell growth and tumor formation *in vivo*.

5. Clinical importance of p53 inactivation in BL
   To evaluate the role of potential target genes in the pathogenesis of BL patients, we integrated our findings from the RNAi screen with molecular and genetic patient profiles.

6. RNAi screens for identification of entity-specific vulnerabilities
   We further explored the potential of genetic perturbation screens across cancer cell lines for identification of novel therapeutic targets in a specific cellular context, such as cell lineage or gene mutation.

3 Materials and Methods

3.1 Materials

3.1.1 List of materials

Reagent	Company
Cell culture	
Dulbecco's Modified Eagle Medium (DMEM)	Thermo Fisher Scientific, Waltham, USA
RPMI medium 1640	Thermo Fisher Scientific, Waltham, USA
Foetal Bovine Serum Premium, South America	PAN-Biotech, Aidenbach, GER
Foetal Bovine Serum	Thermo Fisher Scientific, Waltham, USA
L-Glutamine, 200mM	Thermo Fisher Scientific, Waltham, USA
Penicillin-Streptomycin Solution (100x, 1:1)	Thermo Fisher Scientific, Waltham, USA
Dulbecco's PBS without Ca/Mg (1X)	Thermo Fisher Scientific, Waltham, USA
Trypan Blue Staining solution 0.4%	Thermo Fisher Scientific, Waltham, USA
Dimethyl sulfoxide (DMSO), ≥95%	Sigma-Aldrich, Munich, GER
FastRead 102 Disposable counting chambers	Immune systems, Paignton, UK
Lentiviral packaging, infection and selection	
Opti-MEM® I reduced serum medium	Thermo Fisher Scientific, Waltham, USA
Lipofectamine® Transfection Reagent	Thermo Fisher Scientific, Waltham, USA
PLUS™ Reagent	Thermo Fisher Scientific, Waltham, USA
Puromycin Dihydrocloride	Thermo Fisher Scientific, Waltham, USA
RNAi screen	
shRNA library Human Module 1, DHPAC-M1-P	Cellecta Inc., Mountain View, CA, USA
Buffer P1 (50mM Tris-HCl pH 8.0, 10mM EDTA)	Qiagen, Hilden, GER
RNase A (17,500U)	Qiagen, Hilden, GER
Phenol:Chloroform:Isoamyl Alcohol pH 8.0	Sigma-Aldrich, Munich, GER
DNase I, RNase-free	Epicentre, Madison, WI, USA
Titanium Taq DNA polymerase with PCR buffer	Takara Bio Europe, St-Germain-en-Laye, FR
Magnesium chloride	Sigma-Aldrich, Munich, GER
PCR	
Taq DNA Polymerase	Qiagen, Hilden, GER
Taq Polymerase S (high specificity)	Genaxxon, Ulm, GER
dNTP-Set (Na-salt) - 100 mM	Genaxxon, Ulm, GER
100bp DNA ladder	Thermo Fisher Scientific, Waltham, USA
1 Kb DNA ladder	Thermo Fisher Scientific, Waltham, USA
Agarose for DNA electrophoresis	Serva Electrophoresis, Heidelberg, GER
Agencourt AMPure XP	Beckman Coulter, Krefeld, GER
QIAquick PCR Purification Kit	Qiagen, Hilden, GER
DNA vector cloning	
One Shot® TOP10 Chemically Competent *E.coli*	Thermo Fisher Scientific, Waltham, USA
XL10-Gold Ultracompetent Cells	Agilent Technologies, Böblingen, GER
Ampicillin sodium salt	Sigma-Aldrich, Munich, GER
Spectinomycin	Sigma-Aldrich, Munich, GER
Agar powder	Sigma-Aldrich, Munich, GER
Luria Broth Base (LB) powder	Thermo Fisher Scientific, Waltham, USA
S.O.C Medium	Thermo Fisher Scientific, Waltham, USA
BpiI (BbsI)	Thermo Fisher Scientific, Waltham, USA
Buffer G	Thermo Fisher Scientific, Waltham, USA
BsmBI	Thermo Fisher Scientific, Waltham, USA

Reagent	Company
BamHI	NEB, Ipswitch, MA, USA
SfbI	NEB, Ipswitch, MA, USA
T4 Polynucleotide Kinase incl. 10x buffer	NEB, Ipswitch, MA, USA
T4 DNA Ligase	NEB, Ipswitch, MA, USA
rATP 100mM solution	GE Healthcare, Frankfurt, GER
GeneMatrix Plasmid MiniPrep DNA Purification Kit	EURx, Gdansk, PL
EndoFree Plasmid Maxi Kit	Qiagen, Hilden, GER
QuickExtract DNA Extraction solution	Epicentre, Madison, WI, USA
Plasmid Giga Kit	Qiagen, Hilden, GER
QIAquick Gel Extraction Kit	Qiagen, Hilden, GER
T7 Endonuklease I	NEB, Ipswitch, MA, USA
DNA and RNA purification/quantification	
DNeasy Blood & Tissue Kit	Qiagen, Hilden, GER
RNeasy Mini Kit	Qiagen, Hilden, GER
Quant-it™ PicoGreen® dsDNA Assay Kit	Thermo Fisher Scientific, Waltham, USA
Qubit® dsDNA BR Assay Kit	Thermo Fisher Scientific, Waltham, USA
Qubit® RNA BR Assay Kit	Thermo Fisher Scientific, Waltham, USA
Qubit® Assay Tubes	Thermo Fisher Scientific, Waltham, USA
QIAshredder columns	Qiagen, Hilden, GER
RNAse Away™	Ambion GmbH, Kassel, GER
RiboLock RNase Inhibitor	Thermo Fisher Scientific, Waltham, USA
RNase-Free DNase Set	Qiagen, Hilden, GER
DNA and RNA sequencing	
SUPREMERUN™ sequencing	GATC Biotech AG, Konstanz, GER
twin.tec® PCR plate 96	Eppendorf, Hamburg, GER
GS Junior Titanium emPCR Kit (Lib-A)	Roche, Basel, CH
GS Junior Titanium Sequencing Kit	Roche, Basel, CH
GS Junior Maintenance Wash Kit	Roche, Basel, CH
RT-qPCR	
QuantiFast SYBR Green RT-PCR Kit	Qiagen, Hilden, GER
Western Blot	
Skimmed milk powder	Carl Roth GmbH&Co, Karlsruhe, GER
BSA Protease Free	PAA, Cambridge, UK
Tween® 20	Sigma-Aldrich, Munich, GER
Tris buffer pH 7.5 (1 M)	AppliChem Inc., Maryland Heights MO, USA
Sodium chloride (NaCl)	Sigma-Aldrich, Munich, GER
Kalium chloride (KCl)	Carl Roth GmbH&Co, Karlsruhe, GER
10x RIPA Lysis Buffer	Merck/Millipore, Darmstadt, GER
Benzonase®	Merck/Millipore, Darmstadt, GER
Pierce™ BCA Protein Assay Kit	Thermo Fisher Scientific, Waltham, USA
Pierce™ Bovine Serum Albumin Standard Ampules, 2 mg/ml	Thermo Fisher Scientific, Waltham, USA
PhosSTOP (phosphatase inhibitor cocktail)	Roche Life Science, Indianapolis, IN, USA
cOmplete™, EDTA-free Protease Inhibitor	Sigma-Aldrich, Munich, GER
Laemmli sample buffer, 2x concentrate	Sigma-Aldrich, Munich, GER
Mini-PROTEAN® TGX™ Precast Gels 4-15%	BioRad, Munich, GER
10x Tris/Glycine/SDS Running buffer	BioRad, Munich, GER
PageRuler™ Prestained Protein Ladder	Thermo Fisher Scientific, Waltham, USA
Trans-Blot® Turbo™ RTA Mini LF PVDF Transfer Kit	BioRad, Munich, GER
Fluorescence and luminescence assays	
CellTiter-Glo® Luminescent Cell Viability Assay	Promega GmbH, Mannheim, GER
Annexin V, APC	BD Biosciences, San Jose, CA, USA
Annexin V Binding Buffer, 10x Concentrate	BD Biosciences, San Jose, CA, USA
7-AAD (7-Aminoactinomycin)	BD Biosciences, San Jose, CA, USA
Propidium iodide ≥94% HPLC	Sigma-Aldrich, Munich, GER

Reagent	Company
FISH probes XL 1p32 / 1q21 (D-5049-100-OG)	MetaSystems GmbH, Altlussheim, GER
FISH probes XT MYC BA (D-6023-100-OG)	MetaSystems GmbH, Altlussheim, GER
BREATH-EASY sealing membrane	Sigma-Aldrich, Munich, GER
BD Pharmingen™ APC BrdU Flow Kit	BD Biosciences, San Jose, CA, USA
Formaldehyd, 30%	Carl Roth GmbH&Co, Karlsruhe, GER
FIX/PERM® Solution B	Nordic MUbio, Susteren, NL
Chemicals	
Ethanol absolute	Sigma-Aldrich, Munich, GER
Methanol	Sigma-Aldrich, Munich, GER
Isopropanol	Sigma-Aldrich, Munich, GER
Nutlin-3	Absource Diagnostics, Munich, GER

3.1.2 List of instruments and devices

Instruments and devices	Company
Sonopuls ultrasonic homogenizer	Bandelin, Berlin, GER
Flow Cytometer LSR Fortessa™	BD Biosciences, San Jose, CA, USA
Flow Cytometer LSRII™	BD Biosciences, San Jose, CA, USA
Flow Cytometer FACSAria™ Cell Sorter	BD Biosciences, San Jose, CA, USA
Cobas® z480 Analyzer	Roche, Basel, CH
Mini-PROTEAN® Tetra Vertical Electrophoresis Cell	BioRad, Munich, GER
Trans-Blot® Turbo™ Transfer System	BioRad, Munich, GER
Fluorescence scanner Odyssey®	Li-cor, Lincoln, NE, USA
Microplate reader Infinite® M1000 PRO	Tecan AG, Männedorf, CH
Thermocycler	Biometra, Göttingen, GER
peqSTAR 96X Thermocycler	PeqLab/VWR, Erlangen, GER
GS Junior 454 sequencer	Roche, Basel, CH
NanoDrop® Spectrophotometer ND-1000	PeqLab/VWR, Erlangen, GER
PerfectBlue Gel system	PeqLab/VWR, Erlangen, GER
Liberty 120 rapid gel system	Neuvitro Corp., Vancouver, WA, USA
HighSeq 2000 genome sequencer	Illumina, San Diego, CA, USA
Qubit 2.0 Fluorometer	Thermo Fisher Scientific, Waltham, USA
Bioanalyzer 2100	Agilent Technologies, Böblingen, GER

3.1.3 List of software and operating systems

Software/Operating system	Company/Institution
Barcode Deconvoluter software	Cellecta Inc., Mountain View, CA, USA
Python™ v2.7.10	Python, San Francisco, CA, USA
R v3 and above	R, open source
R Studio™	R Studio, Boston, MA, USA
GENE-E v3.0.204 (for academic use)	Broad Institute, Boston, MA, USA
GSEA	Broad Institute, Boston, MA, USA
LightCycler 480 Software release 1.5.0	Roche, Basel, CH
Odyssey operation software v3	Li-cor, Lincoln, NE, USA
GraphPad Prism v5.03	GraphPad Software, La Jolla, CA, USA
GS Junior Sequencer v2.5	Roche, Basel, CH
GS Amplicon Variant Analyzer v2.5	Roche, Basel, CH
Image Studio Lite v4.0	Li-cor, Lincoln, NE, USA
FlowJo v10	FlowJo, Ashland, OR, USA
FACSDiva™ Software v6/8.1	BD Biosciences, San Jose, CA, USA

3.1.4 List of oligo-nucleotides

RNAi screen		
Name	**Sequence [5'-3']**	**Reaction**
FwdHTS	TTCTCTGGCAAGCAAAAGACGGCATA	1st Round PCR
RevHTS1	TAGCCAACGCATCGCACAAGCCA	1st Round PCR
FwdGex	CAAGCAGAAGACGGCATACGAGA	2nd Round PCR
RevGex	AATGATACGGCGACCACCGAGA	2nd Round PCR
IndA	AATGATACGGCGACCACCGAGATCTACACGCAATGCGCACAACCGCAA	Multiplexing
IndB	AATGATACGGCGACCACCGAGATCTACACGCAGACTGCACAACCGCAA	Multiplexing
IndC	AATGATACGGCGACCACCGAGATCTACACGCATCAGGCACAACCGCAA	Multiplexing
IndD	AATGATACGGCGACCACCGAGATCTACACGCACGTAGCACAACCGCAA	Multiplexing
IndE	AATGATACGGCGACCACCGAGATCTACACGCAAGCGGCACAACCGCAA	Multiplexing
IndF	AATGATACGGCGACCACCGAGATCTACACGCAGATGGCACAACCGCAA	Multiplexing
IndG	AATGATACGGCGACCACCGAGATCTACACGCAGGACGCACAACCGCAA	Multiplexing
IndH	AATGATACGGCGACCACCGAGATCTACACGCAGCGAGCACAACCGCAA	Multiplexing
GexSeqS	AGAGGTTCAGAGTTCTACAGTCCGAA	Barcode sequencing
GexSeqIND	ACGACCACCGAGATCTACACGCA	Indexing

HPLC purified oligo-nucleotides were ordered at MWG Eurofins (Ebersberg, GER).

RT-qPCR		
Name	**Sequence [5'-3']**	**Source**
qMDM4_fwd	TGAAAGACCCAAGCCCTCT	Self-designed
qMDM4_rev	CGAGAGTCTGAGCAGCATCTG	Self-designed
qTP53_fwd	GGAGCACTAAGCGAGCACTG	Self-designed
qTP53_rev	CACGGATCTGAAGGGTGAAA	Self-designed
qMDM2_fwd	CAGTAGCAGTGAATCTACAGGGA	RT-Primer Bank
qMDM2_rev	CTGATCCAACCAATCACCTGAAT	RT-Primer Bank
qBAX_fwd	CCCGAGAGGTCTTTTTCCGAG	RT-Primer Bank
qBAX_rev	CCAGCCCATGATGGTTCTGAT	RT-Primer Bank
qRRM2B_fwd	AGAGGCTCGCTGTTTCTATGG	RT-Primer Bank
qRRM2B_rev	GCAAGGCCCAATCTGCTTTTT	RT-Primer Bank
qCDKN1A_fwd	GACTCTCAGGGTCGAAAACG	self-designed
qCDKN1A_rev	TAGGGCTTCCTCTTGGAGAA	self-designed
qMCM7_fwd	CCTACCAGCCGATCCAGTCT	RT-Primer Bank
qMCM7_rev	CCTCCTGAGCGGTTGGTTT	RT-Primer Bank
qMCM6_fwd	ACCTGCCTACCAGACACAAGA	RT-Primer Bank
qMCM6_rev	ACAGAAAAGTTCCGCTCACAAG	RT-Primer Bank
qMCM10_fwd	TGTCCCTGCGCTACCAAGA	RT-Primer Bank
qMCM10_rev	GATGAGCTTTTGGGATCTGGAG	RT-Primer Bank
qCDKN3_fwd	TCCGGGGCAATACAGACCAT	RT-Primer Bank
qCDKN3_rev	GCAGCTAATTTGTCCCGAAACTC	RT-Primer Bank
qGAPDH_fwd	GGAGCGAGATCCCTCCAAAAT	RT-Primer Bank
qGAPDH_rev	GGCTGTTGTCATACTTCTCATGG	RT-Primer Bank

HPSF purified oligo-nucleotides were ordered at MWG Eurofins (Ebersberg, GER).

shRNA target sequences		
Name	**Sequence [5'-3']**	**Cellecta shRNA ID**
CDKN3_1	CGGGACAAATTAGCTGCACAT	CLL-H-005488
CDKN3_2	TGTTCTCAGTTTCTCGGTTTA	CLL-H-005489
CDKN3_3	CAGACCATCAAGCAATACAAT	CLL-H-005490
CDKN3_4	AGAACTAAAGAGCTGTGGTAT	CLL-H-005491
CDKN3_5	GTGCAGATATTCCTAAAGTTT	CLL-H-005492
CDKN3_6	GACCATGTCTGAAATGTCAGT	CLL-H-005493
MDM2_1	CTTTGGTAGTGGAATAGTGAA	CLL-H-016687
MDM2_2	GATTCCAGAGAGTCATGTGTT	CLL-H-016688
MDM2_3	CGATTATATGATGAGAAGCAA	CLL-H-016689
MDM2_4	CTGTGTGTAATAAGGGAGATA	CLL-H-016690
MDM2_5	CTCAGCCATCAACTTCTAGTA	CLL-H-016691
MDM4_4	CACCTAGAAGTAATGGCTCAA	CLL-H-016692
MDM4_1	GTTCACTGTTAAAGAGGTCAT	CLL-H-016693
MDM4_7	CCCTGATTGTCGAAGAACCAT	CLL-H-016694
MDM4_5	ACAGTCCTTCAGCTATTTCAT	CLL-H-016695
MDM4_6	CTCAACTGATTTACAGACAAA	CLL-H-016696
shNT	CAACAAGATGAAGAGCACCAA	

Design of single-stranded shRNA oligo-nucleotides for cloning into an expression vector is described in chapter 3.4.4. Desalted oligonucleotides were ordered at Sigma-Aldrich (Munich, GER).

sgRNA target sequences		
Name	**Sequence [5'-3']**	**Source**
TP53_3	CATGTGTAACAGTTCCTGCA	Shalem et al., 2014
TP53_7	GAGCGCTGCTCAGATAGCGA	HGLibB_51984
TP53_8	CCCCTTGCCGTCCCAAGCAA	HGLibB_51985

Design of single-stranded sgRNA oligo-nucleotides for cloning into an expression vector is described in chapter 3.4.4. Desalted oligo-nucleotides were ordered at Sigma-Aldrich (Munich, GER).

PCR primer	
Name	**Sequence [5'-3']**
TP53_ex4a_fwd	TGACTGCTCTTTTCACCCATCT
TP53_ex4a_rev	GAAGATGACAGGGGCCAG
TP53_ex4b_fwd	CCTGCACCAGCAGCTCCTAC
TP53_ex4b_rev	CAGGCATTGAAGTCTCATGGA
TP53_ex5_fwd	CAACTCTGTCTCCTTCCTCTTCC
TP53_ex5_rev	GTCGTCTCTCCAGCCCCA
TP53_ex6_fwd	GAGAGA**C**GACAGGGCTGGTT
TP53_ex6_rev	CTTAACCCCTCCTCCCAGAG
TP53_ex7_fwd	CTTGGGCCTGTGTTATCTCC
TP53_ex7_rev	GAGGTGGATGGGTAGTAGTATGG
TP53_ex8_fwd	GCTTCTCTTTTCCTATCCTGAGT
TP53_ex8_rev	GCTTCTTGTCCTGCTTGCT
TP53_ex9_fwd	GTGCAGTTATGCCTCAGATTC
TP53_ex9_rev	CAGTCAAGAAGAAAACGGCAT
TP53_ex10_fwd	GCATGTTGCTTTTGTACCGTC
TP53_ex10_rev	GGAAGGGGCTGAGGTCACT
MYD88_ex5_fwd	GCATGTGTGTGCCTTTTTGT

Name	Sequence [5'-3']
MYD88_ex5_rev	GATGAACCTCAGGATGCTGG
sgTP53_8_fwd	TTCCTGAAAACAACGTTCTGg
sgTP53_8_rev	GGTGTAGGAGCTGCTGGTG
LCIII_fwd	AGTGGCACAGCAGTTAGG
LTR IV_rev	CCTTGCAAAATGGCGTTACT
pRSI12 Colony PCR_fwd	AAAGTATTTCGATTTCTTGGCTTT
pRSI12 sequencing	CAAGGCTGTTAGAGAGATAATTGGAA
pLentiCRISPRv2 sequencing	GTACAAAATACGTGACG

HPLC-purified oligo-nucleotides were ordered at MWG Eurofins. For multiplexed 454 sequencing LCIII sequence was added to forward primers and LTR IV sequence was added to the reverse primers to add universal tails to the PCR products (see chapter 3.4.2).

3.1.5 List of plasmids

Name	Promoter	Genes	Function	Source
pMD2.G	CMV	VSV-G	Lentiviral packaging	Michael Böttcher (DKFZ)
psPAX2	CAG	gag, pol, rev,	Lentiviral packaging	Michael Böttcher (DKFZ)
pRSI12	U6	TagRFP, puroR	shRNA expression	Cellecta Inc.
pLentiCRISPR v2	SV40	puroR, Cas9-FLAG	sgRNA expression	Feng Zhang (Addgene # 52961)

3.1.6 List of antibodies

Gene	MW[kDa]	Company	Clone	Cat. no.	Host	Dilution
MDM4	80	Merck-Millipore	8C6	04-1555	mouse	1:1000
MDM2	75	Merck-Millipore	IF2	OP46	mouse	1:50
GAPDH	37	Abcam	pAb	ab9485	rabbit	1:2500
p53-FITC	53	BD Pharmingen™	DO-1	557026	mouse	1:25
p53	53	BD Pharmingen™	DO-7	554294	mouse	1:5000
p21	21	BD Pharmingen™	SXM30	556431	mouse	1:250
PUMA	24	SantaCruz	pAb	sc-28226	rabbit	1:100
cleaved PARP	89	Cell Signaling	pAb	9546	mouse	1:1000
Anti-mouse		Cell Signaling	DyLight 800	5257	goat	1:15,000
Anti-rabbit		Cell Signaling	DyLight 680	5366	goat	1:15,000

MW = molecular weight pAb = polyclonal antibody

3.1.7 List of web and data resources

Name	Website
NCBI	National Center for Biotechnology Information, Rockville , Bethesda MD, USA (www.ncbi.nlm.nih.gov)
Ensembl	Wellcome Trust Sanger Institute, Hinxton, UK (www.ensembl.org)
UCSC	UC Santa Cruz, California, USA (genome.ucsc.edu)
COSMIC	Wellcome Trust Sanger Institute, Hinxton, UK (cancer.sanger.ac.uk/cosmic)
TP53 Database	IARC, Lyon, France (p53.iarc.fr)
GENE-E	Broad Institute, Boston, USA (broadinstitute.org/cancer/software/GENE-E)
GSEA	Broad Institute, Boston, USA (broadinstitute.org/gsea/index.jsp)
Gene Pattern	Broad Institute, Boston, USA (broadinstitute.org/cancer/software/genepattern)
DSMZ	Leibniz Institute, Braunschweig, GER (dsmz.de)
cBio Portal	Memorial Sloan-Kettering Cancer Center, New York, USA (cbioportal.org)
RT Primer bank	https://pga.mgh.harvard.edu/primerbank/

3.1.8 List of laboratory services

Method	Company/Institution
Capillary sequencing (ABI 3730xl)	GATC Biotech, Konstanz, GER
Next-generation sequencing (Illumina HiSeq2000)	DKFZ genomics and proteomics core facility
Gene expression profiling (Illumina BeadChip HumanHT-12 v4)	DKFZ genomics and proteomics core facility
Gateway Full ORF clone	DKFZ genomics and proteomics core facility
Cell line authentification	Multiplexion, Heidelberg, GER
Cell line contamination test	Multiplexion, Heidelberg, GER
FISH analysis	Prof. Dr. Anna Jauch, University Hospital Heidelberg, Institute of Human Genetics
MYC box mutation analysis	Heiko Trautmann (University Hospital Schleswig-Holstein)
EBV status analysis	Prof. Dr. Henri-Jacques Delecluse, DKFZ

3.2 Primary sample analysis

Data on primary samples from lymphoma patients were generated within the network of the MMML (Molecular Mechanisms of Malignant Lymphoma) consortium, that was founded in 2003. The data set was finalized in 2011. The study was approved by the local ethics commission of the Georg-August University in Göttingen, Germany. The data is available at the Gene Expression Omnibus (http://www.ncbi.nlm.nih.gov/geo) under the accession numbers GSE43677 (for microarray data) and GSE21597 (for SNP array data). Sample processing and generation of micorarray data were described previously[43,49,128]. All bioinformatic analyses on primary patient material in this study were performed in cooperation with Maciej Rosolowski and Markus Kreuz (Institute of Medical Informatics, Statistics and Epidemiology (IMISE), University of Leipzig, Leipzig, GER). Patients were classified into BL, DLBCL and an intermediate group based on a previously described molecular signature[43]. Tumor cell content exceeded 70% in all cases.

DNA was extracted using reagents from Qiagen (Hilden, GER). Copy number variations were analyzed by CGHa using a BAC/PAC array that consisted of 2799 DNA fragments as described elsewhere[129,130]. Interphase FISH analysis was performed on paraffin-embedded or frozen tissue sections to determine *MYC*, *BCL2* and *BCL6* translocations to *IG* enhancer regions.

TP53 mutations were determined by sequencing of exons 4-10 of the coding region.

For gene expression analysis, RNA was extracted using reagents from Qiagen (Hilden, GER) and hybridized to an Affymetrix U133A GeneChip (Santa Clara, CA, USA) according to the manufacturer´s instructions using 5µg of total RNA. For analysis of the most differentially expressed genes in *TP53*mut and *TP53*wt B-NHL, all values were adjusted for subtype-specific effects.

3.3 Cell culture methods

3.3.1 List of cell lines

Name	Depositor
BJAB	DSMZ, Braunschweig, Germany
BL-2	DSMZ, Braunschweig, Germany
CA46	DSMZ, Braunschweig, Germany
Namalwa	DSMZ, Braunschweig, Germany
Ramos	DSMZ, Braunschweig, Germany
Raji	DSMZ, Braunschweig, Germany
BL-41	DSMZ, Braunschweig, Germany
DogKit	DSMZ, Braunschweig, Germany
HEK293T	Stefan Fröhling (DKFZ)

Name	Depositor
DG-75	DSMZ, Braunschweig, Germany
Gumbus	DSMZ, Braunschweig, Germany
BL7	Dr.G.M. Lenoir, IARC, Lyon, France
BL60	Dr.G.M. Lenoir, IARC, Lyon, France
LY47	Dr.G.M. Lenoir, IARC, Lyon, France
Salina	A. Rickinson, Birmingham, UK
Seraphine	A. Rickinson, Birmingham, UK
Cheptanges	A. Rickinson, Birmingham, UK

3.3.2 Cell line cultivation, quality control and cryopreservation

All cell lines were cultured under standard conditions (37°C, 5% CO_2). Lymphoma cell lines were cultured in RPMI and HEK293T cells in DMEM supplemented with 10% FBS (20% for Cheptanges, BL7, Gumbus, DogKit), 2mM fresh glutamine and 1% penicillin/streptomycin. For cell line authentication 200ng genomic DNA were submitted to Multiplexion (Heidelberg, GER) for single nucleotide polymorphism (SNP)-profiling. To test for contamination, cell extracts were prepared from ~$2x10^6$ cells by heating for 15min at 95°C. After removal of cell debris by centrifugation, the supernatant was submitted to Multiplexion for multiplex PCR analysis of 100 contaminants, including 14 mycoplasma strains, EBV, Squirrel Monkey Retrovirus (SMRV) and cross-species cell contaminations. For cryopreservation, cells were frozen in liquid nitrogen at 3-$5x10^6$ cells/ml in the respective cell culture medium containing 30% FBS and 10% DMSO. Cell vials were stored in Mr. Frosty freezing containers (Thermo Fisher Scientific, Schwerte, GER) at -80°C for gradual cool down over 24h.

3.3.3 Cell line characterization

TP53 mutation status was determined by targeted resequencing of exons 4-10 (see 3.4.2). MYC box I and II mutations were determined by Dr. Heiko Trautmann and Dr. Christiane Pott (University Hospital Schleswig-Holstein, Kiel, GER) using Sanger sequencing. Genetic aberrations of chromosome 1q or MYC were reported by the DSMZ cell line bank or the CGHa study from Toujani *et al.,* (2009). In cases with missing data we determined MYC breakpoints or chr1q21 rearrangements by FISH using the MYC break apart probe and 1p32/1q21, respectively (performed by Dr. Anna Jauch at the Institute of Human Genetics, University Hospital Heidelberg, GER). EBV-status was tested by protein staining for EBNA2 (expressed during latency III) and BHRF1 (expressed in Wp-restricted cell lines) (performed in the laboratory of Prof. Delecluse, DKFZ, Heidelberg, GER).

3.3.4 Lentiviral packaging

For lentiviral packaging, HEK293T/17 cells were used, a derivative of the HEK293 cell line that was established from transformed human embryonic kidney cells. HEK293T/17 expresses

Simian Virus-40 (SV-40) T-antigen that allows episomal replication of transfected plasmids and therefore prolongs the effective production of lentiviral particles. The cell line was derived from a single cell clone that was selected for high transfection rates. Cells were seeded out at a density of $2.5x10^5$ cells/ml. After 24h of cultivation cells were growing adherent again and were transfected with three plasmids: the target transfer vector, the envelope vector (pMD2.G) and the packaging plasmid of the 2nd generation (psPAX2). According to the table below, a packaging-plus and a lipofectamine mix were prepared. The packaging-plus mix was incubated for 15min at RT, gently mixed with the lipofectamine mix and again incubated for 15min at RT. The complexed molecules were added to the medium of the HEK293T/17 cells by gentle pipetting and mixed by slow rotation of the plate. After growing the cells for 12-18h in the presence of the transfection mix the medium was replaced and virus-producing cells were cultivated for 24h-36h. Transfection efficiency was estimated based on RFP expression observed in fluorescence microscopy. The supernatant of the HEK293T/17 cells was filtered through a 45µM filter and stored at -80°C.

	Per well	In 6-well [µl]	In 10cm dish [µl]
Packaging-plus mix per shRNA			
OPTI-MEM	190µl	190	950
PACKAGING MIX psPAX2: pMD2.G, 2:1, 500ng/µl	820ng : 410ng	2.5	13
Plus-Reagent	2.5µl	2.5	13
Target plasmid, 50ng/µl	250ng	5	25
Lipofectamine mix			
Opti-MEM	197µl	197	985
Lipofectamine	3.7µl	3.7	19
Add Mix to the well/dish		401	2,004

3.3.5 Lentiviral infection

BL cell lines were seeded out at a final cell density of $5x10^5$ cells/ml. Lentiviral supernatant was added to the cell culture according to previously determined virus titer to achieve desired infection rates. Polybrene is commonly used to increase lentiviral infection rates. However, in BL cell lines polybrene was toxic at low concentrations and no beneficial effect on infection rate was observed.

3.3.6 Puromycin titration and selection

Puromycin was used to select transduced cells that carried a puromycin resistance gene as a selection marker. The optimal concentration of puromycin was titrated on each cell line. Cells were cultivated for 24h or 48h with increasing puromycin concentration (0.5µg/ml – 5µg/ml) and cell viability was measured by flow cytometry based on the forward/sideward scatter and 7-AAD dead cell exclusion staining. The minimal dose that killed >90% of uninfected cells was used to enrich for transduced cells.

3.3.7 Flow cytometric analysis for fluorescent markers

For analysis of lentivirally infected cells expressing fluorescent selection marker RFP 100µl of a dense cell culture (~$1x10^5$ cells) were harvested, washed once with 200µl PBS+2%FBS and resuspended in 100µl PBS+2%FBS. Cells were kept on ice until flow cytometric analysis. RFP

signal was analyzed at the LSRFortessa using the yellow/green (excitation: 561nm) laser. GFP signal was analyzed at the LSRII using the blue laser (excitation: 488nm). Dead cells were excluded by forward/sideward scatter. Duplet cells were excluded by area and height of the forward-scatter (FSC-A and FSC-H).

3.3.8 RFP-growth competition assay

The effect of shRNAs on viability or growth kinetics was tested by infection of BL cell lines at an infection rate of ~50% and subsequent flow cytometric analysis of RFP signal over 14 days. Cells were first measured at day 3 post-infection, when the RFP signal is fully expressed and the fraction of RFP-positive cells measured at later time points was normalized to the initial measurement.

3.3.9 Intracellular staining for flow cytometric analysis

Two alternative fixation methods were used: Methanol (MeOH) which leads to a loss of fluorescent markers and paraformaldehyde (PFA) which retains protein structures and fluorescent signal. ~$2x10^6$ cells were harvested and washed with PBS+2%FBS. For PFA fixation, cells are resuspended in 500µl 2% PFA and incubated for 30min at 4°C. After two washing steps, cells were resuspended in 1ml ice-cold 80% ethanol (EtOH) and incubated over night at -20°C. Before staining, cells were permeabilized in 100µl FIX&PERM Solution B, incubated for 30min at RT in the dark and washed with PBS. For MeOH fixation, cells were resuspended in 100µl PBS and 900µl ice-cold 100% MeOH were added drop-wise while shaking. Cells were incubated over night at -20°C. Before staining, cells were pelleted, resuspended in 1ml PBS and incubated for at least 30min at 4°C.

p53 staining

Fixated cells were resuspended in 100µl p53 staining solution (1:25 antibody dilution in PBS+2%FBS) using DO-1 antibody coupled to FITC (BD Pharmingen, BD Biosciences, San Jose, CA, USA), incubated for 1h at 4°C in the dark and washed and resuspended in PBS+2%FBS.

Cell cycle analysis with 7-AAD

Fixed cells were diluted in 50µl PBS with 100µg/ml RNase A (Qiagen, Hilden GER) and stained with 250µg/ml 7-AAD (BD Pharmingen). Before analysis cells are incubated for 30min at RT in the dark.

3.3.10 Flow cytometric analysis of cell cycle phases by BrdU incorporation

Analysis of cell cycle phases was performed using the BrdU Flow Kit from BD Pharmingen according to the manufacturer´s protocol. Cells were cultivated for 2-3h in the presence of 1mM BrdU, harvested and fixated with PFA-based solutions provided in the kit. DNase I digestion opens up the DNA and makes it accessible to the APC-conjugated BrdU antibody. Total DNA content was stained by 7-AAD for distinction of Sub-G1, G1-phase, S-phase and G2/M-phase. Duplet cells were excluded by FSC-A to FSC-H.

3.3.11 Luminescent growth assay

Cell viability and growth were measured by detection of ATP level using the CellTiter-Glo luminescent assay (Promega). 50µl of cells were seeded out in a white 384-well plate at a density of 1-3x10^5 cells/ml. Cells were incubated for 48h at 37°C. For detection of ATP-levels 14µl CellTiter-Glo reagent was added to each well and incubated for 20min at RT in the dark. Luminescent signal was measured at the Tecan M-1000 multi-well plate reader. Optimal cell density was determined before by Katarzyna Tomska and Marina Lukas.

3.3.12 Compound screen

18 BL cell lines were analyzed by Katarzyna Tomska in a compound screen using 32 substances targeting key signaling pathways of lymphoma (see MD thesis, in preparation). In brief, cell density and incubation time were optimized to achieve logarithmic cell growth. Finally, all cell lines were incubated for 48h with 10 different substance concentrations diluted 1:3 starting from 30µM. As a negative control cells were treated with PBS or 0.1% DMSO corresponding to the final concentration of DMSO for substance dilutions. Cell viability was determined by ATP-levels as described above (3.3.11).

3.4 Molecular biology methods

3.4.1 DNA extraction

Genomic DNA was extracted from 2-5x10^6 cells using the DNeasy Blood&Tissue kit (Qiagen, Hilden, GER) according to the manufacturer´s instructions. In brief, cells were resuspended in lysis buffer, DNA was precipitated with 50% EtOH and bound to the membrane of a spin column. After washing, DNA was eluted from the membrane in pure H_2O and quantified with the Qubit Fluorometer 2.0 using the dsDNA BR DNA kit (Invitrogen, Darmstadt, GER).

3.4.2 Targeted resequencing with 454 technology

For mutation analysis, target sequences in *TP53* and *MYD88* were amplified in two multiplex-PCR reactions using primers that add a universal tag. The reaction mix and PCR program are listed below. PCR products were purified according to the Library Preparation Manual for GS Junior 454 sequencing (Roche, Basel, Switzerland) using 72µl AMPure beads (Invitrogen, Darmstadt, GER), 22.5µl PCR product, 22.5µl H_2O. The mixture was incubated for 10min at RT to let PCR fragments bind to the oligo-nucleotide coated magnetic AMPure beads. The beads were pelleted on a magnet for 5min and washed twice with 70% EtOH. PCR products were eluted from air-dried beads in 10µl H_2O. DNA was quantified using the PicoGreen assay (Invitrogen). Both multiplex-PCR reactions were pooled at equimolar ratios and in a second PCR reaction 454 sequencing adapters and sample-specific multiplex-identifiers were ligated to the PCR products. After AMPure bead purification using 45µl PCR product and 72µl AMPure beads, PCR products were resuspended in 10µl H_2O, quantified in the PicoGreen assay and pooled equimolarly. The sequencing library was diluted to 5x10^5 molecules/µl and mixed with sequencing beads at a ratio of 0.5 molecules/bead. Emulsion PCR (emPCR) and 454 bi-directional sequencing on the GS Junior benchtop sequencer were performed according to the manufacturer´s instructions “emPCR Amplification Method Manual – Lib-A” (March 2012) and

"Sequencing Method Manual" (March 2012) (Roche). Raw sequencing images were processed by the amplicon sequencing pipeline of the GSRunProcessor software (V2.5, Roche) and aligned to the reference sequence in the Amplicon Variant Analyzer software (V2.5, Roche). Variants were annotated according to the COSMIC data base (Sanger Institute).

Mega-PCR	
Reagent	**Volume [µl]**
H_2O	21
10x Buffer	5
dNTPs 10mM each	1
Taq Polymerase	0.5
Primer mix	23
gDNA (5ng/µl)	6
TOTAL	**50**

Mega-PCR		
PCR Step	**Temperature**	**Time [min]**
1	95°C	2:00
2	95°C	0:45
3	57°C	0:45
4	72°C	1:00
5	**GO TO STEP 2**	**30 TIMES**
6	72°C	5:00
7	10°C	**FOREVER**

Titanium-PCR	
Reagent	**Volume [µl]**
H_2O	41.5
10x Buffer	5
dNTPs 10mM each	1
Taq Polymerase	0.5
Titanium fwd+rev primer (10µM)	1
Mega-PCR (5ng/µl)	5
TOTAL	**50**

Titanium-PCR		
PCR Step	**Temperature**	**Time [min]**
1	95°C	2:00
2	95°C	0:45
3	60°C	0:45
4	72°C	1:00
5	**GO TO STEP 2**	**12 TIMES**
6	72°C	5:00
7	10°C	**FOREVER**

3.4.3 Sanger sequencing

Single amplicons were sequenced on the capillary sequencer ABI 3730xl ("Sanger" technology) at GATC Biotech (Constanz, GER). Target sequences were amplified in a PCR reaction according to the layout below, purified using the PCR purification kit (Qiagen, Hilden, GER) and quantified with the nanodrop spectrometer (Peqlab/VWR, Erlangen, GER).

Reagent	Volume [µl]
H_2O	40.5
10x Buffer	5
dNTPs 10mM each	1
Taq Polymerase	0.5
Primer fwd+rev	1
gDNA (5ng/µl)	6
TOTAL	**50**

PCR Step	Temperature	Time [min]
1	95°C	2:00
2	95°C	0:45
3	57°C	0:45
4	72°C	1:00
5	**GO TO STEP 2**	**34 TIMES**
6	72°C	5:00
7	10°C	**FOREVER**

3.4.4 Plasmid cloning

shRNA expression plasmids

shRNA sequences were taken from the DECIPHER human module 1 library (Cellecta Inc. Mountainview, CA, USA) and cloning was performed according to the protocol "Cloning of shRNA Templates into shRNA Expression Vector" (v3a, Cellecta). The sequences contain mismatches in the hairpin of up to 2 nucleotides to promote loading of the leading strand into the RISC complex. Forward and reverse single-stranded oligo-nucleotides were designed according to the schema below consisting of passenger strand, shRNA loop and leading strand. Sequences were flanked by a constant region and 5'-overhangs for restriction enzyme cloning into the pRSI12 vector backbone used for lentiviral expression.

5'-ACCG-G-GCTGG**T**AT**T**GTTGAGAATGAA-GTTAATATTCATAGC-TTCATTCTCAACGATGCCAGC-TTTT-3'

3'- C-CGACCATAACAACTCTTACTT-CAATTATAAGTATCG-AAGTAAGAGTTGCTACGGTCG-AAAA-AAGC-5'

Forward strand

5'-Sticky end-Constant region-Passenger strand-shRNA loop-Leading strand-Constant region-3'

Reverse strand

3'-Const. region-Passenger strand-shRNA loop-Leading strand-Const. region-Sticky end-5'

The empty pRSI12 vector was digested with BsbI restriction enzyme in 1x buffer G for 2h at 37°C. After heat inactivation of the enzyme for 20min at 65°C the vector was purified from a 0.5% preparative agarose gel using the QIAquick Gel Extraction kit (Qiagen, Hilden, GER). Phosphorylated shRNA oligo-nucleotides were ligated into the digested pRSI12 vector. The ligation mix was incubated for 30min on ice with 1µl ultra-competent XL10 Gold *E.coli* cells. Cells were heat-shocked at 42°C for 30sec, kept on ice for 2min and incubated with S.O.C medium for 1h at 37°C while shaking. Cells were plated on LB-agar containing 100µg/ml ampicillin and grown for 12h at 37°C. Insertion of shRNA sequence was tested in a PCR reaction (see template below) from single *E.coli* colonies. The same colonies were used to inoculate LB medium containing ampicillin to expanded cells for plasmid purification using either the GeneMatrix Plasmid MiniPrep kit (EURx, Gdansk, PL) or the EndoFree Plasmid Max kit (Qiagen). Plasmids were sent for sequencing at GATC Biotech using the pRSI9/pRSI12 sequencing primer (CAAGGCTGTTAGAGAGATAATTGGAA). *E.coli* strains were preserved in glycerol solution and stored at -80°C.

PCR Mix	Vol. in µl
H_2O	16.4
10x Buffer	2
dNTPs 10mM each	0.4
Taq Polymerase	0.4
pRSI12-Colony-PCR-Primer mix (5 µM)	0.8
TOTAL	**20**

PCR Step	Temperature	Time in min.
1	94°C	3:00
2	94°C	0:20
3	60°C	0:20
4	72°C	0:20
5	**GO TO 2**	**30 TIMES**
6	72°C	2:00
7	10°C	**FOREVER**

sgRNA expression plasmids

sgRNA sequences were designed according to Shalem, Zhang *et al*., (Science, 2014). Oligonucleotides contained 20bp target sequence (adjacent to "NGG" PAM sequence on genomic DNA) and 5'-overhangs for restriction enzyme cloning. The 5'-end should start with a G.

```
forward 5'-CACCG-20bp target sequence     -3'

reverse 3'-    C-20bp target sequence-CAAA-5'
```

Vector backbone pLentiCRISPRv2 was digested with restriction enzyme BsmBI in FastDigest Buffer. Vector purification and sgRNA ligation was performed as described above for shRNAs. Sequencing was performed by GATC on a capillary sequencer using GTACAAAATACGTGACG sequencing primer.

3.4.5 RNA extraction

Total RNA was extracted from 2-5x10^6 cells using the RNeasy kit (Qiagen, Hilden, GER) according to the manufacturer´s protocol. The cells were washed in PBS, resuspended in lysis buffer and homogenisized through QiaShredder spin columns. RNA was precipitated from the lysate by 35% EtOH and RNA was bound to the membrane of a spin column. After washing, RNA was treated with DNase I for 15min at RT, washed and eluted in 30µl RNase-free H_2O. RNA was quantified using the nanodrop spectrometer or the Qubit fluorometer.

3.4.6 Reverse transcription quantitative PCR (RT-qPCR)

Primers for qPCR were either designed (18-22bp, target region: ~100bp, exon-spanning) or taken from the RT primer bank (https://pga.mgh.harvard.edu/primerbank/). Primer efficiency was tested by RNA dilution series (maximal 30ng RNA, 4 times 1:10 dilutions). RT-qPCR was performed using the QuantiFast kit (Qiagen, Hilden, GER) according to the manufacturer´s protocol. 3-9ng of RNA in 3µl were added to 7µl of reaction mix containing forward and reverse primer (5µM each), enzymes and reagents for reverse transcription and qPCR amplification. qPCR was measured in white 96-well plates on the Cobas® z480 Analyzer (Roche, Basel, CH) using the program shown below. A primer melting curve was recorded to ensure specific target gene amplification.

Step	Cycles	Analysis Mode	Temp [°C]	Acquisition Mode	Time	Ramp Rate	Acquisition (per °C)
Reverse Transcription	1	None	50	None	10min	4.4	
Pre-incubation	1	None	95	None	5min	4.4	
Amplification	40	Quantify	95	None	10sec	4.4	
			60	Single	30sec	2.2	
Melting Curve	1	Melting Curve	95	None	5sec	4.4	
			65	None	1min	2.2	
			97	Continuous		0.11	5
Cooling	1	None	40	None	30sec	2.2	

3.4.7 RNA sequencing

500 ng of total RNA were submitted to the Genomics and Proteomics Core Facility (GPCF) of the DKFZ. RNA quality was tested on a Bioanalyzer system (Agilent Technologies, Böblingen, GER) and quantified by Qubit using the RNA HS Assay Kit (Thermo Fisher Scientific, Waltham, USA). Single-read 50bp sequencing was performed on the HiSeq2000 sequencer (Illumina, San Diego, USA). Analysis of RNA sequencing data was performed by Zhiquin Huang and Marc Zapatka (DKFZ, Division of Molecular Genetics) as follows: RNA sequences were aligned to the hg19 human reference genome using the STAR alignment tool. HTSeq-count was used to calculate gene-level count and RPKM with annotation GENCODE version 19 GTF.

3.4.8 Gene expression array

For gene expression analysis 500ng total RNA were submitted to the DKFZ GPCF for analysis on the Illumina BeadChip® HumanHT-12-v4 containing >47,000 probes for 31,000 annotated human genes. Normalized relative expression values were provided by the GPCF.

3.4.9 Immunoblot analysis

For protein expression analysis cell lysates were prepared with RIPA buffer (150mM NaCl, 0.5% Na-Desoxycholate, 1% NP-40, 0.1% SDS, 50mM Tris pH 7.5; Merck/Millipore). Protein quantification was performed using the Pierce BCA Protein Assay kit (Thermo Fisher Scientific), a colorimetric assay. In brief, the cell lysate was incubated with BCA solution for 30min at 37°C. Protein reduces Cu^{2+} to Cu^{+} ions that react with bicinchoninic acid and form a purple substrate. Light absorption at 562nm is measured with the Tecan plate reader and the protein concentration was calculated based on a standard curve. For immunoblotting 40µg protein containing 1x Laemmli buffer (4% SDS, 20% glycerol, 10% 2-mercaptoethanol, 0.004% bromphenol blue and 0.125 M Tris HCl, pH~6.8; Sigma-Aldrich) were separated by size on pre-casted TGX gradient gels (4-15%) and transferred to a low-fluorescent PVDF membrane using the Trans-Blot Turbo Transfer system (Biorad). The membrane was incubated for at least 2h in TBS-T (137mM NaCl, 2.7mM KCl, 19mM Tris pH 7.4, 0.1% Tween 20) with 5% skim milk to reduce unspecific antibody binding. Primary antibodies were diluted in TBS-T with 5% BSA to increase specificity of binding and incubated over night at 4°C while shaking. Fluorochrome-conjugated DyLight® (CST, Danvers, MA, USA) secondary antibody targeting mouse or rabbit proteins were used at a 1:15,000 dilution. Protein bands were detected using the Odyssey fluorescent scanner (Li-cor, Lincoln, NE, USA) and quantified using the ImageStudio software provided by Li-cor.

3.5 RNAi screen

3.5.1 shRNA library

The DECIPHER™ Human Module 1 shRNA library (#DHPAC-M1-P) was obtained from Cellecta Inc. (Mountainview, CA, USA). It comprises 27,500 pooled shRNA sequences encoded on barcoded pRSI12 vector containing a puromycin resistance gene and red fluorescent protein (RFP) gene. The shRNAs target 5,045 genes in key signaling pathways. The manufacturer provided sequencing results for the plasmid library.

3.5.2 Lentiviral packaging of shRNA library

Lentiviral packaging of the shRNA library was performed according to the Cellecta protocol "Pooled Lentiviral shRNA Libraries" (v5e, 9/6/13). HEK293T/17 cells were plated on 10x 15cm cell culture dishes at $8x10^4$ cells/cm^2 and grown for 24h to reach ~80% confluency. The transfection mix consisting of 300µg packaging plasmid mix (psMD2.G:psPAX2 , 1:2), 60µg of plasmid library DNA, 600µl PLUS reagent and 12ml Opti-MEM was incubated at room temperature for 15min. 900µl lipofectamine in 12ml Opti-MEM were added to the transfection mix and incubated at room temperature for 15min. The final mixture was distributed equally among the plates. After 24h of incubation the supernatant was replaced with fresh medium containing 1U/ml DNase I and 4nM $MgCl_2$ and cells were grown for 24h. The transfection efficiency was estimated based on RFP-expression in fluorescent microscopy. The supernatant from all plates was combined and filtered through a 0.45µm filter and stored in aliquots at -80°C.

3.5.3 Titration of lentiviral supernatant

The lentiviral supernatant of the packaged pRSI12 shRNA library was titrated on BL cell lines selected for the screen to determine the amount of virus needed for ~50% (MOI=0.7) infection rates. Cells were seeded out at $5x10^5$ cells/ml, incubated for 3 days in the presence of increasing volumes of lentiviral supernatant and RFP was measured in flow cytometry using the yellow-green laser (excitation at 561nm) of the LSR Fortessa™ (BD Biosciences, San Jose, CA, USA).

3.5.4 RNAi screen in 8 BL cell lines

Cell lines were transduced with the shRNA library at ~50% infection rate. Every shRNA was infected 80 times ($5.4x10^6$ cells) in three replicates. Cells were cultured for 2 days and ⅓ of the culture was harvested as a baseline. The remaining culture was treated with puromycin for 48h at the minimal lethal dose. After renewal of the medium cells were grown in two separate replicates for 10 days in logarithmic growth phase (cell density $4x10^5$ cells/ml - $1.5x10^6$ cells/ml). During sampling >1,000-fold representation of shRNAs was maintained. Harvested cells were washed with PBS, snap-frozen in liquid nitrogen and stored at -80°C. For extraction of genomic DNA, cells were resuspended in P1 buffer (Qiagen, Hilden, GER) containing 100µg/ml RNase A and 0.5% SDS and incubated for 5min at RT. Genomic DNA was sheared into 10-100kbp fragments by sonication (6 cycles, full power, 10 sec pulse). DNA was extracted with phenol/chloroform (pH 8.0), precipitated with isopropanol in the presence of 3M sodium acetate and washed with 70% EtOH. The air-dried DNA pellet was eluted in water and quantified using Qubit fluorometer (Invitrogen, Darmstadt, GER). shRNA vector barcodes were amplified from 200µg genomic DNA (or the maximum available amount) in 4x 50µl PCR reactions using FwdHTS and RevHTS1 primer.

Reagent	Volume [µl]
H_2O	15.5
10x Titanium Taq buffer	5
Genomic DNA (1µg/µl)	25
FwdHTS (10µM)	1.5
RevHTS1 (10µM)	1.5
dNTP mix (10mM each)	1
Titanium Taq	0.5

	Temperature [°C]	Time [sec]
1	94	180
2	94	30
3	65	10
4	72	20
	Go to 2	16 cycles
5	68	120
6	10	store

In a second, nested PCR target sequences were amplified with optimized number of cycles (to avoid over-cycling) and sample-specific multiplex identifier sequences, that allow pooling of multiple samples on one sequencing lane, were added by the reverse RevGex primer.

Reagent	Volume [µl]
H_2O	37.5
10x Titanium Taq buffer	5
1st round PCR product	1
FwdGex (10µM)	2.5
RevGex (10µM)	2.5
dNTP mix (10mM each)	1
Titanium Taq	0.5

	Temperature [°C]	Time [sec]
1	94	180
2	94	30
3	65	10
4	72	20
	Go to 2	12-18 cycles
5	68	120
6	10	store

PCR products of 255bp were analyzed on a 2.5% agarose gel, purified using the QIA quick PCR purification kit (Qiagen) and quantified with nanodrop (Peqlab, Erlangen, GER).

3.5.5 Sequencing of shRNA vector barcodes

Six samples each were pooled at equimolar ratios and submitted at 10nM to the DKFZ GPCF for 50bp single-end sequencing on one lane of the Illumina HiSeq2000 (Table 1). The GexSeqS sequencing primer binds directly in front of the 18nt shRNA barcode and is added first to the sequencing reaction (Figure 9).

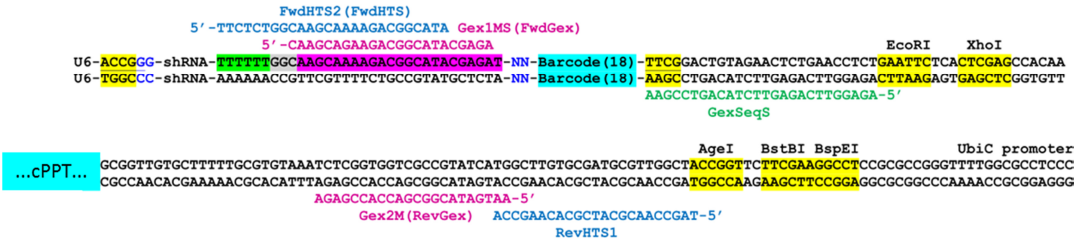

Figure 9: Primers for sequencing of the shRNA library
Part of the pRSI12 vector sequence with indicated shRNA barcode sequence, amplification (1st round PCR: blue; 2nd round PCR: pink) and sequencing (green) primers.

In order to avoid that the sequencer loses the focus "random" sequences from PhiX virus were added to the library to dilute the signal of the vector backbone (60% library : 40% PhiX). The indexing sequences were read in a second sequencing reaction replacing the Gex2M (sequencing primer for uniplex samples) with the GexSeqIND.

Table 1: Indexed shRNA screening samples

Cell line	Time point	# of cells	DNA [µg]	Lane	Index	Coverage
BJAB	Day 2	$3.7x10^7$	122	1	ATGC	27,050,695
	Day 14_rep1	$1.5x10^8$	970		GACT	16,556,211
	Day 14_rep2	$1.5x10^8$	714		TCAG	7,184,670
BL60	Day 2	$3.0x10^7$	62	1	CGTA	34,250,997
	Day 14_rep1	$2.5x10^8$	1650		AGCG	12,908,933
	Day 14_rep2	$2.5x10^8$	1920		GATG	14,104,821
Raji	Day 2	$2.0x10^7$	116	2	ATGC	18,474,328
	Day 14_rep1	$2.3x10^8$	1420		GACT	20,090,539
	Day 14_rep2	$2.3x10^8$	1580		TCAG	30,158,731
Ramos	Day 2	$4.3x10^7$	123	2	CGTA	20,471,635
	Day 14_rep1	$3.2x10^8$	1080		AGCG	13,286,388
	Day 14_rep2	$3.2x10^8$	1120		GATG	17,430,929
BL-2	Day 2	$3.1x10^7$	50	3	ATGC	23,851,748
	Day 14_rep1	$3.2x10^8$	915		GACT	8,080,939
	Day 14_rep2	$3.2x10^8$	1479		TCAG	22,043,318
LY47	Day 2	$1.1x10^7$	30	3	CGTA	25,713,683
	Day 14_rep1	$2.3x10^8$	415		AGCG	7,416,915
	Day 14_rep2	$2.3x10^8$	418		GATG	5,452,051
Salina	Day 2	$1.5x10^7$	52	4	ATGC	25,011,187
	Day 14_rep1	$4.4x10^8$	1275		GACT	10,023,296
	Day 14_rep2	$4.4x10^8$	1856		TCAG	23,214,458
Seraphine	Day 2	$1.1x10^7$	37	4	CGTA	33,684,767
	Day 14_rep1	$1.7x10^8$	668		AGCG	13,147,547
	Day 14_rep2	$1.7x10^8$	538		GATG	20,649,830

3.5.6 RNAi data analysis

Barcode identification. Multiplexed samples were deconvoluted by the DKFZ GPCF based on the index sequence. Raw sequencing reads were trimmed to 20bp reads using the python script “Gzim_Trim”. Barcode sequences were identified using the DECIPHER bar code deconvoluter software (version 2010-10-05) and the library reference file (BLIB). Settings of the software were changed to “Allow 1 error” and “Correct N symbol”. The 2bp module identifier (AT for module 1) was not needed, as we did not pool different modules. The software created a tab delimited file containing the counts for all identified barcodes.

Normalization. To account for differences in the coverage of the samples, relative shRNA counts were calculated by dividing of every raw read count with the mean read count of the same sample. As replicates on day 14 were highly correlated, the mean of both replicates was calculated for every shRNA. Relative shRNA counts on day 14 were divided by relative counts on day 2 to calculate fold-changes (FC) for each cell line. After logarithmic transformation with the basis 2 all values were normalized across cell lines by peak median absolute deviation (PMAD) using the GenePattern module “NormLines” provided by the Broad Institute. For each cell line, every shRNA value is divided by the modeled peak value and divided by the median absolute deviation.

Class comparison. Analysis of differentially expressed shRNAs was performed using GENE-E software with RIGER extension provided by the Broad Institute. The table of PMAD-normalized logarithmic fold-changes was saved as a .gct format (tab delimited file containing two header rows: “#1.2” in A1, “# of data columns” in B1, “# of data rows” in B2) and opened in GENE-E.

TP53 status of cell lines was added using the .cls class definition file and scores for differential shRNA representation were calculated using RIGER algorithm. shRNAs were scored and ranked for their ability to distinguish between two classes using „Weight of evidence" (WoE) statistics. WoE scores for shRNAs targeting the same gene were combined into gene scores and ranks using Kolmogorov-Smirnov (KS) statistics.

edgeR. Gene depletion scores were calculated using the edgeR package and Fisher z-transformation as described previously[131,132]. In brief, raw sequencing reads for all samples were combined. The pipeline requires replicate measurements that were not available for day 2 samples. However, as shRNA representation on day 2 was highly correlated within all cell lines, an artificial replicate for each cell line was calculated based on the mean shRNA count for the remaining cell lines. shRNAs were sorted by abundance on day 2 (mean over all cell lines) and the top 5% were removed to avoid strong outliers when the fold-changes were calculated. Control shRNAs that were represented in triplicates were removed and missing values were replaced by 10. For every cell line, the edgeR package was used to normalize every sample for library size, calculate the dispersion of the data and fit a negative binomial model. P-values for shRNA distribution were calculated by carrying out a likelihood ratio test and adjusted for multiplicity of testing by FDR method. P-values for shRNAs targeting the same gene were combined into gene depletion scores using weighted z-transformation (wZ-scores).

Removal of overlapping shRNAs. A script for identification of shRNAs with overlapping target region was generated by Agnes Hotz-Wagenblatt (DKFZ) shRNA sequences were mapped against the human transcriptome using Tophat2 algorithm (Ensembl v75).

To identify candidate genes we applied the following criteria:

(1) Genes with significantly lower shRNA counts in p53wt by KS score (p-value < 0.05): Using the KS gene scores as described above we identified 324 genes that had significantly lower shRNA counts in p53wt cell lines.

(2) Genes with significantly lower shRNA counts in p53wt by 2nd best shRNA (p-value < 0.05): Following a similar approach as for the calculation of KS gene scores, all shRNAs were ranked for their differential representation. Instead of calculating a combined score over all shRNAs genes were ranked by the second strongest shRNA that discriminates between the groups. This step selects genes with at least two strong differential shRNAs. 150 genes showed significantly lower shRNA counts using both ranking methods from step (1) and step (2).

(3) Genes essential in p53wt (median wZ-score < -0.5): We further classified genes with lower shRNA counts in p53wt by their wZ-score into genes depleted in p53wt or genes enriched in p53mut. For example, the pro-apoptotic gene BAD was on rank 21 by KS score, but was not essential in p53wt by wZ-score (median wZ = -0.15). Instead, shRNAs targeting BAD were enriched in p53mut cell lines (median wZ = 1.37). In comparison, the gene MDM4 which was the highest ranking gene by KS score was essential in p53wt (median wZ = -1.79), but not in

p53mut (median wZ = 0.29). To select for essential genes in p53wt, we set the cut-off to a median wZ-score of -0.5 and identified 59 genes fulfilling this criteria.

(4) Filtering for expressed genes: We further filtered out genes that were not found to be expressed in published RNA sequencing data of three BL cell lines, including the Raji cell line[133]. 46 out of 59 genes (78%) were expressed indicating low noise in the data.

(5) Removal of shRNAs with overlapping target region: Some of the shRNAs have overlapping target regions. These shRNAs may exert similar effects resulting into biased gene scores. We mapped all shRNAs against the genome and calculated the number of base pairs that overlap within the same gene (see 3.5.6). Four genes were removed from the list of candidates because the gene score was influenced by overlapping shRNAs.

(6) Significant difference of gene depletion score ($p<0.05$): We further prioritized 12 genes that show a significant difference in their wZ-score meaning that they are significantly stronger depleted across all four p53wt cell lines.

(7) Common essential genes (median wZ in p53mut<-0.5): Four genes that showed a median wZ-score below -0.5 in the p53mut cell lines were categorized as common essential genes.

# of genes in p53wt	Filtering criteria	# of genes in p53mut
324	Significant by KS score	**269**
150	Significant by 2nd best shRNA	**132**
59	Depleted in this class	**52**
46	Expressed by RNA sequencing	**46**
42	After removal of biased shRNAs	**44**
12	Significant difference in gene wZ-score	**19**
4	Generally toxic	**16**

4 Results

For the systematic identification of genes essential in Burkitt lymphomagenesis, we analyzed associations of recurrent genetic alterations in primary BL samples from the MMML consortium and integrated our findings with a functional genomics screen for p53-specific vulnerabilities in BL cell lines.

4.1 Pattern of recurrent mutations and CNVs in BL

To improve our understanding of failsafe mechanisms in MYC-driven lymphoma we systematically analyzed the pattern of recurrent genomic alterations in 59 primary BL samples (MMML consortium).

The pattern of *MYC* and *TP53* mutations in BL patients is shown in Figure 10. The *MYC* gene was mutated in 59% of BL patients (n=37) and carried multiple mutations as a result of somatic hypermutation (average number of mutations in conserved regions: 1.7). *MYC* box I mutations increase oncogenic potential by impaired induction of pro-apoptotic Bim, presumably as an alternative to p53 inactivation[65]. The conserved *MYC* box I residues P57 and T58 were affected in 17% of patients (n=11). *TP53* mutations were frequently observed (n=27, 43%) and mainly comprised missense mutations in the DNA binding domain that lead to a loss of its tumor suppressor function. Notably, *MYC* box I mutations occurred independent of *TP53* mutations.

Figure 10: *TP53* and *MYC* box I mutations in Burkitt lymphoma patients.
Incidence and co-occurrence of *TP53* and *MYC* box I mutation in 59 BL patients (MMML consortium). Each column represents one patient and the mutation status is indicated.

To study their clinical impact we analyzed correlations between *TP53* mutation and clinical parameters. Patients carrying *TP53* mutations displayed with higher clinical stage (p=0.017) and more extranodal involvement (p=0.016) (Figure 11A). However, we did not observe a significant difference in overall survival of *TP53* mutant and wild type patients (Figure 11B).

A

		p53mut	p53wt	p-value
Stage	I/II	6 (21%)	15 (39%)	0.017
	III/IV	11 (38%)	4 (11%)	
Nodal/ Extranodal	E	0 (0%)	6 (16%)	0.016
	N	4 (14%)	5 (13%)	
	NE	11 (38%)	5 (13%)	

B

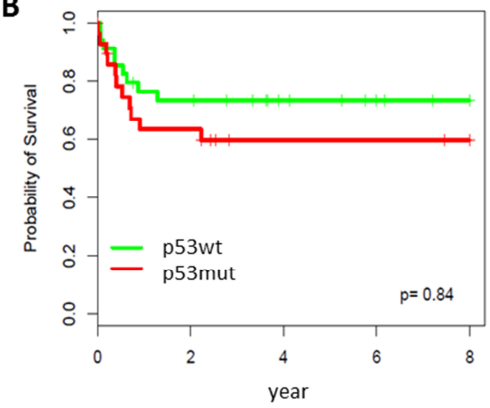

Figure 11: Clinical impact of *TP53* mutations in Burkitt lymphoma
(A) Clinical parameters were correlated to the *TP53* mutation status. The table shows significantly correlated parameters (p<0.05). E=extranodal; N= nodal; NE=nodal and extranodel
(B) Overall survival of 34 p53wt and 29 p53mut BL patients.

To find alternative mechanisms that may contribute to failsafe checkpoint inactivation in BL, we compared recurrent copy number variations (CNVs) in 38 p53 wild-type (p53wt) and 29 p53 mutant (p53mut) BL samples (Figure 12A). p53mut samples showed a trend towards a more complex karyotype compared to p53wt BL (p=0.107). p53 mutations co-occurred with deletion of the p53 locus chr17p13 (5/6 patients, p=0.075). In addition, we observed an unexpected overrepresentation of chromosome 1q32 gain in p53wt BL (p53mut=24%, p53wt=42%, p=0.055). The gain on chr1q was the second most common CNV besides of the *MYC* translocation, confirming previous findings[33,48]. An association of chr1q gain with p53 status in BL has not been described before and suggests a novel oncogenic mechanism exclusive to p53 mutation.

A detailed analysis of the architecture of chr1q CNV in p53wt BL showed partial chromosomal gains in 37%, while in 5% the complete chr1q arm was affected. Minimally gained regions (MGR) comprised 1q21.1-q23.3, 1q24-q25 and 1q32.1 (Figure 12B *left*). Chr1q amplifications affect large regions and the pathogenic role of single deregulated genes remains elusive. We used RNA expression analysis to query potential genes involved in chr1q gain. Figure 12C lists cancer consensus genes that were located within MGR and found to be upregulated in patients with chr1q gain.The association of chr1q gain with p53 mutation status was specific for BL and not observed in diffuse large B-cell lymphoma (DLBCL), where amplifications on chr1q were equally distributed in p53wt and p53mut patients (p53mut=22%, p53wt=23%) and mostly affected the whole arm of the chromosome rather than partial trisomies (B, *right*).

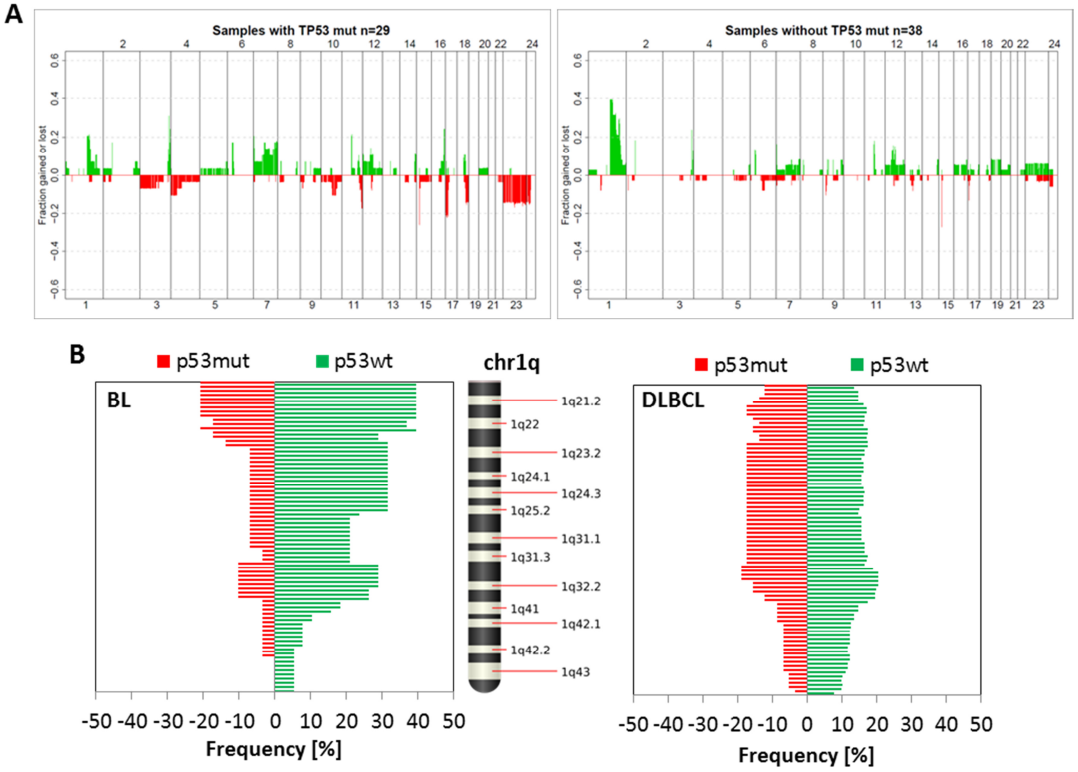

C

Cancer consensus gene	Genomic region	Chromosomal band	p53wt	p53mut	p-value
BCL9; FCRL4; ARNT; MUC1; MCL-1; CKS1B; MLLT11; SDHC; NTRK1; PRCC; LMNA	1:147611837-154183119	1q21-q22	15 (39%)	6 (21%)	0.101
PRRX1; ABL2; TPR	1:170664220-186375028	1q24-q25	12 (32%)	2 (7%)	0.014
PTPRC	1:198639275-198756181	1q31-q32	8 (21%)	1 (3%)	0.036
ELK4; MDM4; SLC45A3	1:205616546-205664656	1q32	11 (30%)	3 (10%)	0.056

Figure 12: Differential copy number variations in p53wt Burkitt lymphoma.
(A) Copy number variations (CNVs) determined by comparative genome hybridization array (CGHa) in 29 p53mut and 38 p53wt BL. Gains (positive values) are shown in green and losses (negative values) are shown in red. **(B)** Fraction of gains on chromosome 1q at a higher resolution in p53mut (red) and p53wt (green) patients. *left*: BL; *right*: DLBCL. **(C)** List of cancer consensus genes located within minimally gained regions of p53wt BL that show a gene-dosage effect.

4.2 RNAi screen identifies p53-specific vulnerabilities

4.2.1 Selection of cell line models

To study specific dependences in BL with wild-type p53 we selected cell line models representing p53wt and p53mut patients. The majority of BL cell lines harbors p53 mutations (80%). We obtained 6 p53wt cell lines and selected 8 commonly used p53mut cell lines for further characterization. The mutation status was confirmed by targeted resequencing of exons 4-10. Four out of six p53wt cell lines could be efficiently infected with lentiviral vectors and were chosen for the screen (BL-2, LY47, Salina, Seraphine). According to the published cytogenetic profile all of them harbor a gain on chr1q[47]. Seraphine carries a duplication of the whole chr1q-arm. BL-2 and Salina show a partial duplication of chr1q21.2-q31.3 and LY47 of the distal chr1q43-q44 region. All p53mut cell lines could be infected with lentiviral vectors, therefore we chose four cell lines that differ in their p53 mutation and have normal chr1q copy number (BJAB, BL60, Raji, Ramos), reflecting the karyotype of BL patients. All cell line characteristics are listed in Table 2.

Table 2: Genetic characteristics of cell lines used in the RNAi screen
WT = wild-type; MUT = mutant; EBV = Epstein-Barr-Virus; +(III) = EBV latency III phase; +(Wp) = EBV Wp-restricted latency III

Name	*TP53* status	*MYC* box I status	Chr1q gain	EBV status	t(MYC)
BJAB	p.H193R	WT	Normal	-	t(8;14)
BL60	p.R248W	WT	Normal	+ (III)	FISH+
Raji	p.R213Q; p.Y234H	MUT (boxI)	Normal	+ (III)	t(8;14)
Ramos	p.I254D	WT	Normal	-	t(8;14)
BL-2	WT	MUT (boxI)	+1q21.1q31.3	-	t(8;22)
LY47	WT	WT	+1q43q44	+ (III)	t(8;22)
Salina	WT	WT	+1q21.2q31.3	+ (Wp)	t(8;14)
Seraphine	WT	WT	+1q21.1qter	+ (III)	t(8;14)

To further characterize the cell lines, we investigated additional features which could impact the screen results. The *MYC* translocation characteristic for Burkitt lymphoma was reported in seven cell lines and in BL60 we confirmed its presence by FISH analysis. *MYC* box I mutations were present in one cell line of each group. Many BL cell lines are naturally infected and transformed by EBV. This has to be taken into consideration as viral proteins expressed in the latency III phase of the virus (like EBNA-3C and LMP-2A) deactivate the p53 pathway and promote survival[134,135]. In the group of p53wt cell lines BL-2 was EBV-negative while the remaining three cell lines were EBV-positive and expressed latency III genes. LY47 and Seraphine expressed genes from the Cp-promoter leading to a single transcript encoding all genes, while Salina expressed a shorter transcript from the alternative Wp-promoter containing genes of the restricted latency III phase. Two of the p53mut cell lines, BL60 and Raji, were positive for EBV and expressed full latency III genes, whereas Ramos and BJAB were EBV-negative.

In summary, we ensured an equal distribution of MYC box I mutations and EBV infection between p53wt and p53mut cell lines to avoid biases in group comparison analysis.

4.2.2 shRNA screening layout

To identify genes that are essential in p53wt, but not in p53mut BL cell lines, we performed a loss-of-function RNAi screen in the selected cell lines (Figure 13). We used a pooled shRNA library for systematic downregulation of 5,045 genes in key signaling pathways with five to six independent silencing trigger per gene. After lentiviral delivery, the shRNAs integrate into the genome, are stably expressed and target a complementary mRNA for degradation. The shRNA representation was determined on day 2 and on day 14 after transduction by high-throughput sequencing of sequence-optimized vector barcodes. Silencing trigger that target essential genes were lost over time. While common essential genes showed shRNA depletion in all cell lines p53-specific essential genes were only lost within the group of p53wt or p53mut cell lines, respectively.

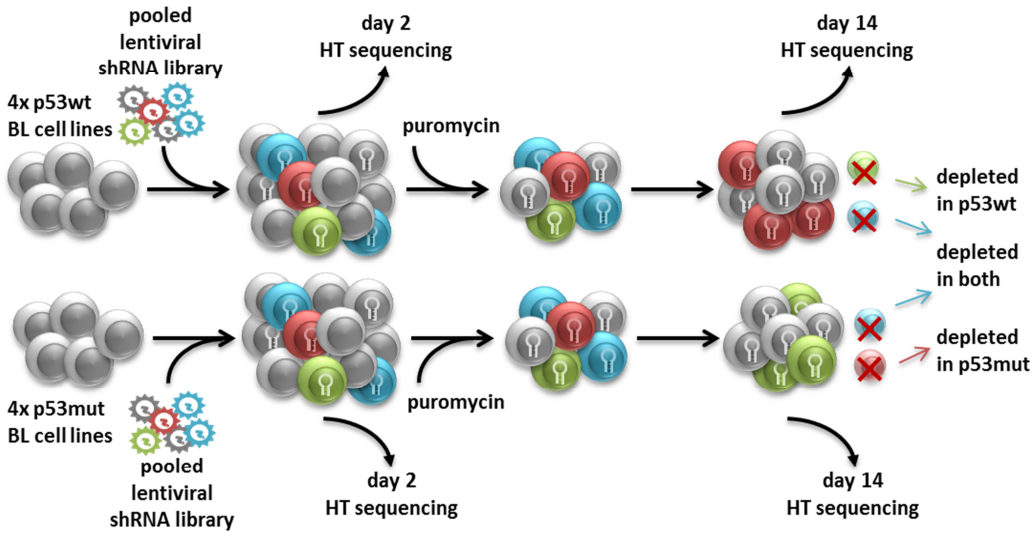

Figure 13: Scheme of the shRNA screen for identification of p53-specific vulnerabilities.
4 p53wt and 4 p53mut BL cell lines were transduced in triplicates with a pooled shRNA library using lentiviral transfer. On day 2 one replicate was harvested as baseline control. After enrichment of infected cells with puromycin the cell pool was divided into half for technical replicates. Both replicates were harvested on day 14 post-infection. shRNA representation on day 2 and day 14 was determined by high-throughput sequencing of vector barcodes. shRNAs targeting essential genes (blue) were depleted from the pool in both cell line groups, while cells infected with shRNAs against non-essential genes (grey) were propagating normally. shRNAs that are depleted only from the group of p53mut (red) or p53wt (green) cell lines identify p53-specific essential genes.

4.2.3 Establishment of the RNAi screen

The shRNA plasmid library was packaged into lentiviral particles using HEK293T/17 cells and the efficiency of packaging was monitored by RFP-expression in fluorescent microscopy (Figure 14A). The lentiviral supernatant was titrated on the target cells to determine the amount needed to infect ~50% of cells. Using low virus titers in the screen reduced the number of cells infected with multiple shRNAs. Infection rates were measured by flow cytometric analysis of RFP signal on day 3 post-infection (Figure 14B). First, 20µl, 50µl and 100µl of the lentiviral supernatant were added to BL-2 and Raji (Figure 14C, *left*). Optimal infection rate was obtained for lower volumes of added viral supernatant and similar volumes were used for titration on the six remaining cell lines (Figure 14C, *right*). For all cell lines, the rate of infected cells increased linearly with the volume of added virus, which allowed determining the optimal condition for each cell line. To test cytotoxic effects of the shRNA library the ratio of RFP+/shRNA+ and RFP-/shRNA- cells was monitored over time. RFP was stably expressed in cells infected with a non-targeting shRNA (shNT), while RFP-signal was depleted in cells infected with the shRNA library (Figure 14D). This suggests that shRNAs targeting essential genes were depleted during this time course and we chose 14 days of incubation for the screen as this resulted into a drop of RFP-signal of at least 50%. We did not observe an increase in apoptosis by Annexin-V staining (data not shown). Apoptosis is a fast process and as the expression of shRNAs was not synchronized in the cells we cannot exclude that our method was not sensitive enough to detect an increase in apoptotic cells.

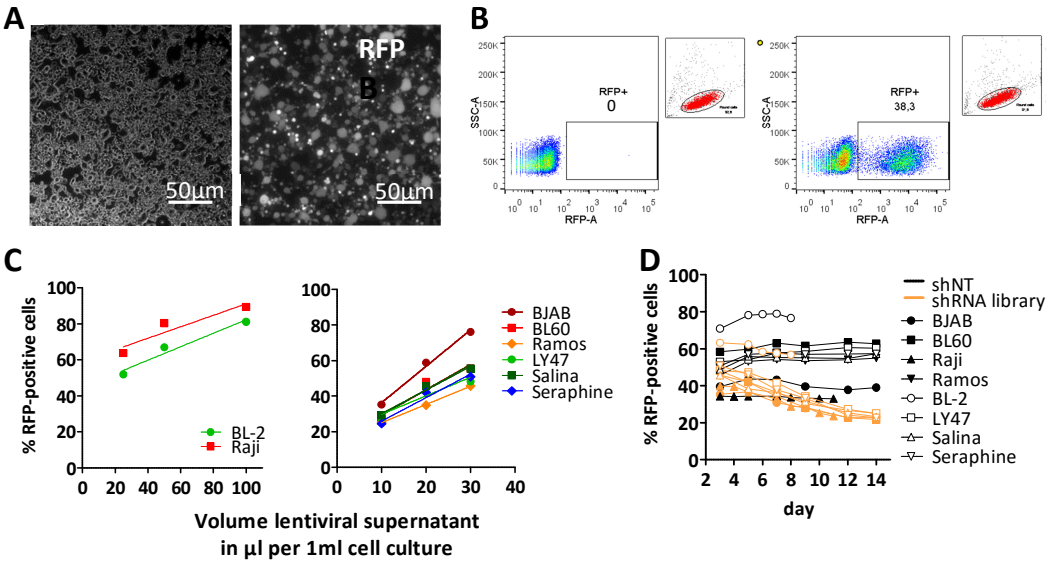

Figure 14: Establishment of the RNAi screen
(A) HEK293T/17 cells in light microscopy (*left*) and fluorescent microscopy (yellow/green filter; *right*) during lentiviral packaging of the shRNA library; scale: 50µm. **(B)** Exemplary analysis of RFP signal in flow cytometry (*left*: uninfected; *right*: infected). Dead cells were excluded by FSC/SSC. **(C)** Titration of lentiviral supernatant on BL cell lines. RFP signal was measured on day 3 post transduction. **(D)** Time course for RFP-signal depletion in cell lines infected with a non-targeting shRNA (shNT, black) or the shRNA library (orange).

4.2.4 RNAi screen

The RNAi screen was performed according to the layout described in section 4.2.2. The infection rates were determined in a small sub-culture that was not treated with puromycin. For all cell lines we achieved the desired infection rate between 40% and 60% (Figure 15A, *left*). Starting from day 5 post-infection, the RFP-signal dropped steadily in all cell lines as observed previously (Figure 15A, *right*). Puromycin treatment efficiently enriched infected cells to 88-99% (Figure 15A, *right*). Cell lines with >90% enriched cells stably expressed RFP over 14 days. Three cell lines with <90% enriched cells (LY47, Seraphine and Raji) showed a drop of RFP-signal to ~70% of the total population. Genomic DNA was extracted from cells on day 2 and day 14 (2 replicates) after infection and unique barcode sequences corresponding to shRNA vectors were amplified in a two-step PCR reaction. We pooled six samples for sequencing on one lane of the HiSeq2000 (Illumina, San Diego, CA, USA) and controlled the quality of pooled PCR amplicons on a Bioanalyzer (Agilent Technologies, Böblingen, GER) (Figure 15B). The analysis showed a single PCR product of the expected size.

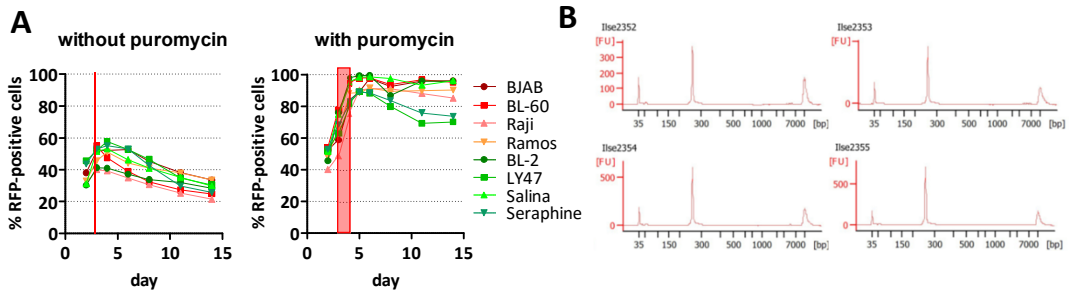

Figure 15: Infection rates and library preparation
(A) RFP-signal was determined over 14 days in a subculture without puromycin and in the main bulk of the culture treated with puromycin for 48h (red area) to enrich for infected cells. The infection rate was determined by the fraction of RFP-positive cells on day 3 post-infection without puromycin (red line). **(B)** Electrophoresis of amplified and indexed barcode sequences on the Bioanalyzer (Agilent Technologies, Böblingen, GER). The PCR products have a size of 255bp. The lower and the upper peak are DNA markers used for calibration.

4.2.5 Visualization of shRNA screening results

To assess the quality of obtained screen results we first compared the representation of shRNAs within the plasmid library (as provided by the manufacturer) with the shRNA representation on day 2 post-transduction in all eight cell lines. All shRNAs were detected and highly correlated with the plasmid library (R^2>0.8) (Figure 16A). The correlation between cell lines was even stronger (R^2>0.9), suggesting that lentiviral packaging and batch effects of the plasmid library have a greater impact than lentiviral infection (Figure 16B). The distribution of shRNA counts resembled a Gaussian distribution (Figure 16C) confirming that no major toxicity effects were visible on day 2.

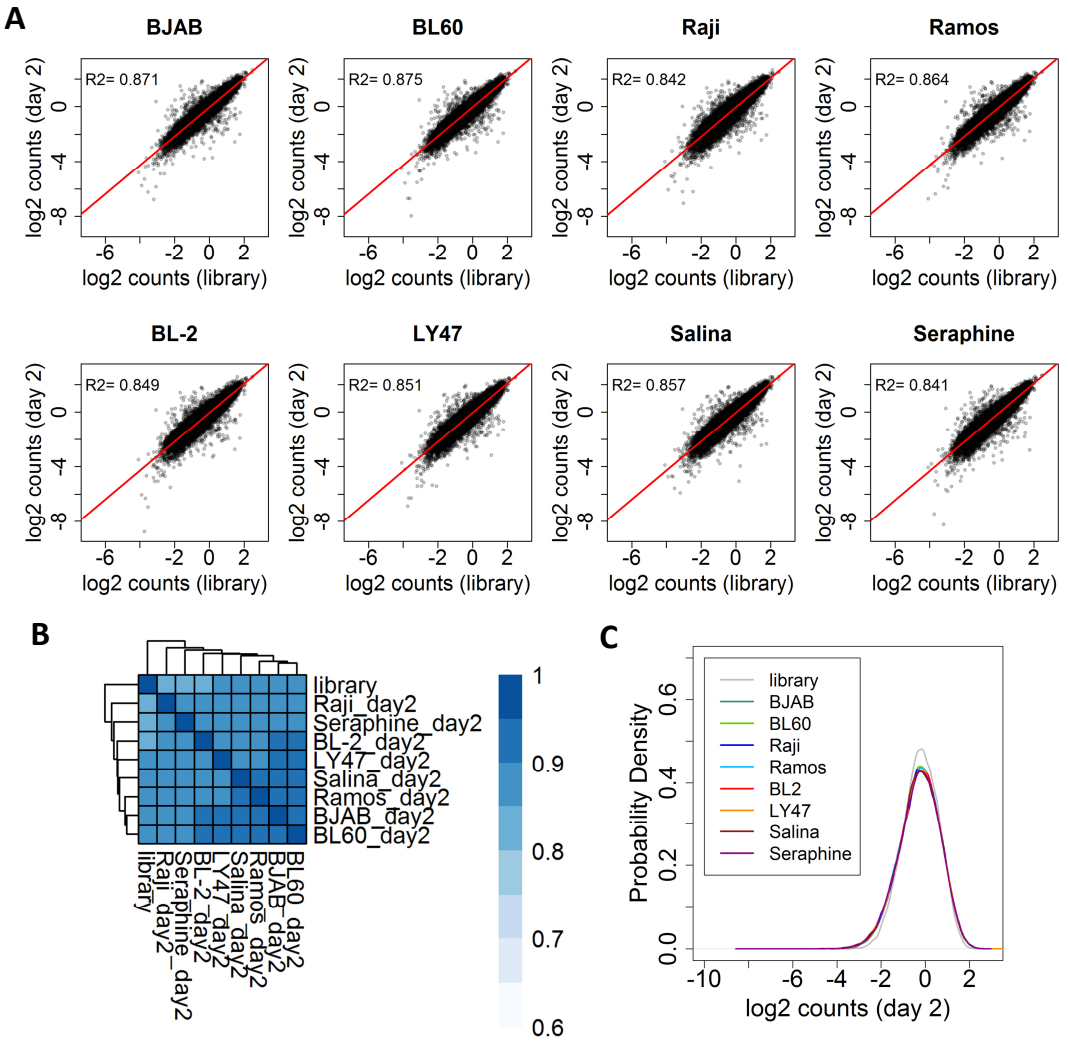

Figure 16: shRNA library representation on day 2.
(A) Raw shRNA counts were normalized for different library abundance. After logarithmic transformation relative shRNA counts on day 2 were plotted against the library representation and the correlation was calculated. **(B)** Correlation matrix between library and day 2 shRNA counts. The color scale displays R^2-values. **(C)** Density plot displaying the distribution of shRNA counts.

Replicate measurements on day 14 were highly correlated within the same cell line (R^2>0.9), but differed across cell lines (median R^2=0.65) indicating cell line specific shRNA depletion (Figure 17B). Using the average over both replicates, we analyzed changes in shRNA representation compared to day 2 (Figure 17A, C). In all cell lines shRNAs were depleted on day 14, but no enrichment could be observed. The strength of shRNA depletion was not influenced by the number of cell divisions, as cytotoxic effects were strong in LY47, the slowest growing cell line, but weak in Ramos, the fastest growing cell line.

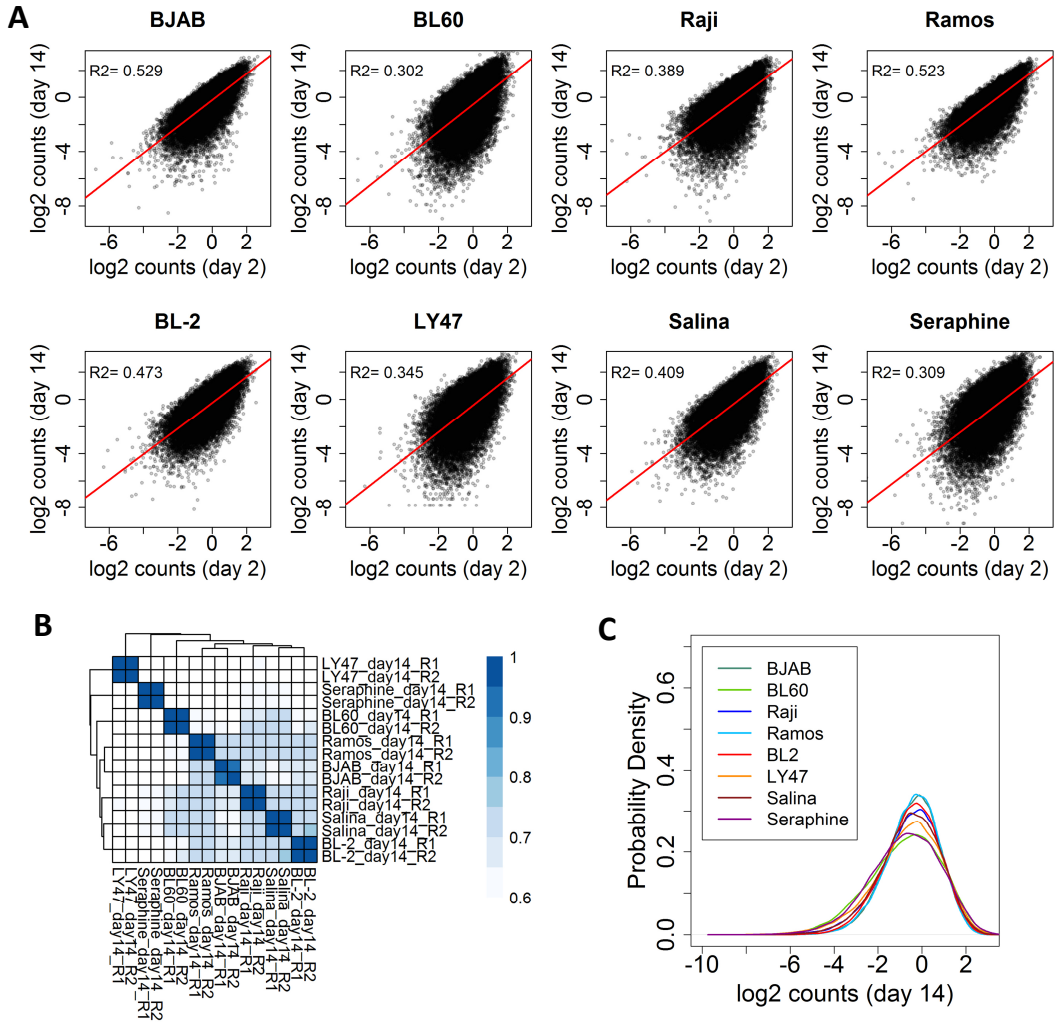

Figure 17: shRNA library representation on day 14.
(A) As described for the day 2 time point, raw shRNA counts were normalized for differences in library abundance. In addition, the mean over both replicates was calculated. After logarithmic transformation mean relative shRNA counts on day 14 were plotted against relative counts on day 2 of the same cell line and the correlation was calculated. **(B)** Correlation matrix for day 2 and day 14 replicate (R1 and R2) shRNA counts. **(C)** Density plot displaying the distribution of shRNA counts on day 14 (mean of both replicates).

4.2.6 Common essential and non-essential genes

To identify essential genes, we established an analysis pipeline based on published algorithms[131,132]. A detailed description can be found in the methods section 3.5.6. In brief, using the edgeR Bioconductor package we fitted a generalized linear model that tests if shRNAs were preferentially depleted or enriched. The resulting p-values were adjusted for multiple testing. We then combined p-values of shRNAs targeting the same gene by weighted z-transformation into gene depletion scores (wZ-scores). Figure 18A shows an exemplary shRNA distribution for the essential ribosomal protein *RPL30* and the non-essential gene *APOA4*. While shRNAs against *APOA4* were randomly distributed across the whole data set,

shRNAs targeting *RPL30* were significantly depleted. After collapsing of shRNA values into gene depletion scores, *RPL30* was specifically identified as one of the top-ranking essential genes (Figure 18B).

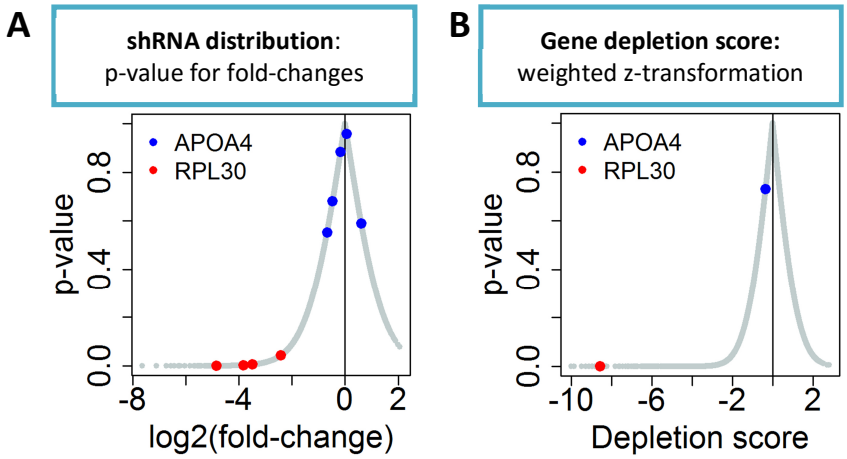

Figure 18: Identification of essential and non-essential genes from the RNAi screen.
Exemplary graphs depicting the data analysis approach using the edgeR package for comparison of count data. **(A)** Likelihood for shRNAs of being randomly distributed across the whole data set. The grey curve marks all data points. Distribution of shRNAs targeting the essential *RPL30* gene (red), compared to the non-essential *APOA4* gene (blue) are indicated. **(B)** Based on the shRNA distribution gene depletion scores were calculated by weighted z-transformation. Every data point represents one gene and genes with significantly depleted shRNAs were located within the tails of the curve.

To evaluate the performance of our screen, we first analyzed the most essential genes common to all cell lines based on the median depletion score. Within the 100 top-scoring genes we observed a strong enrichment for ribosomal, proteasomal and spliceosomal genes (Figure 19A). Furthermore, we probed the depletion scores against a published gene set of general essential and non-essential genes[115]. Our screen covered 222 genes that were classified as “non-essential” (NE) or “constitutive core essential” (CCE) based on the overlay of multiple independent RNAi screens in cell lines across cancer entities. Our data showed a high overlap: While genes classified as NE had unchanged shRNA counts, genes classified as CCE showed strong negative depletion scores (Figure 19B). Genes from the three enriched KEGG signaling pathways were found in the group of CCE, but not in NE genes (Figure 19C). Within the 100 most essential genes 35 genes were classified as “CCE” while 1-2 would be expected by chance. Notably, cell lines did not cluster by *TP53* mutation status. Therefore, the strength of shRNA depletion for common viability genes was not influenced by the presence of mutant or wild-type p53. This data suggests that the screen can reliably identify genes essential for cell viability and growth.

A

KEGG gene set	# of genes	FDR q-value
Ribosome	16	2.09×10^{-24}
Proteasome	13	2.1×10^{-22}
Spliceosome	8	4.7×10^{-8}

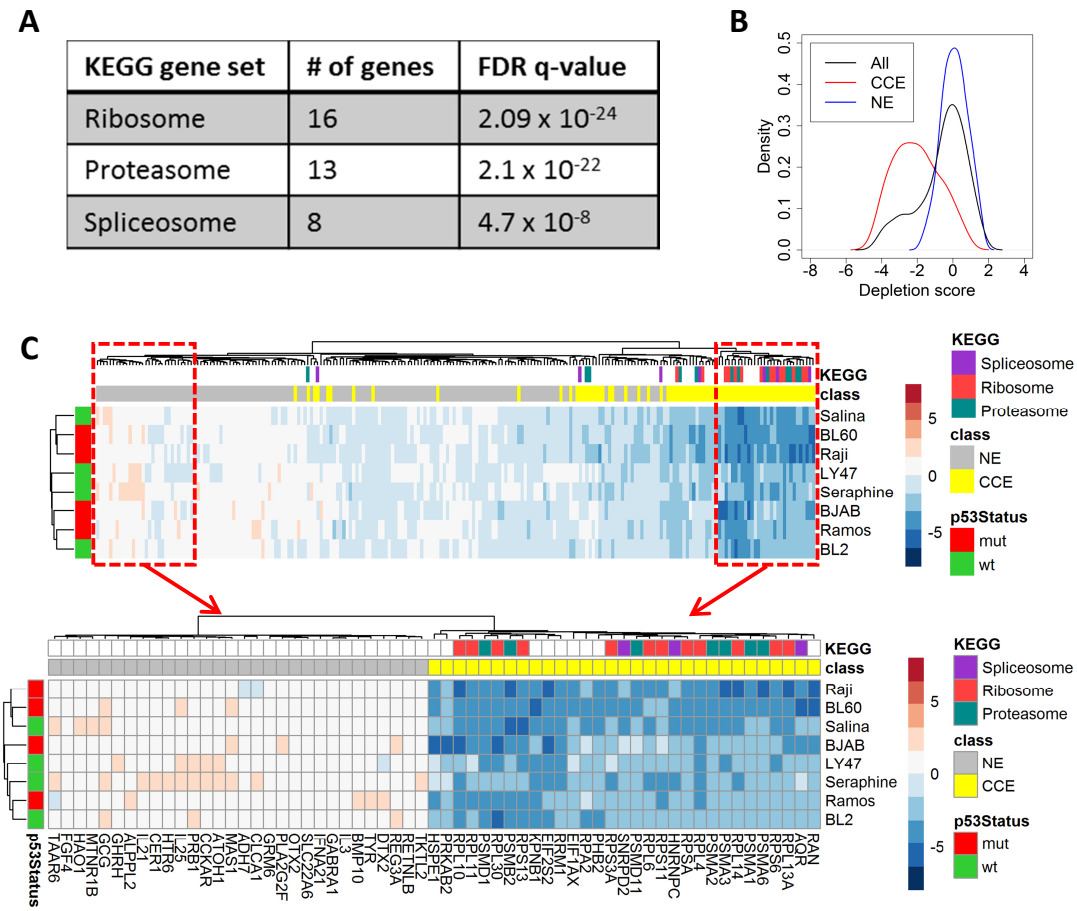

Figure 19: General essential and non-essential genes
(A) For every gene the median depletion score over all cell lines was calculated. The 100 top ranking genes were probed against KEGG gene sets using the GSEA tool from the Broad Institute. **(B)** Distribution of gene depletion scores for all genes (black) and genes classified as "constitutive core essential" (CCE, red) or "non-essential" (NE, blue)[115]. **(C)** Clustering of gene depletion scores by Euclidian distance for 220 genes classified as CCE or NE (*top*). The lower heatmap shows a magnification of the two most distinct gene clusters.

4.2.7 Genotype-specific essential genes

To identify genes essential in a subset of cell lines with defined genetic background, we adapted bioinformatics tools provided by the Broad Institute to rank genes based on their differential shRNA representation. The tools were developed and optimized to analyze loss-of-function screens in hundreds of human cancer cell lines as part of the "Achilles" project that is discussed in further detail in section 4.3.8[113]. The layout of the analysis pipeline is depicted in Figure 20A and further details can be found in the method section 3.5.6. In brief, for every cell line we calculated fold-changes of shRNA counts between day 14 and day 2. To account for differences in data dispersion we normalized the shRNA values for each cell line using peak median absolute deviation (PMAD) (Figure 20B). We then examined the position of every shRNA across the whole data set in p53wt versus p53mut cell lines and compared if shRNA

counts were significantly lower/higher in one of the groups. The comparison was performed using "weight-of-evidence" statistics that ranks shRNAs according to their strength to differentiate between two groups. Finally, we collapsed shRNA scores into gene scores using KS statistic to test if shRNAs targeting the same gene are biased towards lower/higher representation in one of the groups. This group comparison can be performed in both directions: Genes on top of the ranking list show consistently lower shRNA counts in group A, while genes on the other side of the ranking show lower shRNA counts in group B.

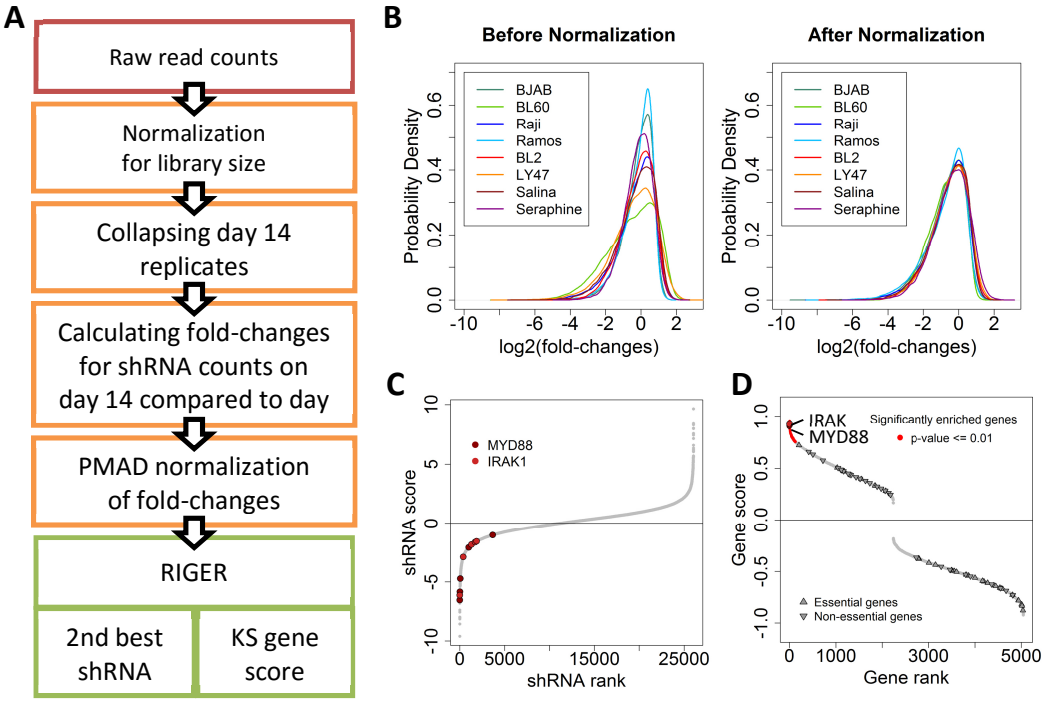

Figure 20: Identification of genotype-specific essential genes
(A) Schematic overview of the analysis pipeline for identification of genotype-specific essential genes. PMAD = peak median absolute deviation, KS = Kolmogorov-Smirnov statistic **(B)** Normalization of shRNA fold-changes between cell lines using PMAD. **(C)** Ranked shRNAs scored by differential representation in BL-2 (*MYD88* mutant) and 7 *MYD88* wild-type BL cell lines. **(D)** Genes ranked based on the power of the shRNAs to discriminate between *MYD88* mutant and wild-type BL cell lines. The essential and non-essential genes shown here are the genes from Figure 19C.

We tested the approach on a previously described genetic dependence. Using a self-established platform for targeted resequencing of genes that are recurrently mutated in lymphoma we identified the *MYD88* mutation S219C in the BL-2 cell line. A previous study reported a strong dependence of *MYD88*-mutant ABC DLBLC on MYD88 itself or its downstream mediator IRAK1[136]. This was shown for the characteristic hotspot mutation L265P which occurs most frequently in ABC DLBCL, as well as for the less frequent S219C mutation. In our RNAi screen, shRNAs targeting *MYD88* or *IRAK1* showed significantly lower shRNA counts

in BL-2 (Figure 20C). Importantly, using our class comparison approach we identified *IRAK1* on rank 4 and *MYD88* on rank 5 of genes specifically essential in BL-2 (Figure 20D). This suggests that the pipeline can be used as an unbiased statistical approach to identify novel gene dependences.

4.2.8 p53-specific essential genes

We applied the same analysis pipeline as described for MYD88 to identify p53-specific essential genes. shRNAs were ranked according to their differential representation in 4 p53wt versus 4 p53mut cell lines. As shown in Figure 21A shRNAs targeting general essential (e.g. *RPL30*) or non-essential (e.g. *APOA4*) genes were equally represented in both groups, while individual genes (e.g. *MDM4*, *CDKN3*) showed consistently lower shRNA counts in p53wt cell lines as indicated by negative shRNA scores.

shRNA scores were collapsed into gene scores using KS statistics. Genes on top of the ranking list had lower shRNA counts in p53wt cell lines and genes on the bottom had lower shRNA counts in p53mut cell lines (Figure 21B). The most robust candidates were selected by stringent filtering criteria as described in section 3.5.6. In brief, we selected genes with at least two significantly underrepresented shRNAs and significantly lower ($p<0.05$), negative gene depletion scores (weighted z-score (wZ)<-0.5) in p53wt cell lines. We removed genes that were not found to be expressed in RNA sequencing or that scored with shRNAs that had overlapping target regions. Twelve genes were fullfilling all criteria (Figure 21C). Four of these genes were also essential in p53mut cell lines (wZ-score<-0.5), but significantly stronger depleted in p53wt cell lines. These included two metabolic genes (*GALNTL4*, *CYP39A1*), one methyltransferase (*BHTM2*) and one histone subunit (*HIST3H3*).

The p53 inhibitor MDM4 was identified as the strongest gene specifically essential in p53wt cell lines. MDM4 is located on 1q32. As chr1q gain was associated with p53wt BL patients (see section 4.1), we wanted to know if genes on chr1q were more essential in p53wt cell lines. Figure 21D shows the median gene depletion scores in p53wt versus p53mut cell lines. The shRNA library covered 237 genes located on chr1q (indicated in dark grey). We did not observe a p53-specific dependence of chr1q genes. Besides of *MDM4*, the cell cycle regulator *CDKN3* (rank 8) was the strongest outlier here and both genes were chosen for validation.

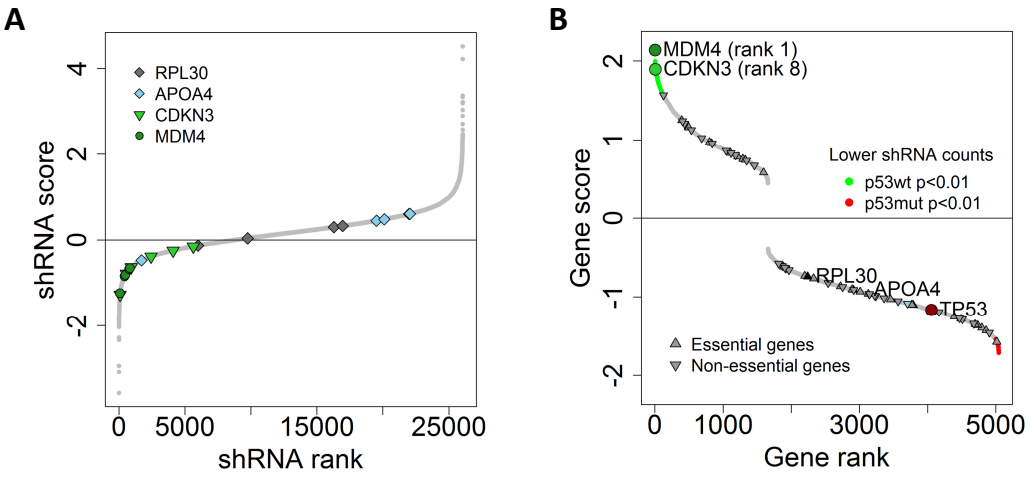

C

Gene	Chr locus	Gene score	Median wZ (p53wt)	Median wZ (p53mut)
MDM4	1q32.1	1	-1.79	0.29
MMP14	14q11.2	7	-1.14	0.04
CDKN3	14q22.2	8	-1.00	0.65
PYCR1	17q25.3	209	-0.94	0.13
AMT	3p21.31	105	-0.66	0.24
GATM	15q21.1	319	-0.64	0.05
ABCC3	17q21.33	49	-0.61	0.36
ATP6V1F	7q32.1	5	-0.55	0.10
GALNTL4	11p15.3	12	-1.82	-0.96
CYP39A1	6p12.3	206	-1.61	-0.92
BHMT2	5q14.1	54	-1.13	-0.57
HIST3H3	1q42.13	27	-1.57	-0.57

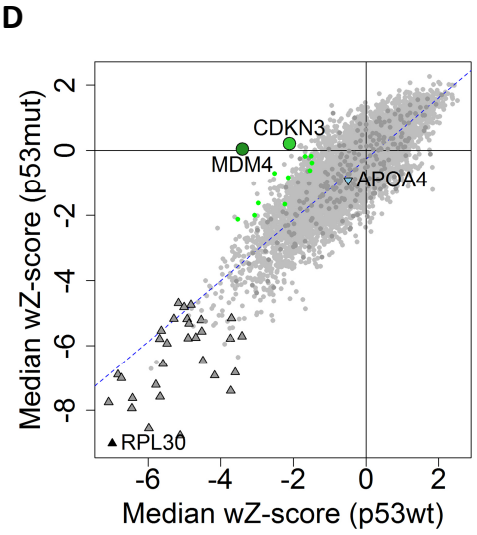

Figure 21: Identification of essential genes specific to p53wt BL cell lines.
(A) Ranking of shRNAs by differential representation in 4 p53wt vs. 4 p53mut cell lines. *RPL30* (essential) and *APOA4* (non-essential) are shown as controls. *MDM4* and *CDKN3* were two candidate genes chosen for validation. **(B)** Ranking of p53-specific essential genes. Low ranking genes showed lower shRNA counts in p53wt and high ranking genes had lower counts in p53mut. **(C)** Overview of 12 high-reliability candidate genes essential specifically in p53wt cell lines. The list shows the gene score and the median wZ-score calculated over 4 p53wt or 4 p53mut cell lines. **(D)** Median wZ-score over 4 p53wt and 4 p53mut cell lines with indicated common essential genes (grey triangle), genes on chr1q (grey dots), 12 high-reliability candidates (green dots), control *APOA4* (non-essential) and *RPL30* (essential) and *MDM4* and *CDKN3* chosen for validation.

4.3 MDM4 depletion induces p53-dependent cell cycle arrest

4.3.1 Validation of RNAi screening

To validate the observed phenotype we first tested the effect of shMDM4_1–5 on MDM4 mRNA and protein level. After lentiviral delivery of targeted shRNAs or shNT transduced cells were selected with puromycin to ensure that >90% of cells carry the shRNA vector. MDM4 mRNA level were quantified using RT-qPCR and protein level were determined in immunoblot analysis (Figure 22A, B). All shRNAs led to a significant downregulation of MDM4 mRNA and protein level between 40-60%.

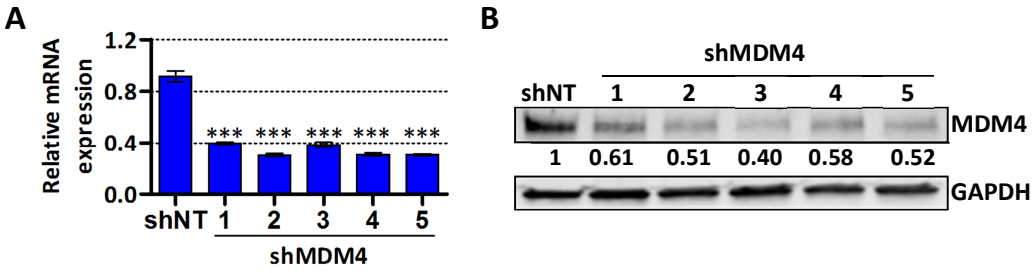

Figure 22: On-target effect of shRNAs directed against MDM4.
Quantification of MDM4 level in the BL-2 cell line 5 days after transduction with 5 shRNAs targeting MDM4 and a non-targeting control shNT. **(A)** mRNA level of MDM4 and GAPDH were determined by quantitative real-time PCR. The expression values were normalized to the house keeping gene GAPDH and to shNT. The error bars indicate the mean standard error of three independent biological replicates. ***=p-value<0.001 **(B)** Immunoblot analysis for MDM4 and GAPDH. MDM4 protein expression was normalized to GAPDH and shNT.

We tested the effect of MDM4 depletion on cell viability and proliferation in an RFP-competition assay. Cells were transduced with lentiviral shRNA vectors at ~50% and co-expressed RFP. Essential genes were identified by loss of RFP-signal as quantified by flow cytometric analysis (Figure 23A). For validation experiments we extended the panel of BL cell lines. Besides of the eight BL cell lines from the screen, four additional p53mut cell lines were included. Two shRNAs located in different exons of MDM4 (shMDM4_1: spanning exon 3-4 boundary; shMDM4_2: exon 7) were chosen for validation. Three out of four p53wt cell lines showed strong depletion of RFP signal, indicating toxicity of the target gene knock-down (shMDM4_1: Ø17%; shMDM4_2: Ø35%), while all p53mut cell lines showed moderate effects to MDM4 depletion (shMDM4_1: Ø74%; shMDM4_2: Ø81%) (Figure 23B). The p53wt BL-2 cell line was insensitive towards MDM4 knock-down and behaved like a p53mut cell line (shMDM4_1: 76%; shMDM4_2: 85%). Comparison of RFP depletion in single knock-down experiments with loss of shRNA counts in the RNAi screen showed high reproducibility confirming the robustness of the RNAi screen (Figure 23C).

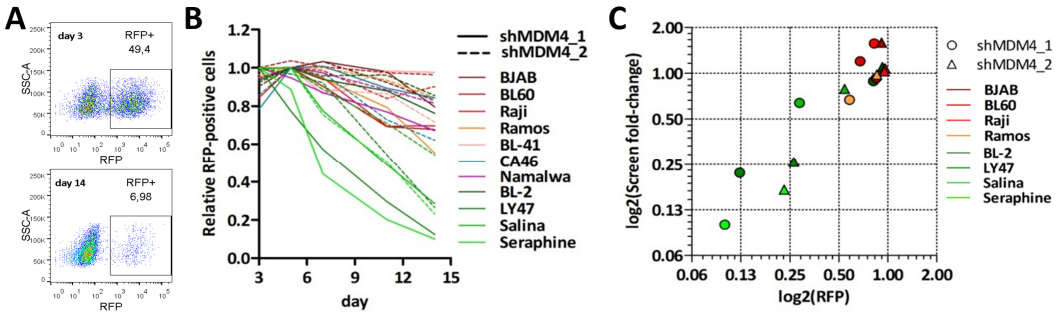

Figure 23: RFP competition assay after MDM4 depletion.
(A) Exemplary plots from flow cytometric analysis of RFP-signal in cells transduced with toxic shRNAs. The upper plot shows the RFP-signal on day 3 post-transduction and the lower plot on day 14. **(B)** Relative RFP-signal over 14 days in 12 BL cell lines transduced with shMDM4_1 and shMDM4_2 (green: p53wt, rest: p53mut). The RFP-signal was fully established between day 3 and day 5 post-transduction and all RFP-values were normalized to the maximal expression. **(C)** Loss of RFP-signal in single knock-down experiments and depletion of shRNA counts in the RNAi screen on day 14 post-transduction. (green: p53wt; red/orange: p53mut)

4.3.2 Generation and characterization of a p53 knock-out model

To test if effects seen after MDM4 depletion depend on p53, we generated an isogenic p53 knock-out (p53ko) cell line from p53wt Seraphine using the CRISPR/Cas9 technology. In a one-vector system, the microbial endonuclease Cas9 was co-expressed with single-guide RNAs (sgRNA) targeting *TP53* in exon 4 (sgRNA#1), exon 5 (sgRNA#2) or exon 7 (sgRNA#3). The sgRNAs bind to their complementary sequence on the genomic DNA and direct Cas9 to the desired target region. Cas9 induces double strand breaks that are repaired by error-prone non-homologous end joining (NHEJ). As a result, deletions and, in rare cases, insertions are introduced that lead to a loss of gene function.

We tested the efficiency of disrupting p53 function of three independent guide RNAs targeting different exons. Cells transduced with CRISPR/Cas9 expression vectors co-expressed a puromycin resistance gene and were first selected with puromycin. To remove clones still carrying functional p53 protein (either by lack of a cut or in-frame deletions), cells were propagated in the presence of the small molecule inhibitor nutlin-3, that induces p53-dependent apoptosis by MDM2 inhibition. All three sgRNAs conferred resistance towards nutlin-3 indicating inactivation of p53 (data not shown). For further studies we selected the Seraphine cell line infected with sgRNA#1. We confirmed the presence of deletions in p53 exon 4 using a DNA mismatch repair assay (Figure 24). As NHEJ introduces various random deletions, efficient targeting of *TP53* results into a pool of cells carrying different mutations. After DNA extraction and amplification of the genetic locus, DNA double strands were denatured and re-annealed in a thermocycler. Annealing between the original DNA strand and a shorter strand carrying a deletion leads to formation of a loop. The T7 endonuclease cuts the

DNA at the site of the loop and produces fragments of various sizes (Figure 24A). In the parental p53wt cell line addition of the T7 endonuclease to the PCR product resulted into two smaller bands besides of the full length PCR product (581bp) (Figure 24B). The same pattern was seen for sgRNA#2 and sgRNA#3 that target different exons. For sgRNA#1, which targets the amplified region, three bands with a unique pattern were observed.

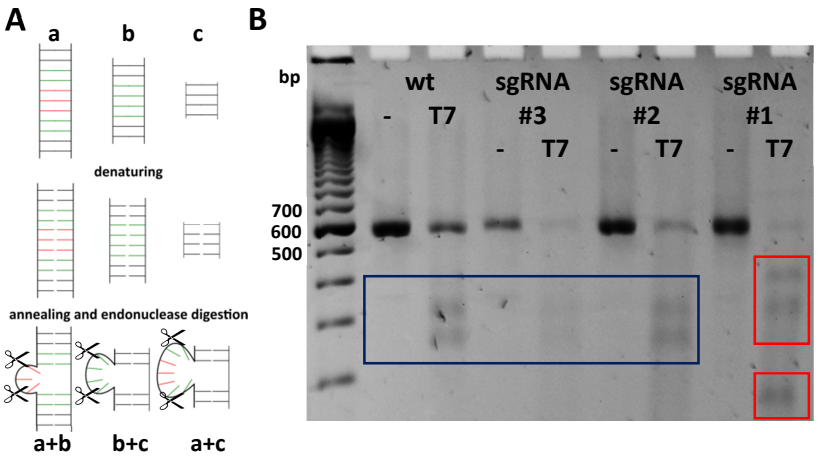

Figure 24: Generation and characterization of a p53 knock-out cell line
(A) Schema of the mismatch repair assay. The target sequence of the sgRNA was amplified from genomic DNA of a mixed pool of cells carrying different deletions (a=full-length, b=short deletion, c=long deletion). After denaturing and re-annealing of the DNA double strands, loops were forming at the sites of missing base pairs that were targeted by T7 endonuclease. **(B)** Mismatch repair assay in Seraphine cell line. The exon 4 of *TP53* was amplified from the parental p53 wild-type (wt) cell line or modified cell lines expressing sgRNA#1, #2 or #3 and either left untreated (-) or incubated with T7 endonuclease (T7).

The p53ko cell line was included in a compound screen on 28 cell lines (including 18 BL cell lines) that was performed by Marina Lukas and Katarzyna Tomska. Nutlin-3 that was also included in the screen showed the strongest p53-specific toxicity. All p53wt cell lines were sensitive towards nutlin-3 starting from a concentration of 3µM, while p53mut and the p53ko cell lines did not respond to concentrations up to 10µM (Figure 25A). The toxicity that can be seen at 30µM might be explained by unspecific effects or by disruption of the p73-MDM2 binding[137]. Using flow cytometry we analyzed p53 protein level in the p53wt and the p53ko cell line treated with nutlin-3 or dissolvent (DMSO) after intracellular staining with fluorophore-labeled antibodies (Figure 25B). The basal expression level of p53 was lower in the p53ko cell line and nutlin-3 treatment increased p53 level in the p53wt, but not in the p53ko cell line. Accordingly, nutlin-3 induced apoptosis in the p53wt, but not in the p53ko isogenic cell line as shown in flow cytometry using APC-labeled Annexin V to stain the membrane of apoptotic cells and 7-AAD to stain exposed DNA of dying cells.

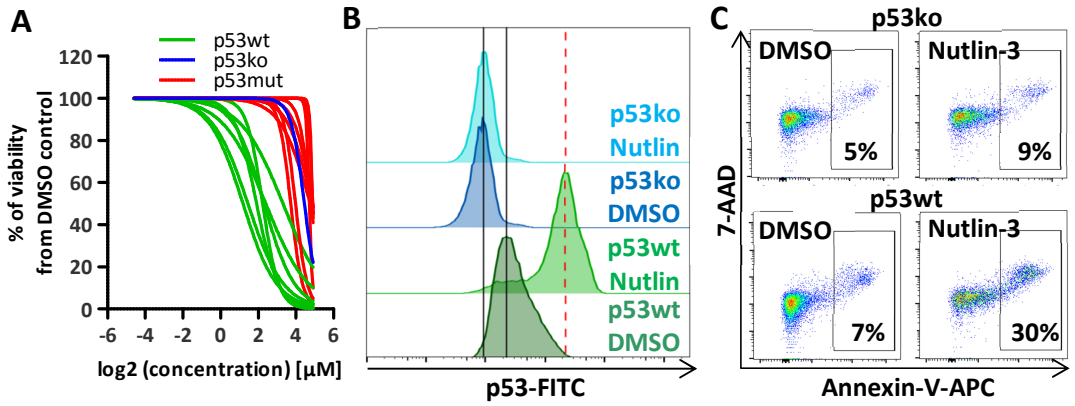

Figure 25: Nutlin-3 treatment of the p53ko cell line
(A) Titration of nutlin-3 in 18 BL cell lines (7 p53wt, 1 p53ko, 10 p53mut). All cell lines were incubated with 10 different concentrations of nutlin-3, DMSO or PBS for 48h. Cell content was measured by ATP level using a luminescent assay and normalized to DMSO. The curves were generated with a non-linear fit. The data was kindly provided by Katarzyna Tomska. **(B)** Flow cytometric analysis of p53 level after intracellular staining. Seraphine p53wt and p53ko cells were grown in the presence of 10µM nutlin-3 or 0.1% DMSO for 10h. Cells were fixated and permeabilized for intracellular staining using a p53-antibody coupled to the fluorophore FITC. **(C)** Flow cytometric analysis of apoptotic cells after nutlin-3 treatment. Seraphine p53wt and p53ko were incubated with 10µM nutlin-3 or DMSO (0.1%) for 10h. Early apoptotic and dead cells were stained with Annexin V-APC and 7-AAD.

To test if cytotoxic effects of MDM4 knock-down were p53-dependent we performed the RFP competition assay in the isogenic p53ko and p53wt cell lines. shNT was stably expressed in both cell lines. In the p53wt cell line, 80% of cells expressing shMDM4_2 were lost 14 day post-transduction, while cells of the p53ko cell line were unaffected. shMDM4_1 showed strong cytotoxic effects in the p53wt cell line. 56% of cells were depleted after 7 days and 90% after 14 days. In the p53ko cell line the effect of shMDM4_1 was much weaker. 10% of RFP-positive cells were lost on day 7 and 56% on day 14, suggesting p53-dependent cytotoxicity.

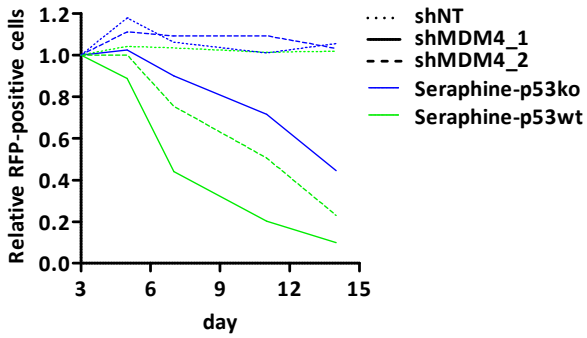

Figure 26: MDM4 knock-down in the p53ko cell line
RFP-competition assay in Seraphine-p53wt (green) and Serapine-p53ko (blue) after MDM4 knock-down. Isogenic Seraphine cells were infected with shNT, shMDM4_1 or shMDM4_2 at an infection rate of ~50% and infected cells were monitored in flow cytometry by RFP expression over 14 days. Fraction of RFP-positive cells was normalized to day 3.

4.3.3 Cell cycle analysis after MDM4 depletion

MDM4 depletion did not induce apoptosis (data not shown). Therefore, we analyzed the effect of MDM4 knock-down on the cell cycle profile in the presence or absence of functional p53. In Seraphine-p53wt and Seraphine-p53ko 28% and 27%, respectively, incorporated BrdU into their genomic DNA within 3h of culturing, while 62% of Raji (p53mut) cells were BrdU-positive (Figure 27A). In the p53wt cell line both shRNAs targeting MDM4 led to a ~50% decrease in cycling cells compared to shNT, while no significant effect was seen in the p53mut cell line (Figure 27B). In the p53ko cell line, shMDM4_2 had no effect on the cell cycle and shMDM4_1 induced a moderate G1 arrest of about 20%, in line with the results from the RFP competition assay. In immunoblot analysis of the p53wt cell line following MDM4 knock-down we detected increased expression of p53 with both shRNAs (1.4/1.7) and p53 target genes p21 (1.3/1.3) and PUMA (1.6/1.5), but not PARP cleavage that would indicate apoptosis.

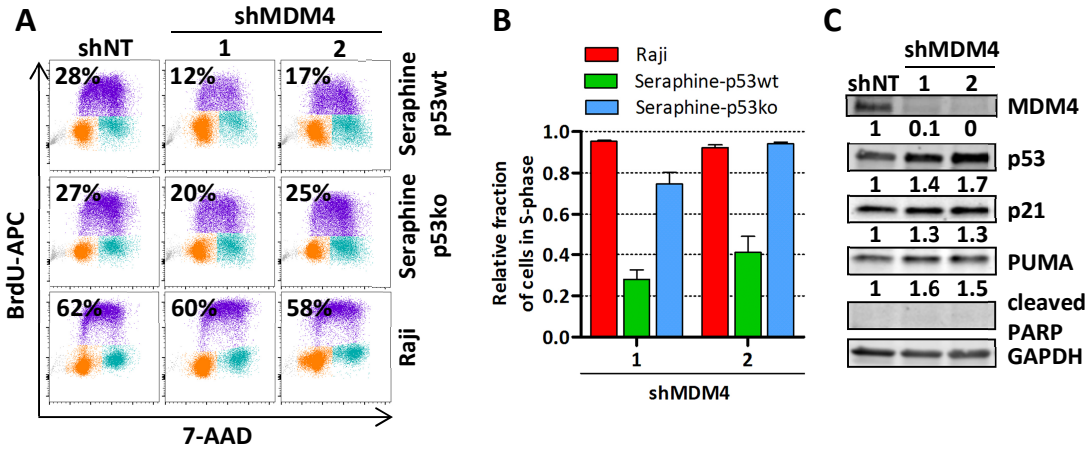

Figure 27: p53-mediated cell cycle arrest after MDM4 knock-down
(A) Exemplary plots from flow cytometric analysis of cell cycle phases in p53wt, p53ko and p53mut cell lines. Cells were grown in the presence of the nucleotide analogue BrdU that was incorporated into cycling cells. After cell fixation and permeabilization BrdU was stained with APC-labeled antibody. Total DNA amount was stained with 7-AAD. orange = G1-phase, violet = S-phase, blue = G2/M phase, grey = Sub-G1-phase. **(B)** Quantification of cells in the DNA synthesis phase (S-phase). The bars represent triplicate measurements of cell fractions in the S-phase normalized to shNT. **(C)** Immunoblot analysis in Seraphine-p53wt transduced with shNT, shMDM4_1 and shMDM4_2. Protein levels were normalized to GAPDH and to shNT. Cleaved PARP was not detected above background and could not be quantified.

4.3.4 The MDM4 homologue MDM2 shows similar effects on cell cycle progression

The p53 inhibitor MDM2 shares a similar structure with MDM4 and both proteins are needed to suppress p53. In our screen MDM2 was not identified as a p53-specific essential gene. To investigate the role of MDM2 in p53wt BL, we analyzed the effect of MDM2 targeting shRNAs in the screen (Figure 28). One out of five shRNAs (shMDM2_1) was underrepresented in the p53wt group (Figure 28A). After collapsing of all shRNAs into gene scores MDM2 showed a

tendency towards p53wt-specific toxicity (p=0.05, Figure 28B). As this score was driven by a single shRNA, MDM2 was not considered as a candidate gene. We tested the on-target effect of all 5 shRNAs on mRNA and protein level (Figure 28C). To avoid MDM2 upregulation by activation of the p53-dependent negative feedback loop, the p53ko cell line was chosen. MDM2 mRNA and protein level were reduced by two shRNAs, shMDM2_1 (27%/35%) and shMDM2_3 (54%/53%). To conclude, the shRNA that gives the strongest on-target effect on MDM2 was specifically toxic in p53wt, but not p53mut BL cell lines. The gene MDM2 did not score in the screen due to lack of on-target effect for most shRNAs.

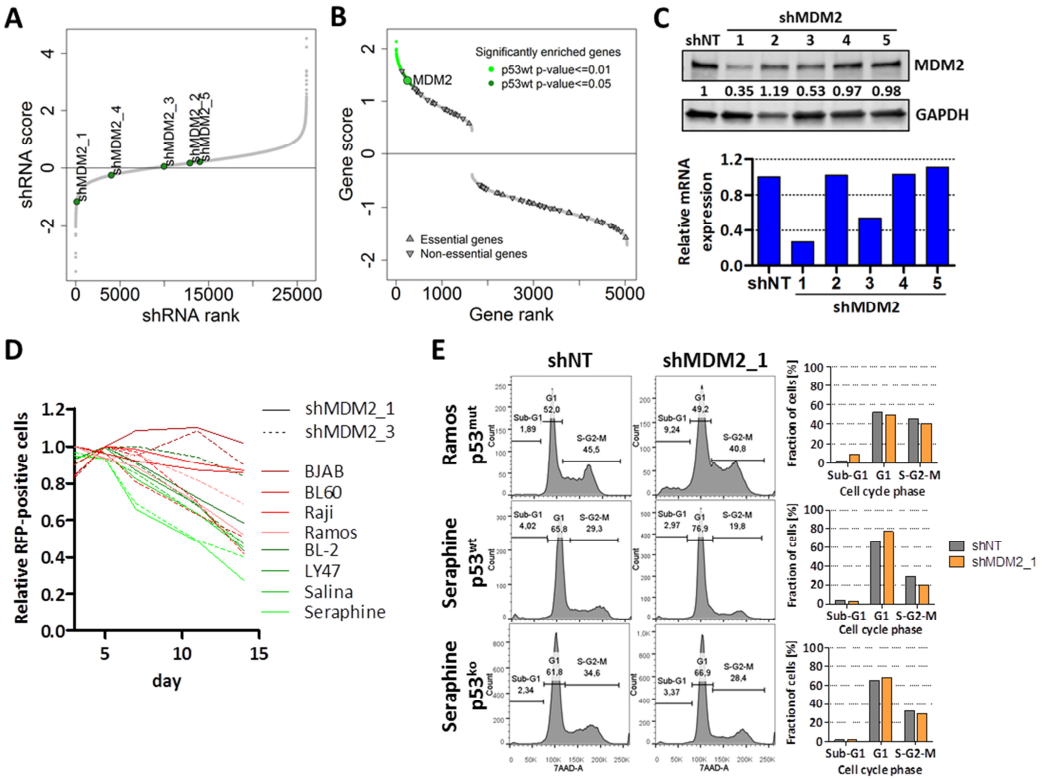

Figure 28: MDM2 knock-down in the RNAi screen

(A) shRNAs from the RNAi screen ranked by differential representation in p53wt vs. p53mut cell lines. shRNAs 1-5 targeting MDM2 are highlighted. shRNAs with negative shRNA scores were underrepresented in p53wt cell lines. **(B)** Genes ranked by differential shRNA representation. Genes with significantly lower shRNA counts in p53wt cell lines are marked in light green (p-value<0.01) and dark green (p-value<0.05). **(C)** Protein and mRNA level of MDM2 in Seraphine-p53ko cell line 3 days after lentiviral delivery of shNT or shMDM2_1-5. More than 80% of cells were RFP-positive. MDM2 mRNA level were determined in RT-qPCR and protein level in immunoblot analysis. All values were normalized to GAPDH and to shNT. **(D)** RFP competition assay in all eight screening cell lines. Cells were transduced with shNT, shMDM2_1 or shMDM2_3 at ~50% transduction rate and RFP-signal was measured over 14 days. Fraction of RFP-positive cells was normalized to day 5 post-transduction. **(E)** Cell cycle profiling in Seraphine-p53wt, Seraphine-p53ko and Ramos (p53mut) transduced with shNT or shMDM2_1. Cells were fixated and permeabilized. Total DNA was stained with 7-AAD and measured in flow cytometric analysis. Cells in G1-phase, Sub-G1-phase and S-G2-M-phase were quantified.

To test if MDM2 is essential in BL cell lines with or without functional p53 we performed the RFP competition assay in all screening cell lines using both shRNAs with confirmed on-target effect (Figure 28D). shMDM2_1 showed strong viability effects in all p53wt cell lines (Ø44%), but not in p53mut cell lines (Ø78%). shMDM2_3 was depleted in 3/4 p53wt cell lines (Ø55%), but also in 2/4 p53mut cell lines (Ø60%). We tested the effect of MDM2_1 on the cell cycle of the isogenic Seraphine cells and Ramos (p53mut) (Figure 28E). Total DNA was stained with 7-AAD after permeabilization of cell that either expressed shNT or shMDM2_1. The p53wt cell line showed a reduction of cycling cells of 9% after MDM2 depletion, while 4% and 5% reduction was observed in the p53ko and p53mut cell line, respectively.

4.3.5 Basal expression of MDM4 and MDM2 in BL cell lines

To see if vulnerabilities towards MDM2 and MDM4 depletion correlated with protein and/or mRNA abundance, we used qPCR and immunoblot analysis to determine the basal expression levels of p53, MDM2 and MDM4 in all screening cell lines and eight additional BL lines. In total, our analysis included 8 p53wt and 8 p53mut BL cell lines (Figure 29). In p53wt cell lines, we observed low or undetectable levels of p53 protein. Under physiologial conditions, p53 protein levels are tightly regulated and protein levels are kept low by rapid proteasomal turnover. Mutant p53 is resistant towards MDM2-mediated proteasomal degradation and therefore accumulates in the cell. This is in accordance with our observations in BL cell lines. All p53mut cell lines showed high p53 protein expression. Protein levels were not correlated with mRNA level in either group. Most p53mut cell lines expressed low p53 mRNA, while about half of p53wt cell lines showed elevated level.

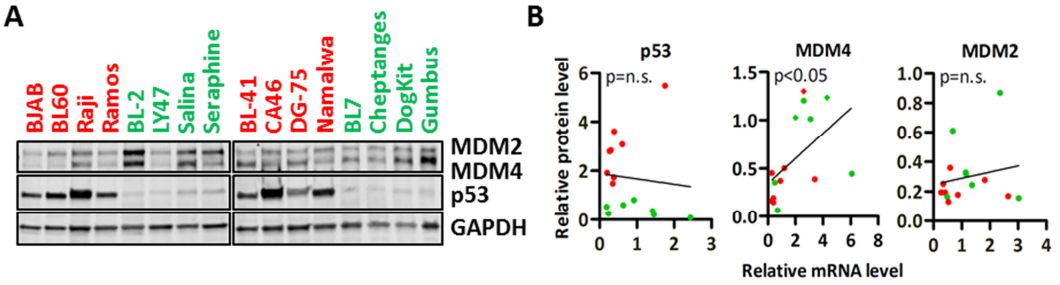

Figure 29: Basal expression of p53, MDM2 and MDM4 in BL cell lines
(A) Correlation of protein and mRNA for p53, MDM4 and MDM2 in p53wt (green) and p53mut (red) BL cell lines. **(B)** Immunoblot for p53, MDM2 and MDM4 in 8 p53wt (green) and 8 p53mut (red) BL cell lines. GAPDH was used as a control.

For MDM4, we observed a significant correlation between mRNA and protein level (Figure 29B). Most cell lines with high expression level belonged to the group of p53wt cell lines (4 out of 5). For MDM2, protein expression levels were low in most cell lines and not correlated with mRNA. BL-2 (p53wt) was the only cell line with high MDM2 mRNA and protein level. In addition, BL-2 expressed high MDM4, while most p53wt cell lines expressed either high MDM2

(Seraphine) or MDM4 (Salina, DogKit and Gumbus). MDM4 and MDM2 expression level did not correlate with sensitivity towards protein depletion.

4.3.6 Gene expression profiling after MDM4 and MDM2 knock-down

To determine the signaling pathways that were influenced by depletion of MDM4 and MDM2 we performed gene expression profiling in the Seraphine-p53wt and Seraphine-p53ko cell line after MDM4 and MDM2 knock-down. Cells were transduced at high infection rates (>80% RFP+ cells) with shNT, two shRNAs targeting MDM4 (shMDM4_2, shMDM4_3) and one shRNA targeting MDM2 (shMDM2_1, the only validated shRNA showing strong on-target effect and p53-specific viability effects). On day 5 post-transduction RNA was extracted and hybridized on an Illumina BeadChip. In all samples ~16,700 gene probes (corresponding to ~13,000 genes) were found to be expressed above the background signal. MDM4 and MDM2 expression could not be detected, because of the low resolution of the assay. Therefore, depletion of the target gene was validated by qPCR (Figure 30A). shRNAs targeting MDM4 efficiently depleted MDM4 mRNA in both cell lines (shMDM4_2: 0.3; shMDM4_3: 0.4) and increased MDM2 level exclusively in the p53wt cell line (shMDM4_2: 2.5; shMDM4_3: 2.7). shMDM2_1 efficiently reduced MDM2 level in the p53ko cell line (0.4). The on-target effect was not visible in the p53wt cell line (1.1). As mentioned previously, the p53-dependent negative feedback loop might lead to an upregulation of MDM2 mRNA.

The p53wt cell line showed more dynamic changes of the gene expression (90-560 gene probes with at least 2-fold difference) compared to the p53ko cell line (1-120 gene probes with at least 2-fold difference) (Figure 30B). shMDM4_3 showed the strongest effects on gene expression, in the p53wt as well as the p53ko cell line. This may indicate p53-independent effects specific to this shRNA.

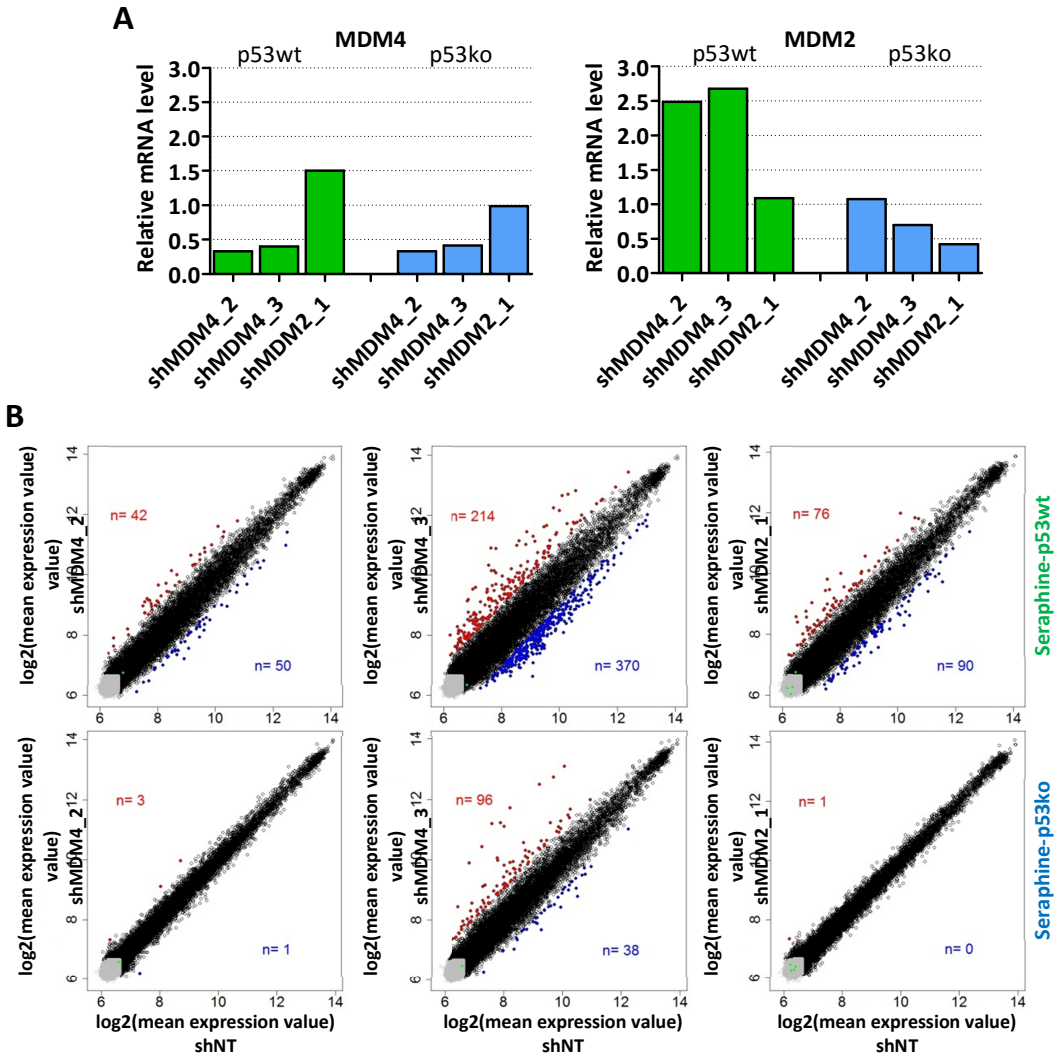

Figure 30: Gene expression profiling after MDM4 and MDM2 knock-down
(A) Relative mRNA level of MDM4 (*left*) and MDM2 (*right*) in Seraphine-p53wt (green) and Seraphine-ko (blue) transduced with the indicated shRNAs. mRNA levels were normalized to shNT. **(B)** Gene expression values in Seraphine-p53wt and Seraphine-p53ko transduced with shMDM4_2, shMDM4_3, shMDM2_1 or shNT. Genes with more than two-fold increase (red) or decrease (blue) are indicated. Gene probes of the respective targets, MDM4 or MDM2, are shown in green. Gene probes in the range of background noise (p-value>0.05, mean expression value<110) are marked in grey.

We tested if genes within pre-defined gene sets were specifically deregulated. Using gene set enrichment analysis (GSEA) the distribution of genes within hallmark sets was compared to the overall distribution of the data and an enrichment score (ES) was calculated. Figure 31A shows the results from GSEA for shMDM4_2 as an example. p53 target genes showed the strongest ES (0.55) for upregulated genes. Downregulated genes were strongly enriched for genes in key pro-survival and proliferation pathways including E2F targets (ES=-0.63), G2M checkpoint (ES= -0.51) and MYC targets (ES=-0.54). The same pathways were significantly deregulated by

shMDM4_3 and shMDM2_1 (Figure 31B). To validate these findings, we measured mRNA level of selected p53 target genes and cell cycle regulators following MDM4 knock-down (Figure31C). MDM4 was stably repressed between days 3 and 5. p53 targets MDM2, p21, BAX and RRM2B were about 1.5-fold elevated on day 3 after transduction of cells with shMDM4_2 and further increased up to 2-fold on day 5, while p53 mRNA level remained unchanged. To a similar extent, cell cycle regulators of the MCM-family were depleted between days 3 and 5. CDKN3 level were unchanged on day 3 and 4, but rapidly decreased on day 5.

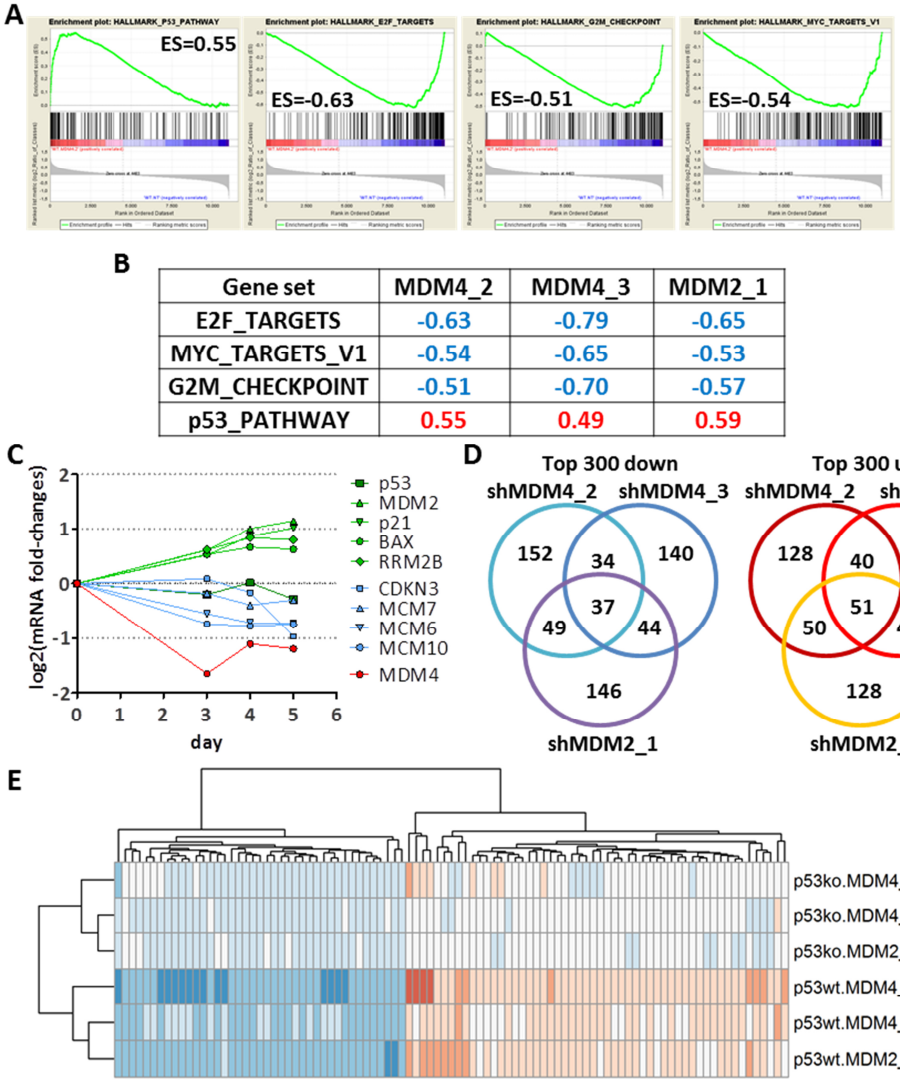

Gene set	MDM4_2	MDM4_3	MDM2_1
E2F_TARGETS	-0.63	-0.79	-0.65
MYC_TARGETS_V1	-0.54	-0.65	-0.53
G2M_CHECKPOINT	-0.51	-0.70	-0.57
p53_PATHWAY	0.55	0.49	0.59

Figure 31: GSEA for differentially expressed genes following MDM4 and MDM2 depletion
(A) Gene set enrichment analysis (GSEA) for differential gene expression in Seraphine-p53wt transduced with shNT or shMDM4_2. The graphs were generated with software provided by the Broad Institute. All genes were sorted by their fold-change from genes higher in shMDM4_2 (red) to genes lower in shMDM4_2 (blue). Based on the distribution of shRNAs within respective gene sets (black bars), an enrichment score (ES) was calculated. **(B)** ES for hallmark pathways. Positive ES = upregulation; negative ES = downregulation. **(C)** Time course of mRNA level in Seraphine-p53wt infected with shMDM4_2 for p53 targets (green), cell cycle regulators (blue) and shRNA target (red). **(D)** Overlap of the 300 most up- or downregulated genes between three shRNAs. **(E)** Heatmap for commonly regulated genes.

The observation that MDM4 knock-down represses CDKN3 is interesting as p53wt cell lines were specifically dependent on CDKN3 in the RNAi screen. To investigate genes that were commonly regulated after MDM4 or MDM2 knock-down we selected the 300 most up- and downregulated genes in either sample and compared the overlap (Figure 31D). 37 genes were among the most downregulated genes with either shRNA, while 51 genes were commonly upregulated. The fold-changes of commonly regulated genes are shown as a heatmap in Figure 31E.

4.3.7 MDM4 depletion in a mouse xenograft model

To evaluate if MDM4 serves as a potential target in tumor therapy the influence of MDM4 depletion on xenograft formation in mice was tested. shMDM4_2 was used to knock-down MDM4 in isogenic Seraphine cell lines (p53wt, p53ko) and in Raji (p53mut). The non-targeting control shNT was used as a reference. After transduction and puromycin selection, shRNA expressing cells were injected subcutaneously into the left (shMDM4_2) or right (shNT) flank of three mice per cell line. For quantification of tumor growth the metabolic activity of the tumor cells in the xenograft was determined by uptake of the glucose analogue fluordesoxyglucose (FDG) using positron emission tomography (PET) (Figure 32A). Tumor size was also measured after sacrificing of the mice (Figure 32B). In the p53wt cell line tumor growth was significantly reduced after MDM4 knock-down, compared to the control shRNA (average 59%, $p<0.05$). Tumors were also smaller post-mortem (73%).

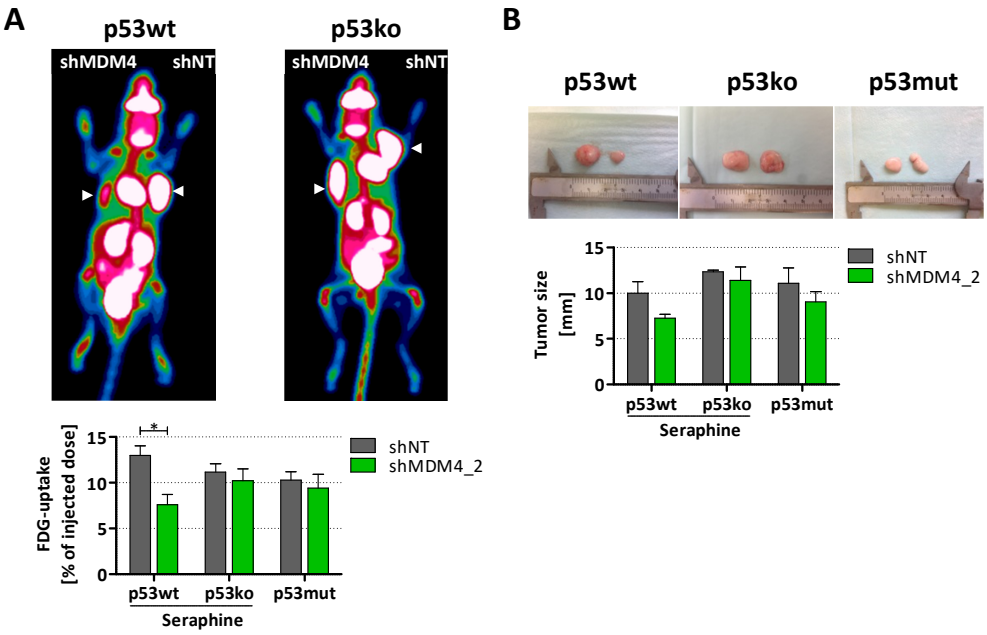

Figure 32: MDM4 knock-down decreases xenograft formation in mice.
(A) Exemplary figures of the FDG-PET scanning. The white arrows mark the tumor xenograft. The graph shows the quantification of FDG-uptake with error bars indicating the mean standard error of three mice. **(B)** Exemplary figures of excised tumors of sacrificed mice. The graph shows the quantification of tumor size. Error bars show the mean standard error of three mice. The experiment was performed in collaboration with Dr. Stefan Habringer in the research group of Professor Dr. Ulrich Keller (Medical clinic III, Munich, GER).

4.3.8 MDM4 dependence across p53wt cancer cell lines

To test if p53-specific dependence on MDM4 is limited to BL cell lines, we re-analyzed a publically available loss-of-function RNAi screen in 216 cell lines representing 19 tumor entities[112]. On a genome-wide scale the Broad Institute screened 54,020 shRNAs from the TRC library targeting ~11,000 genes. Based on the COSMIC data base (Sanger Institute, http://cancer.sanger.ac.uk/cosmic) and published RNA sequencing data[133] we could determine the p53 status for 158 cell lines. 77 cell lines carried p53 mutations (49%) and 81 cell lines were p53 wild-type (51%) (Figure 33A).

We ranked the genes according to their differential shRNA representation in both groups. MDM4 showed significant underrepresentation of shRNAs in p53wt cell lines and was identified on rank 20 ($p<0.001$) (Figure 33C). For seven tumor entities at least 4 cell lines were available per group which allowed an analysis for p53-specific gene dependences in single entities (CNS, haematopioetic&lymphoid, ovary, lung, large intestine, pancreas, breast) (Figure 33B). The strongest association was found in large intestine (rank 7, $p<0.001$) and ovary carcinoma cell lines (rank 173, $p=0.01$) (Figure 33D). In a comparison of common p53-specific essential genes identified in both our BL screen and the Achilles project we also found the cell

cycle regulator *CDKN3* (rank=127, p=0.01). However, *CDKN3* was not significantly associated with p53 status in entity-specific analysis.

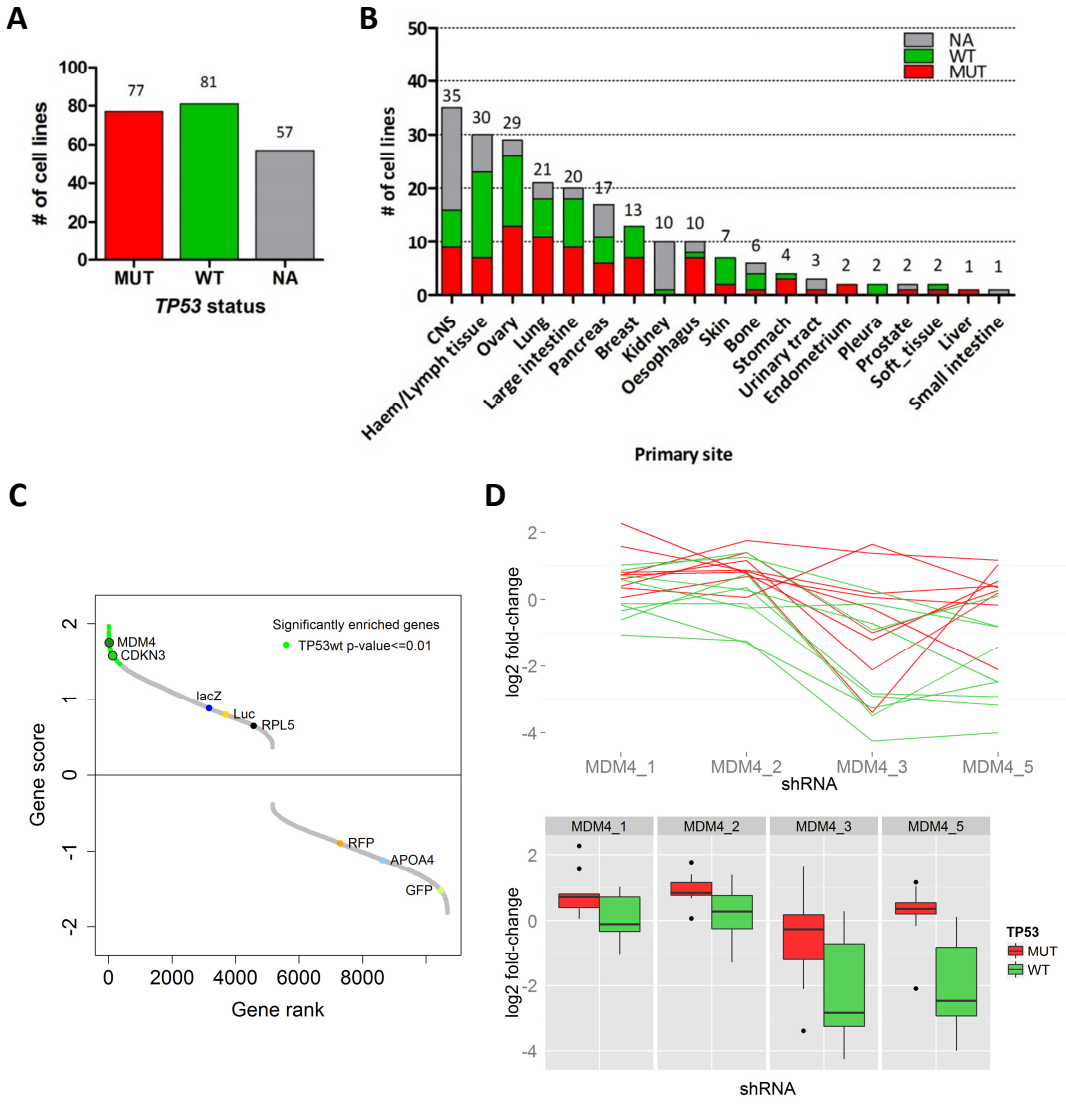

Figure 33: p53-specific gene dependences across cancer
(A) Number of cell lines from the Achilles Project v2.4.3 with available p53 mutation status (Broad Institute)[112]. **(B)** Representation of cancer entities with indicated p53 mutation status. **(C)** Ranking of genes by differential shRNA representation in p53wt vs. p53mut cell lines. Genes marked in green show significantly lower shRNA counts in p53wt cell lines (p≤0.01). Two candidate genes (*MDM4* and *CDKN3*) and p53-independent control genes are indicated. **(D)** Depletion of shRNAs targeting MDM4 in 9 p53wt (green) and 9 p53mut (red) large intestine cell lines.

4.3.9 BL patients express a strong p53 signature

To study the effect and function of p53 mutation on cellular pathways, we generated a molecular signature for mutant p53 based on differentially expressed genes in 430 B-NHL primary samples where gene expression data was available (MMML). Data analysis was performed by Dr. Maciej Rosolowski and Dr. Markus Kreuz (Interdisciplinary Centre for Bioinformatics, University of Leipzig, GER). Samples from mBL, non-mBL and intermediate patients (as defined by Hummel *et al.*, 2006) were grouped by p53 mutation status to derive a p53 mutant signature across all patients (Figure 34A). The signature includes 50 gene probes with the highest reliability of higher or lower expression, respectively, in p53mut compared to p53wt patients.

Genes expressed higher in p53mut patients were not enriched for hallmark gene sets. Interestingly, the gene *CDKN2A*, encoding for the tumor suppressors $p14^{ARF}$ and $p16^{INK4a}$, showed the strongest differential expression with two gene probes (Figure 34B, *left*). *CDKN2A* is often deactivated in cancers without p53 mutations, either by deletion or hypermethylation. In BL, deletion of the *CDKN2A* locus on chr9p21 is rare. Therefore, alternative mechanisms must exist. Unfortunately, methylation data was only available on a limited number of patients and we could not test an association of *CDKN2A* methylation status and p53 mutation.

Genes expressed lower in p53mut patients were strongly enriched for p53 target genes (n=9; *MDM2*, *BAX*, *RPS27L*, *TNFRSF10B*, *TRIM22*, *DDB2*, *CCNG1*, *CDKN1A*, *FDXR*) (Figure 34B *right*, C). These data suggest that a portion of B-NHL retain active p53 signaling. This finding allowed us to query both disease specific differences and measure activity of p53 pathway activation in the context of wild-type and mutant p53.

In addition, gene set enrichment analysis for chromosomal regions identified genes on 17p13 (n=11) and 1q32 (n=3) (Figure 34B *right*, C) associated with p53 status. This effect might reflect gene dosage effects. Loss of 17p13 mainly affects p53mut patients and results into decreased expression of genes within this locus. Gain of 1q32 associates with p53wt and results into increased expression in p53wt patients. As shown in Figure 34D, elevated expression of *MDM4* and *RNPEP* was specifically observed in BL, but not in non-BL patient samples. While *MDM4* level in p53mut BL were comparable to either p53wt or p53mut non-BL, p53wt BL expressed higher level (Figure 34E). At the same time, p53 target genes were stronger activated in p53wt non-BL (Figure 34F, G).

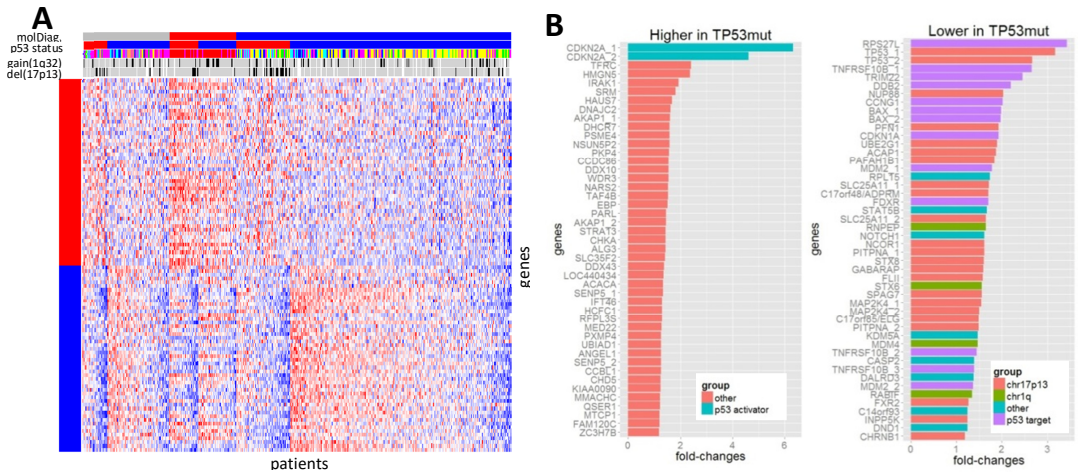

C

Gene set	# of genes	FDR q-value
HALLMARK_P53_PATHWAY	9	5.7×10^{-12}
Chr17p13	11	3.8×10^{-13}
Chr1q32	3	5.7×10^{-2}

D

	Relative expression (p53wt-p53mut)	
Gene	**BL**	**Non-BL**
MDM4	**1.26**	**1.05**
RNPEP	1.22	1.07
RABIF	1.04	1.08

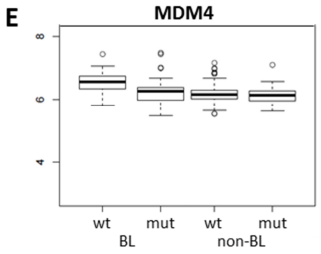

F

	Relative expression (p53wt-p53mut)	
Gene	**BL**	**Non-BL**
CCNG1	0.93	1.62
FDXR	1.05	1.42
CDKN1A	1.15	1.31
DDB2	1.16	1.4
BAX	1.23	1.35
RPS27L	1.24	1.73
TRIM22	1.24	1.34
MDM2	1.26	1.2
TNFRSF10B	1.41	1.3
Mean	**1.19**	**1.41**
P-value	**0.007**	

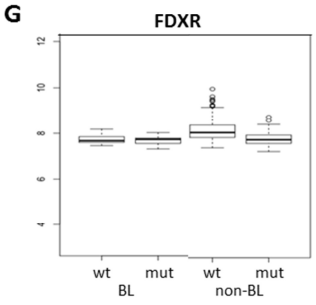

Figure 34: p53 gene expression signature

(A) Supervised hierarchical clustering of differentially expressed gene probes in 430 B-NHL. Every column represents a patient and every row represents a gene. Patients were clustered by molecular diagnosis into intermediate (grey), BL (red) and DLBCL (blue) and by p53 status into mutant (red) and wild-type (blue). Deletion of chr17p13 and gain of chr1q32 are indicated (black=mutation, grey=normal, white=unknown). 50 gene probes higher (red) or lower (blue) in p53mut were sorted by their strength to differentiate between the groups with the strongest discriminators on the bottom. **(B)** Fold-changes for 50 gene probes expressed lower (*left*) or higher (*right*) in p53mut samples. **(C)** Genes from the 50 gene probes expressed lower in p53mut were tested for enrichment in hallmark gene sets and chromosomal positions. **(D)** Differential expression of genes on chr1q32 in BL and non-BL samples. **(E)** Expression of MDM4 in BL and non-BL samples with and without p53mut. **(F)** Differential expression of p53 targets in BL and non-BL samples. **(G)** Exemplary expression of p53 targets in BL and non-BL.

4.4 p53-specific effects of the cell cycle regulator CDKN3

The dual-specificity phosphatase CDKN3 controls the spindle checkpoint and is needed to ensure correct chromosomal segregation during mitosis. In our RNAi screen CDKN3 knock-down was toxic exclusively to p53wt BL cell lines. Using RT-qPCR we confirmed depletion of CDKN3 mRNA by all of the six shRNAs included in the shRNA library (Figure 35A). Validated antibodies for CDKN3 were lacking. Therefore, the on-target effect on protein level could not be tested. We selected two shRNAs and performed the RFP-assay as described above to validate the phenotype observed in the RNAi screen. All eight screening cell lines and the isogenic p53ko cell line were transduced with lentiviral vectors and transduced cells were monitored for RFP-expression over 14 days using flow cytometry (Figure35B, C). Both shRNAs were depleted stronger in p53wt cell lines compared to p53mut cell lines (p53wt: Ø 37%, p53mut: Ø 64%, $p<0.05$). shCDKN3_5 that was toxic in the Seraphine-p53wt cell line (30%) showed limited effect in the Seraphine-p53ko line (70%). shCDKN3_6 was toxic to both cell lines, but exerted a stronger effect in the p53wt cell line (p53wt: 16%, p53ko: 24%). To study the effect of CDKN3 depletion we performed cell cycle profiling in the isogenic Seraphine lines and Ramos (p53mut). After CDKN3 knock-down using two independent shRNAs total DNA amount was stained by 7-AAD and measured in flow cytometry (Figure 35D). After CDKN3 depletion Seraphine-p53wt showed an arrest in the G1-phase and a reduction of cycling cells (54%). This effect was not observed in the p53mut cell lines (93%) and the p53ko cell lines (88%).

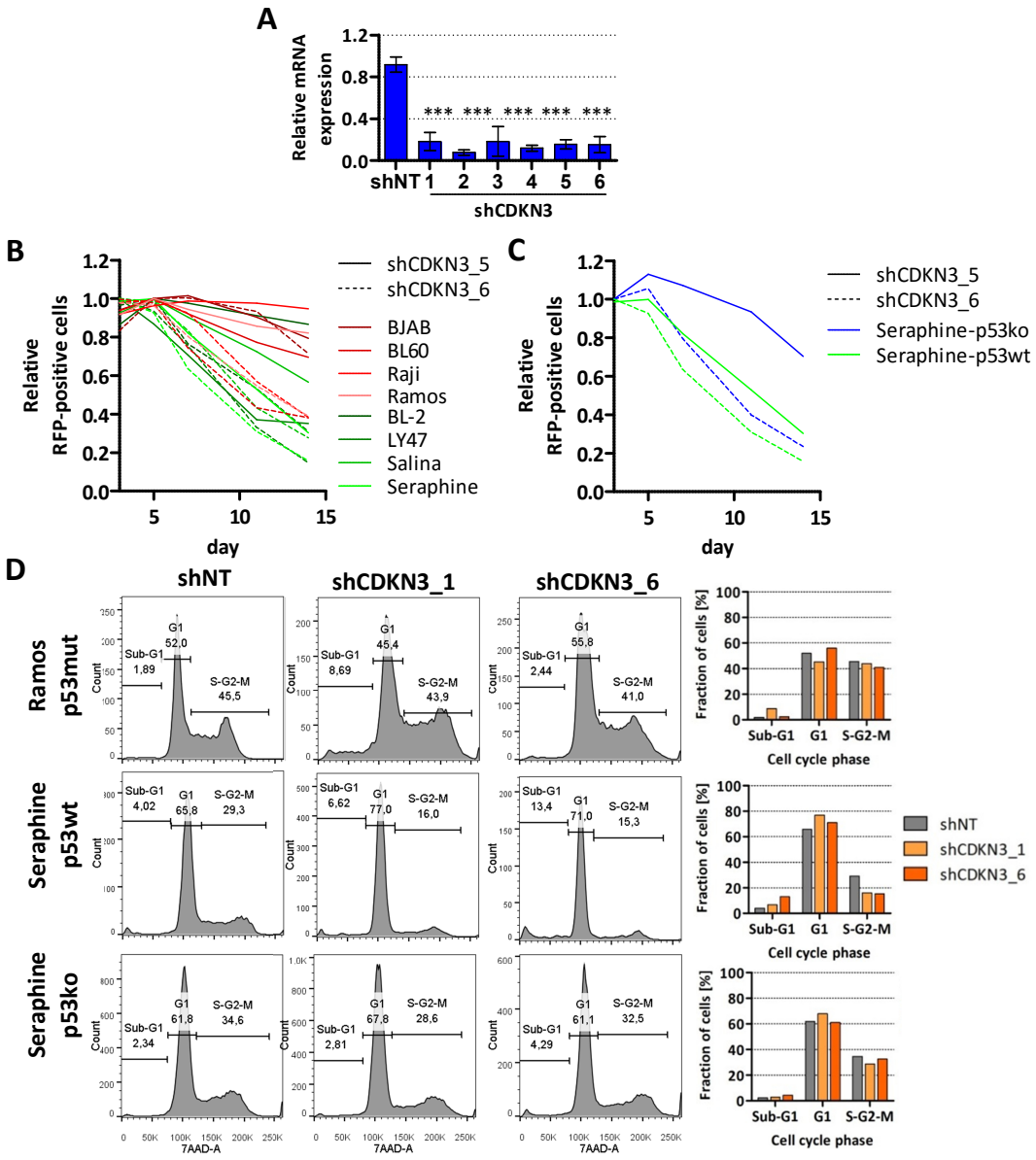

Figure 35: Depletion of CDKN3 induces G1-arrest in p53wt BL

(A) mRNA level for CDKN3 were measured by RT-qPCR in the Seraphine-p53ko cell line infected with shNT or shCDKN3_1-6. The measurements were performed in triplicates. Error bars indicate the mean with standard deviation. **(B)** Relative RFP-signal in cells transduced with two shRNAs targeting CDKN3. In a partially transduced cell culture the fraction of RFP+/shRNA+ cells was normalized to day 3. red=p53mut, green=p53wt **(C)** Comparison of RFP-signal depletion in the isogenic Seraphine cell lines. green=p53wt, blue=p53ko; **(D)** Cell cycle profiling in isogenic Seraphine and Ramos (p53mut). Total DNA was stained in fixated cells using 7-AAD.

4.5 Entity-specific essential genes

We performed an RNAi screen in a large panel of BL cell lines (n=8) and could robustly identify general as well as genotype-specific essential genes. BL cell lines were not represented in the Achilles project and according to our knowledge this is one of the largest genetic perturbation screens in BL. Therefore, we asked if our data could also help to predict specific vulnerabilities in B-cell lymphoma or Burkitt lymphoma. The provider of the DECIPHER Module 1 library (Cellecta Inc., Mountain View, CA, USA) generated RNAi screening data in 12 cell lines representing seven different entities (Table 3). The data can directly be compared to our RNAi screening data in BL, because the same library and protocols were used.

Table 3: Cell lines used in external RNAi screens
List of pooled shRNA screens performed by Cellecta company.

Screen	Cell lines	Entity	# of replicates	Time-point	Library version
HDM1_p23	K562	CML-myeloid	4	9 days	NA
	Jurkat	ALL T-lymphocyte	4	9 days	
	DU-145	Prostate carcinoma	3	8 days	
HDM1_v1	MDA-MB-231	Breast carcinoma	3	11 days	pRSI9
	A2780	Breast carcinoma	3	10 days	
HDM1_v2	C4-2	Prostate carcinoma	3	8 days	pRSI12
	R22v1	Prostate carcinoma	3	8 days	
	PC3	Prostate carcinoma	3	8 days	
	THP1_RPCI	Monocyte	3	9 days	
	THP1_ATCC	Monocyte	3	10 days	
	U937	DLBCL	3	10 days	
	AML19310	AML myeloid	3	10 days	

We applied the same analysis pipeline as described for our own screen to data from Cellecta. As no sequencing data was provided for early time points after infection, shRNA counts were normalized to their abundance in the respective plasmid libraries. shRNA fold-changes for all screens were combined and normalized for differences in data dispersion between cell lines (Figure 36A). In a class comparison approach, we identified genes with significantly lower shRNA counts in BL cell lines (n=8) compared to non-lymphoid cell lines (prostate and breast carcinoma, n=6) (Figure 36B, *left*). We then further selected candidate genes by the strength of shRNA depletion. For this, we calculated the median over the logarithmic fold-change for respective cell line groups (Figure 36B, *right*). Common essential genes showed strong shRNA depletion in all three groups, while non-essential genes were unchanged.

Among the genes essential specifically in BL we identified *PAX5*, that plays an important role in B-cell differentiation, and the proto-oncogene *FLI1*, that was first described in erythroleukemias. *PAX5* was among the 50 most essential genes in BL (rank=46; median $\log_2$(fold-change)=-2.03), while its knock-down did not affect non-lymphoid cell lines (rank=2663; median $\log_2$(fold-change)=-0.31). *FLI1* was on rank 169 of toxic genes in BL (median $\log_2$(fold-change)=-1.47), but was dispensable in non-lymphoid lines (rank=2186; median $\log_2$(fold-change)=-0.41).

Both transcription factors are mainly expressed in cells of the lymphoid lineage. To further investigate if candidate genes play a specific role in the pathogenesis of Burkitt lymphoma, we repeated the analysis as described above comparing essential genes in BL with essential genes in five hematopoietic-lymphoid, non-BL cell lines. *PAX5* was again identified as a gene with significant lower shRNA counts in BL (Figure 36C, *left*). Depletion of *PAX5* did not have an effect in hematopoietic-lymphoid cell lines (rank=2186; median $\log_2$(fold-change)=-0.41) (Figure 36C, *right*). shRNAs targeting *FLI1* were also strongly depleted in hematopoietic-lymphoid cell lines, specifically in the three lymphoid lines (rank=132; median $\log_2$(fold-change) =-1.6) and therefore *FLI1* did not score in the comparison for genes with differential shRNA representation. In addition, we could also identify genes (e.g. *ALLC*) that were essential in BL and some non-lymphoid cell lines, but not in hematopoietic-lymphoid cell lines. Figure 36D shows the logarithmic fold-changes for all shRNAs targeting *PAX5*, *FLI1* or *ALLC* in BL, hematopoietic-lymphoid and non-lymphoid cell lines.

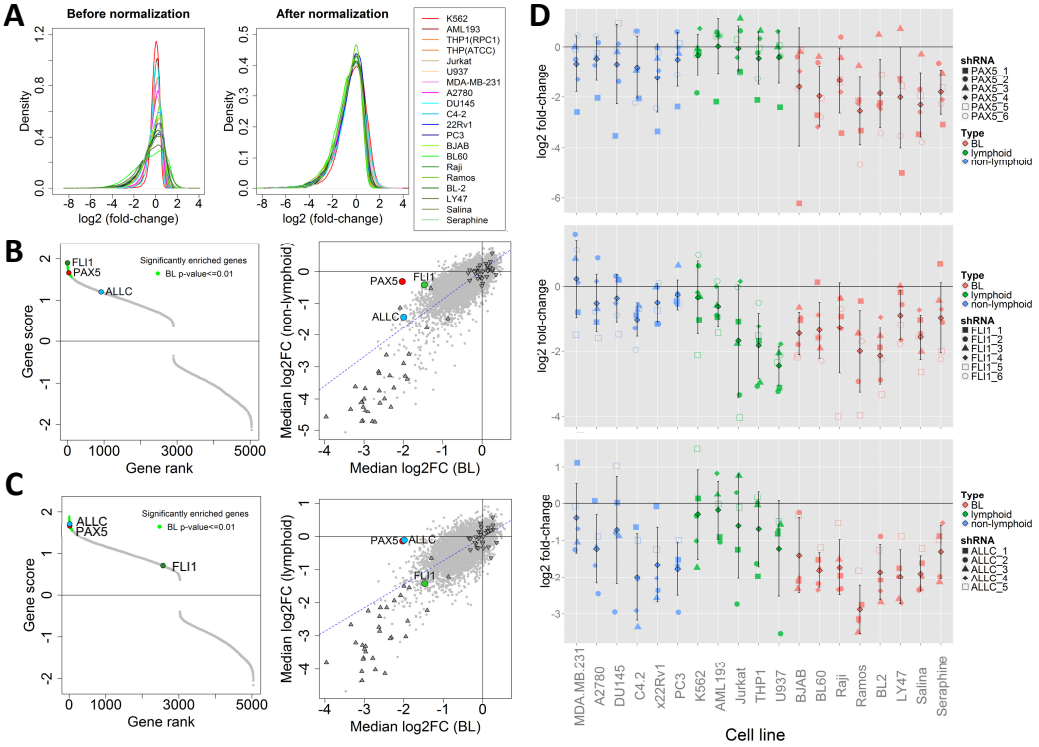

Figure 36: Identification of entity-specific gene dependences
(A) PMAD (peak median absolute deviation) normalization of logarithmic fold-changes for cell lines from our own RNAi screen and RNAi screens provided by Cellecta. **(B)** *left*: Analysis of genes with differential shRNA representation in BL and non-lymphoid cell lines. Genes with significantly lower shRNA counts in BL are highlighted in green. *right:* Median logarithmic fold-change (log2FC) for 8 BL and 6 non-BL cell lines. **(C)** *left*: Analysis of genes with differential shRNA representation in BL and hematopoietic-lymphoid cell lines. Genes with significantly lower shRNA counts in BL are highlighted in green. *right:* Median logarithmic fold-change (log2FC) for 8 BL and 5 hematopoietic-lymphoid cell lines. △ common essential genes; ▽ common non-essential genes. **(D)** Logarithmic shRNA fold-changes for all shRNAs targeting *PAX5*, *FLI1* and *ALLC* in cell lines from our BL or the Cellecta RNAi screen.

For future validation studies we selected 2 independent shRNAs targeting genes with significant lower shRNA counts in BL compared to non-lymphoid cell lines and a mean depletion of -0.5 in BL (Figure 37).

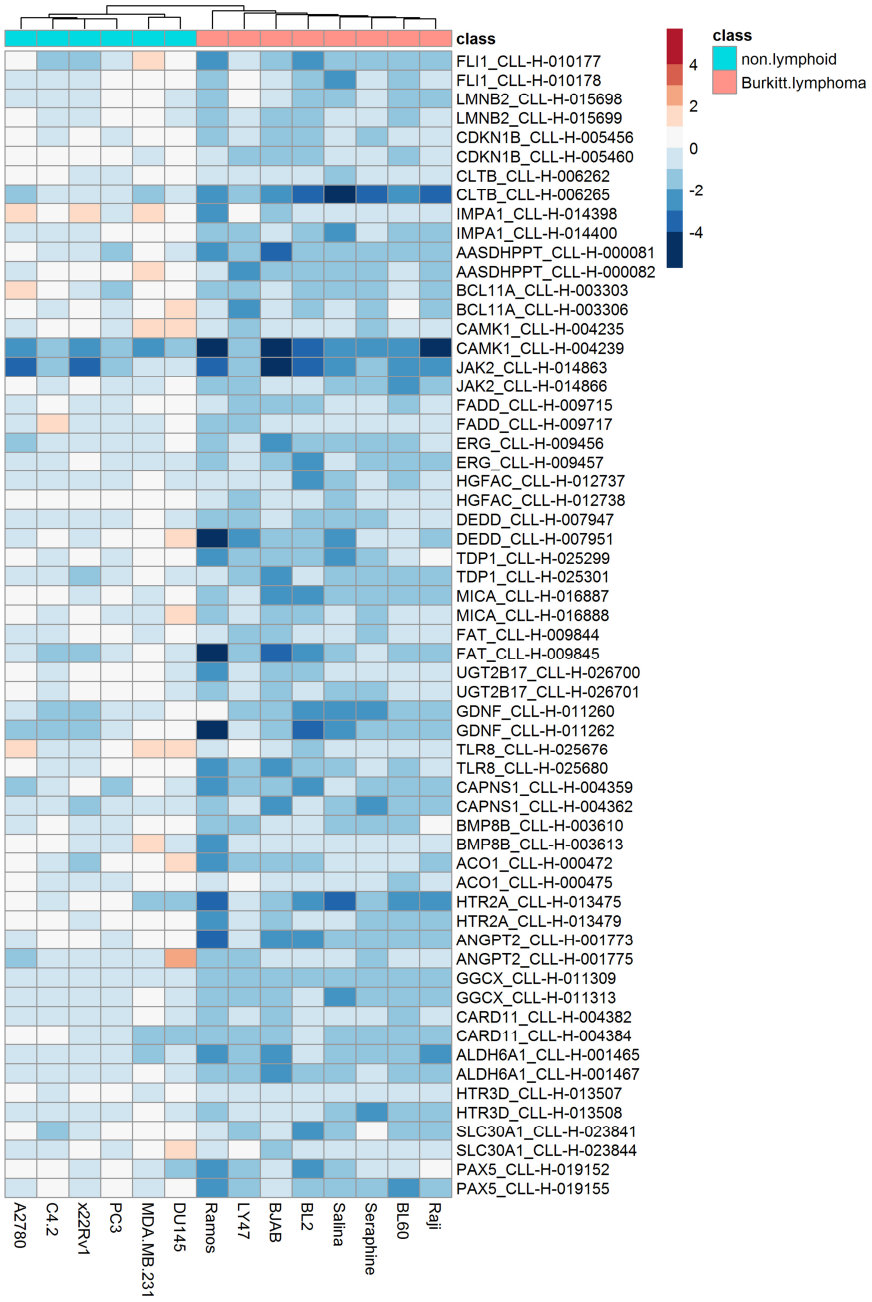

Figure 37: Selection of shRNAs targeting entity-specific essential genes
The heatmap shows logarithmic fold-changes of shRNAs that target genes essential in BL, but not in non-lymphoid cell lines. For every gene, two independent shRNAs that were significantly lower in BL and had a mean logarithmic fold-change of -0.5 were selected.

4.6 Summary

We investigated mechanisms of evading apoptosis in MYC-driven Burkitt lymphoma. Besides of aberrations in the *TP53* gene, mutations within the conserved *MYC* box I were shown to promote survival. In our analysis of 67 BL primary samples, 43% of BL patients carried mutations in *TP53* and 27% in *MYC* box I. Most importantly, both mutations were not exclusive and in about 50% of BL patients genetic aberrations that contribute to the evasion of MYC-induced apoptosis were not known.

To identify alternative mechanisms, we correlated *TP53* mutation with clinical parameters and chromosomal aberrations. Patients carrying mutant *TP53* displayed with higher clinical stage and advanced disease. However, overall survival was independent of *TP53* status, indicating that additional factors contribute to the aggressiveness of the disease. In patients retaining wild-type p53 (p53wt) we observed a high frequency of chromosome 1q gains, mainly partial trisomies, leading to upregulation of cancer consensus genes within minimally gained regions.

Essential genes specific to p53wt BL were studied in an unbiased functional genomics approach. We performed an RNAi screen in a panel of representative cell lines using a pooled shRNA library targeting genes beyond chr1q. Results obtained from the screen were robust and sensitive for identification of common as well as genotype-specific gene dependences. We identified the p53 inhibitor MDM4 as the strongest p53-dependent essential gene. Effects seen in the screen were highly reproducible and p53-dependence was confirmed in a p53 knock-out model.

Depletion of MDM4 in p53wt cell lines activated the p53 pathway resulting into p53 target gene expression, downregulation of proliferation signals (E2F targets, G2M checkpoint, MYC targets) and cell cycle arrest. In a mouse xenograft model, knock-down of MDM4 significantly reduced tumor growth, suggesting MDM4 as a promising therapeutic target. Moreover, a specific dependence of p53wt cell lines on MDM4 could be shown in a meta-analysis of a large genome-wide RNAi screen across cancer entities.

To understand the molecular impact of *TP53* mutations in aggressive B-cell lymphoma we derived a gene expression signature discriminating between patients with and without p53 mutation. MDM4 was exclusively upregulated in Burkitt lymphoma, but not in diffuse large B-cell lymphoma, while p53 pathway activity was reduced.

p53-specific effects were also validated for an additional candidate gene from our RNAi screen, *CDKN3*. Our data suggest a yet unknown mechanism of cell cycle regulation in the presence of wild-type p53. Furthermore, we expanded the data analysis of our RNAi screen to identify entity-specific vulnerabilities and distinguished Burkitt lymphoma and B-cell lymphoma essential genes that inquire further studies.

5 Discussion

Oncogenic MYC activation is the hallmark of Burkitt lymphoma (BL), but is not sufficient for tumorigenesis. Essential survival and proliferation signals are provided by mutations that activate the E2A transcription factor, tonic B-cell receptor signaling and PI3K signaling. In addition, the p53 tumor suppressor pathway is inactivated in 40% of BL by mutations of the *TP53* gene, but alternative mechanisms to escape MYC-driven p53 response in the remaining 60% are not known. In this study, we identified an association of chr1q32 gain with wild-type p53 patients. We further provide a functional genomics resource for identification of gene dependences in cell line models with defined p53 status. Among the candidate genes identified in an unbiased screening approach, the p53 inhibitor MDM4 was identified as an essential gene in BL retaining functional wild-type p53.

5.1 Recurrent genetic aberrations in Burkitt Lymphoma

Burkitt lymphoma is seen as a relatively homogeneous disease. Translocation of MYC is a hallmark characteristic of all BL and mutations that activate E2A transcription factor are found in 70% of BL. In addition, *TP53* mutations are found in 40% of patients, indicating the need for additional aberrations that abrogate MYC-induced oncogenic stress responses. To study alternative mechanisms besides of *TP53* mutation we analyzed the pattern of recurrent genetic aberrations in 67 BL cases (MMML consortium). *MYC* box I mutations, that abrogate activation of pro-apoptotic Bim, were previously reported to occur exclusively to *TP53* mutation[65]. We observed that *TP53* and *MYC* box I mutations occurred independent of each other and accounted for 54% of patients, while failsafe mechanisms in the remaining 46% of patients still remained elusive.

Correlation of p53 mutation status with recurrent copy number variations (CNVs) revealed an overrepresentation of chr1q gain in p53wt BL patients, and this observation was specific seen to BL, but not DLBCL. We observed a preference for partial trisomies of the proximal chr1q21-q23 bands and an additional minimally gained region at chr1q32. Chr1q gain is the most frequent CNV in BL (25%)[48,49,138]. Sequential karyotyping in relapsed patients revealed a higher incidence of chr1q gain in high-grade BL at diagnosis (39%) and upon relapse (64%)[139]. However, an association with p53 mutation status has not been reported.

Aberrations on chr1q are the most frequent CNV across cancer and mainly comprise amplifications or gains, rather than losses[61]. Cancer entities that show high frequency of chr1q gain include hepatocellular carcinoma (60%)[140,141], breast cancer (50-60%)[142,143], ovarian carcinoma (21%)[144], multiple myeloma (40% at diagnosis, 70% at relapse)[145,146] and non-Hodgkin´s lymphoma[147]. Amplified regions contain multiple well characterized oncogenes displaying a gene dosage effect (e.g. *CKS1B*, *MCL-1*, *UCK2*).

5.2 RNAi screen identifies p53-specific vulnerabilities

Analysis of the genetic landscape of BL greatly improved our understanding of its pathogenesis. However, the molecular impact of genetic aberrations is often not fully understood. Copy number variations affect large chromosomal regions and the contribution of single genes to tumorigenesis is not known. Genetic perturbation screens are a powerful technology to identify genes that are essential for cell proliferation or viability in an unbiased approach. The Broad Institute performed an RNAi screen in a large panel of cell lines across cancers and observed that cell lines carrying hotspot mutations in *BRAF* or *KRAS* strongly depend on the activated oncogene[113]. Melanoma patients carrying the *BRAF* V600E mutation were treated in clinical trials with the small molecule inhibitor vemurafenib that specifically inhibits the mutant isoform[148], but some patients acquire resistance[149]. RNAi screening in cell lines was used to identify resistance mechanisms that could guide future therapeutic approaches[150]. The oncogene *KRAS* is deemed to be an undruggable target for cancer therapy. Therefore, synthetic lethality screens were performed to find alternative druggable targets in *KRAS* mutant cancer[151-153]. As shown on cell lines from the Achilles project, loss-of-function mutations in tumor suppressors can lead to dependence on close homologs that compensate for the loss. Inactivating mutations in *ARID1A*, a member of the SWI/SNF nucleosome remodeling complex, are found in many human cancers and promote tumor formation. RNAi screen revealed that depletion of its homolog *ARID1B* is toxic to *ARID1A* mutant cancer cell lines[154]. These examples demonstrate that RNAi screens in representative cell line models are useful tools to assess differential functional dependences in defined subgroups beyond genetic characteristics.

To identify genes essential in MYC-driven BL that do not acquire *TP53* mutation we performed a shRNA screen in BL cell line models representing genetic patient subgroups. Four p53 wild-type (p53wt) BL cell lines that carried a chr1q gain were compared to four p53 mutant (p53mut) cell lines with normal copy number. A pooled shRNA library consisting of 27,500 shRNAs targeting more than 5,000 genes was used. For an unbiased approach we decided to use a shRNA library that was not limited to genes located on chromosome 1q, even though genetic data suggested p53-specific functions for this region. 237 of these genes were located on chr1q. ENSEMBL BioMart lists 945 protein coding genes on chr1q. Therefore, we covered 25% of all genes on chr1q, including characterized oncogenes.

As an indication of data robustness, common essential and non-essential genes across cell lines defined in a previous study[115] showed high concordance. Common essential genes were among the genes with the strongest shRNA depletion and were significantly enriched for proteasomal, ribosomal and spliceosomal genes, while non-essential genes showed unchanged shRNA counts and no enriched gene sets. Importantly, these effects were independent of the p53 mutation status. A high dynamic range allowed us to reliably distinguish between essential and non-essential genes.

To identify differential shRNA loss in genetically defined subgroups we combined two data analysis pipelines that were previously applied to pooled shRNA screens. The first pipeline compares differences in shRNA counts in two groups irrespectively of the actual depletion of shRNAs[113]. The second pipeline is a measurement of the strength of shRNA depletion and therefore the toxicity effects of the gene knock-down[131,132]. As described above, cell lines carrying *BRAF* or *KRAS* mutations strongly depend on the activated oncogene and RNAi screen identified both genes as the highest ranking genes based on differential shRNA representation in mutant versus wild-type cell lines. We tested the reliability of our screen to identify genotype-specific viability effects. The BL-2 cell line carries a *MYD88* mutation leading to activation of interleukin and Toll-Like receptor pathway. As shown previously in DLBCL of the ABC-subtype, MYD88 mutant cell lines depend on MYD88 itself and its downstream target, IRAK1[136]. By comparison of differential shRNA losses in BL-2 versus seven remaining cell lines we identified both *MYD88* and *IRAK1* among the highest-ranking genes with significant lower shRNA counts in the *MYD88*-mutant cell line. This example serves as a positive control demonstrating that we can identify genotype-specific effects even within single cell lines.

By comparison of differential shRNA losses in four p53wt and four p53mut BL cell lines we identified 12 candidate genes that were essential specifically in p53wt cell lines. Four genes, including two metabolic proteins (*GALNTL4*, *CYP39A1*) and two modulators of transcription (*BHMT2*, *HIST3H3*), were found to be essential in both groups of cell lines, but the dependence was stronger in p53wt cell lines. The highest ranking gene that was essential only in the presence of wild-type was the p53 inhibitor MDM4 that is located on chr1q32. Besides of MDM4 only HIST3H3 was located on chr1q and we did not observe an enrichment of genotype-specific essential genes by chromosomal location. A second candidate gene chosen for validation was the cell cycle regulator CDKN3.

5.3 MDM4 in Burkitt Lymphoma

The tumor suppressor p53 is the most frequently mutated gene in human cancer. p53 senses cellular stress such as DNA damage, hypoxia or oncogene activation and prevents uncontrolled proliferation and malignant transformation by transactivation of multiple target genes that regulate DNA repair, cell cycle, apoptosis, senescence, differentiation, metabolism and angiogenesis[155]. Over 80% of mutations occur in the DNA binding domain and many mutations inactivate its transcriptional activity[156,157]. p53 mutations are found on average in 50% of human cancers. However, the incidence strongly varies by entity and ranges from 5% in renal cell carcinoma and 10% in melanoma to 70% of small cell lung cancer and 90% in ovarian cancer[158,159]. The high incidence of p53 mutations in cancer suggests that probably all tumor cells inactive this tumor suppressor pathway, either by p53 mutation or by alternative mechanisms. Identification of factors that suppress p53 response may constitute an important strategy to develop targeted therapies based on the restoration of p53 activity.

We identified *MDM4* as an essential gene in Burkitt lymphoma cell lines without p53 mutation. p53-dependence was confirmed in an isogenic p53-/- cell line. MDM4 and its close homologue MDM2 are the two major p53 inhibitors consisting of a highly conserved C-terminal p53 binding domain, an internal acidic domain and an N-terminal RING finger domain[82,84]. Binding to the N-terminal transactivation domain of p53 suppresses p53-mediated transcription[160]. MDM2, but not MDM4, acts as an E3-ubiquitin ligase and targets p53 for proteasomal degradation[83]. This process involves the RING finger domain of MDM2 and its less conserved acidic domain[161]. The RING finger domain also mediates homo- and heterodimerization of MDM2 and MDM4, an important regulatory element which can both stabilize or destabilize the proteins[162,163]. Mutations within the RING finger domain and loss of either MDM2 or MDM4 are embryonic lethal in the presence of p53 and concomitant loss of p53 rescues the observed toxicity, demonstrating that both MDM proteins are needed for full suppression of p53[164-168]. In unstressed cells, MDM4 evades MDM2-mediated degradation by association with the deubiquitinase HAUSP. Stabilized MDM4 translocates MDM2 to the nucleus and protects it from self-ubiquitination[169,170]. Therefore, MDM4 can indirectly influence p53 level by regulation of MDM2. Upon DNA damage, MDM4 is phosphorylated by ARF which decreases binding affinity towards HAUSP and increases association with 14-3-3 protein, which redirects the E3-ubiquitin-ligase activity of MDM2 from p53 towards MDM4[171,172]. While MDM2 is a transcriptional target of p53 and inhibits p53 activity in a negative feedback loop, MDM4 is constitutively expressed independent of p53 and regulated on a post-transcriptional and post-translational level[160].

MDM2 and MDM4 are often overexpressed in a mutually exclusive pattern in cancers that retain wild-type p53[173]. Amplification of the MDM4 locus on chr1q32 was first described in glioblastoma[174] and further characterized by the Cancer Genome Atlas Research Network. Focal gains of MDM4 were detected in 4% of gliomas and were mutually exclusive to MDM2 amplifications on chr12q15, that occurred in 11%, or p53 aberrations present in 38% of untreated and 58% of treated patients[175]. MDM4 is also amplified in 10-14% of breast cancer, while MDM2 amplification is seen in about 4%[159,176,177]. MDM4 and *TP53* aberrations were mutually exclusive (p=0.013) and MDM2 showed tendencies towards exclusivity with MDM4 amplification and *TP53* aberrations[159]. In a mouse xenograft model, MDM4 amplification promoted clonal outgrowth[178]. In 17% of soft tissue sarcomas MDM4 was found to be amplified[179]. A more detailed analysis revealed a subtype-specific pattern for MDM4 and MDM2 amplifications. Both genes were equally amplified in osteosarcoma (MDM2/MDM4, 35%/35%), while MDM2 prevailed in well-differentiated liposarcoma (70%/0%) and de-differentiated liposarcoma (50%/13%) and MDM4 was more frequently amplified in Ewing´s sarcoma (38%/50%) and synovial sarcoma (33%/44%)[180]. Prevalence for MDM4 amplification was also observed in retinoblastoma (10%/65%) and ectopically overexpressed MDM4 in *Rb*-deficient retinal cells promoted retinoblastoma[181]. Notably, elevated MDM4 protein level was detected in 65% of cutaneous melanoma, a disease that rarely acquires *TP53* mutations (17%) and poorly responds to chemotherapy. MDM4 overexpression was not observed on mRNA

level and MDM4 amplifications are rare (8%)[159]. These findings suggest that the role of MDM4 deregulation in cancer might be underestimated. In BL, little is known about the role of MDM4. One study in pediatric BL identified MDM4 amplification in 5/25 patients which was correlated with elevated mRNA level, but not with protein level[182]. Amplifications of chr1q are the most frequent copy number alteration in BL[49]. In our study, we show for the first time an association of chr1q32 gain with wild-type p53 in BL patients.

MDM2 and MDM4 amplifications often occur exclusive to each other and overexpression of one member is sufficient to suppress p53. The distinct pattern of amplifications indicates yet unknown specific molecular mechanisms for MDM2 and MDM4. Overexpression of MDM4 overcomes cellular senescence triggered by oncogenic Ras activation in murine and human fibroblasts[176,183,184]. In addition, pro-survival signaling through the PI3K/AKT/mTOR signaling axis in hepatocellular carcinoma was shown to suppress the p53 pathway by phosphorylation and stabilization of MDM4[185].

Restoration of p53 activity by targeting of MDM2 and MDM4 is a promising therapeutic approach. The small molecule inhibitor nutlin-3 was identified in a chemical screen for compounds that target the p53-binding pocket of MDM2 and therefore competes with p53 binding[186]. Nutlin-3 activates the p53 pathway in cancer cell lines without *TP53* mutation[187] and induces cell cycle arrest or apoptosis in a cell line dependent context[188]. Factors that influence the decision on p53 response were studied in a synthetic lethality screen, but are still incompletely understood[189]. Thereby, the use of nutlin-3 as a single agent in the clinic is limited[190,191]. In combination with genotoxic reagents or cyclin-dependent kinase inhibitors, nutlin-3 synergizes in the induction of apoptosis[187,192,193]. The strong conservation and high structural similarity of the p53 binding pocket with MDM4 suggested dual-specificity[194]. However, nutlin-3 shows much lower binding affinities for MDM4 and MDM4 overexpression can confer resistance towards nutin-3 induced apoptosis[195,196]. A small-molecule inhibitor with high specificity for the MDM4 p53-binding site[197] showed anti-proliferative effects in p53 wild-type HCC cell lines[185]. However, the efficiency of this inhibitor was limited by the instability of the MDM4-inhibitor complex[198]. The development of peptide inhibitors did not result into promising therapeutic reagents so far, mostly hampered by poor biochemical properties[199]. Modification of α-helical peptides modified with side chains, such as hydrocarbons, result into so called stapled peptides with increased cell permeability and stability[200]. The stapled peptide SAH-p53-8 that mimics the p53 α-helical peptide shows high binding affinity towards MDM4 and exerts cytotoxic effects in HCC cell lines by activation of the p53 pathway[201]. The peptide was also shown to be active in cutaneous melanoma[202] and uveal melanoma[203].

Following MDM4 knock-down, we observed activation of the p53 pathway and cell cycle arrest in BL cell lines. For future therapeutic approaches, understanding the switch between cell cycle arrest and apoptotic response is of great importance. The sensitivity of p53wt BL cell lines towards MDM2 knock-down and nutlin-3 suggests that dual inhibition might be more effective. Reasonable drug combinations of p53 reactivation and DNA-damaging reagents may

show improved cytotoxic effects. MDM4 was also identified as a gene significantly more toxic in p53wt cancer cell lines across entities, emphasizing that MDM4 is a promising therapeutic target.

5.4 Potential role of the cell cycle regulator CDKN3 in the p53 pathway

We identified *CDKN3* as a specifically essential gene in Burkitt lymphoma with wild-type p53. CDKN3 is a dual-specificity phosphatase that removes phosphorylation from serine as well as threonine and controls chromosomal integrity during mitosis in three major ways: (1) CDKN3 inactivates CDK2, a key initiator of G1-S transition, and hereby induces G1 checkpoint arrest[204-206]. (2) CDKN3 dephosphorylates CDK1 during mitotic exit. Knock-down of CDKN3 increases the number of centrosomes and weakens spindle assembly checkpoint which can subsequently lead to aneuploidy[207]. (3) CDKN3 directly targets Mps-1 (monopolar spindle 1), a regulator of centrosome duplication, formation and chromosomal spindle attachment that is activated during mitosis by CDK2[208]. Depletion of CDKN3 leads to excess Mps-1 levels resulting into overduplication of centrosomes and multinucleated cells[209].

In our study CDKN3 knock-down in BL cell lines decreased proliferation and induced G1 cell cycle arrest. This is in line with previous studies in cervical cancer lines[204,210,211] and the hepatocellular carcinoma cell line Huh-7[212]. In HeLa cells, a strong increase of CDKN3 expression was observed during G1-S transition, which could explain the preference for G1-arrest[204].

CDKN3 was found to be overexpressed in many cancers, including renal cell carcinoma[213], hepatocellular carcinoma[214], thyroid cancers[215], cervical cancer[211], ovarian carcinoma[216], breast and prostate cancer[210]. Overexpression was not caused by amplification of the CDKN3 chromosomal location on chr14q22 and the mechanism of CDKN3 regulation is still unknown. It might be a surrogate marker for proliferating cells. However, it was not tested if CDKN3 level fluctuated during cell cycle as shown for HeLa cells[204]. High CDKN3 level was frequently observed to be associated with higher tumor grade and poor patient outcome[213,214,216,217]. During B cell differentiation CDKN3 expression was characteristic for germinal center B cells of the dark zone, while a strong downregulation in light zone B cells was observed[9]. Therefore, high CDKN3 expression might be an additional centroblast-specific characteristic that is retained during transformation of post-germinal center B cells. Burkitt lymphoma is characterized by a high proliferation rate (Ki67>95%), but CDKN3 expression level were not reported yet. Analysis of published microarray data showed that CDKN3 was highly expressed in studies on aggressive B-NHL, and especially studies including Burkitt lymphoma (Figure 38A). In the study of Hummel et al. (2005), that was used to derive a molecular signature for Burkitt lymphoma, CDKN3 was significantly overexpressed in the group of molecular Burkitt lymphoma, compared to non-Burkitt lymphoma (DLBCL) (Figure 38B).

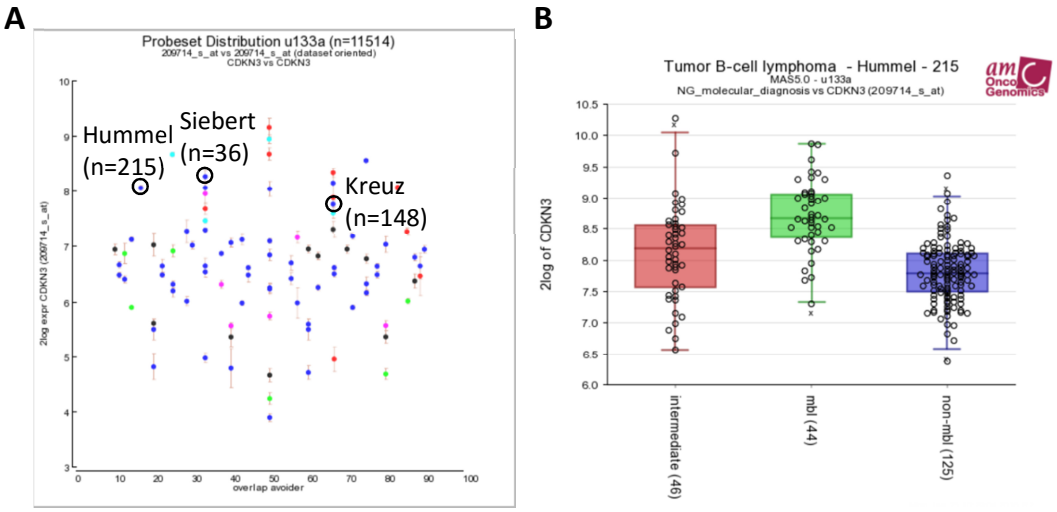

Figure 38: Microarray data on CDKN3 expression in aggressive lymphomas
(A) Expression of CDKN3 in publically available gene expression studies using Affymetrix U133a microarray. The visualization was created by the R2 platform (http://r2.amc.nl). Highlighted are studies including aggressive B-NHL (MMML consortium). **(B)** CDKN3 expression level in 215 aggressive B-NHL by molecular classification. (green: molecular Burkitt lymphoma – mbl; blue: non-molecular Burkitt lymphoma – non-mbl; red: intermediated cases)

CDKN3 expression did not contribute to the p53 signature that differentiated p53wt and p53mut cases. However, we observed p53-specific effects in our cell line models. MDM4 knock-down led to p53-dependent depletion of CDKN3 mRNA. In a time course experiment, CDKN3 depletion seems to occur with a delay following activation of the p53 pathway. The exact mechanisms by which CDKN3 might be regulated, is unknown. A previous study showed that the p53 target p21, that mediates cell cycle arrest, was inversely correlated with CDKN3, and p21 knock-down increased CDKN3 levels[218]. The phosphatase Cdc25a exerts similar functions than CDKN3 and is a well characterized oncogene[219]. Cdc25a is a transcriptional target of MYC and mediates G1-S transition by activation of the CDK2/cyclin E complex[220]. Moreover, Cdc25a competes with p21 for CDK2-binding and is therefore counterbalancing the tumor suppressive function of p53[221]. Upon DNA damage, Cdc25a is downregulated by a mechanisms involving checkpoint kinase 1 (Chk1)[222]. p53 can lead to downregulation of Cdc25a by transcriptional activation of miR-365 that targets Cdc25a mRNA for degradation[223].

Upon CDKN3 depletion we observed upregulation of p53 target genes. Whether these effects are direct or indirect via DNA stress response is currently unclear.

5.5 BL-specific vulnerability

Our study was designed to identify p53-specific essential genes. To further understand the pathogenesis of BL we wanted to also identify entity-specific essential genes. The Achilles

project included 216 cell lines, but Burkitt lymphoma was not represented[112]. One study on the pathogenesis of BL included a RNAi drop-out screen in several BL cell lines, but the shRNA library was restricted to selected genes mainly within the B-cell receptor pathway[44]. Therefore, our screen is the largest and most comprehensive genetic perturbation screen in Burkitt lymphoma. To find entity-specific essential genes, we combined our data set with three RNAi screens performed by Cellecta.

We identified the genes *PAX5* and *FLI1* as the most robust candidate genes. In a comparison of BL versus other haematopoietic/lymphoid cell lines we also identified *PAX5* as one of the highest scoring genes. In a recent genetic perturbation screen using genome-wide CRISPR/Cas9 sgRNA libraries, *PAX5* was identified as one of the top candidate genes that was essential in two BL cell lines, but dispensable in two CML cell lines[126]. *PAX5* is a transcription factor of the conserved paired box (PAX) protein family. It is highly expressed in all mature B-cells except for plasma cells and initiates B-cell specific programs both by activation and repression of its target genes[224,225]. *PAX5* deregulation has been implicated in the pathogenesis of B cell malignancies, such as acute lymphoblastic leukemia and some non-Hodgkin´s lymphomas. Deletion of *PAX5* on 9p13 has been described in some cases, as well as translocation to various sites within the genome, that can either activate or deactivate *PAX5*. Therefore, *PAX5* can function as a tumor suppressor or oncogene[226-228]. Chromosomal aberration of *PAX5* has not been described in BL and further studies are needed to clarify, why *PAX5* is essential in all BL cell lines, but not in other B-cell derived lymphoma cell lines.

The transcription factor *FLI1* (Friend Leukemia integration factor, synonym ERGB) was identified in our RNAi screen comparison as an essential gene in BL as well as non-BL cell lines of the lymphoid lineage. We compared published RNA sequencing data in more than 600 cell lines and found an overexpression of *FLI1* in lymphoid compared to non-lymphoid cell lines[133]. *FLI1* belongs to the ETS (E26 transformation specific) transcription protein family and plays a key role in normal hematopoiesis by regulation of stem cell maintenance and differentiation[229-231]. This proto-oncogene was first identified in erythroleukemias induced by Friend Murine Leukemia Virus-infected erythroblasts[232]. However, overexpression of *FLI1* in transgenic mice induces B cell lymphomas rather than erythroleukemias[233]. Besides of virally induced tumors, *FLI1* has been shown to be involved in the pathogenesis of the pediatric bone cancer Ewing´s sarcoma that is positive for the *EWS-FLI1* fusion protein in 80% of the cases[234]. High level of *FLI1* can also provoke autoimmune diseases, such as systemic lupus erythematosus. The multiple involvements of *FLI1* in disease formation motivated attempts to develop FLI1-specific inhibitors[235]. Topoisomerase inhibitors were also reported to work in part by FLI1 inhibition in Ewing´s sarcoma[236,237]. *FLI1* is not described to be deregulated in BL and its role in leukemogenesis has to be evaluated in further studies.

The identification B cell specific vulnerabilities using RNAi screens enables development of targeted therapies with reduced overall toxicity compared to chemotherapeutic reagents.

6 Conclusion and Perspective

Insights into the pathogenesis of Burkitt lymphoma beyond oncogenic MYC activation were gained from molecular and genetic profiling. Here we describe the association of chr1q gain with wild-type p53. Using an RNAi screen in a panel of representative cell lines we were able to identify essential genes and to link specific gene dependences to the genotype. We identified a strong dependence of the BL-2 cell line on the mutated *MYD88* oncogene, as well as downstream members of the associated signaling pathway, proving the validity of our approach. Moreover, we identified p53-specific gene dependences in BL. Integration of observed genetic dependences and molecular patient profiles revealed, that amplification and overexpression of MDM4 contributes to BL pathogenesis in the absence of p53 mutations. We identified MDM4 as the main target of chr1q amplification essential for cell propagation. MDM4 also ranked among the prime candidate genes when our analysis was expanded to a large genome-wide RNAi screen across cancer. Therefore, reactivation of p53 following MDM4 depletion or inhibition is a promising therapeutic approach.

We observed p53-specific effects following knock-down of the phosphatase CDKN3 that is often overexpressed in cancer. So far, CDKN3 was not linked to the p53 pathway and further studies are needed to clarify the interaction between CDKN3 and p53. Cell cycle deregulation by mutation of *CCND3*, a cyclin that is expressed during G1/S-transition, is frequently observed in BL. Our data provides further evidence for the role of cell cycle regulation and safety checkpoints in BL and might help to find future therapeutic targets.

BL was not represented in the Achilles project, that characterized gene dependences in 216 cancer cell lines[112], and previous genetic perturbation studies in BL were either based on pathway specific RNAi libraries[44] or limited in the number of cell lines[126]. Our data set presents the most comprehensive study on genetic vulnerabilities in BL. Beyond the scope of our p53-based project, we identified entity-specific genes by integration of multiple RNAi screens. Validation and functional characterization is still ongoing, but based on our previous experience, data obtained from the drop-out screen is very robust and reproducible. We conclude that functional screens are a valuable resource for identification of cellular context-specific essential genes. The novel CRISPR-technology rapidly evolves as an alternative to RNAi and may guide future genetic perturbation screens. Combination with primary patient data adds an additional layer to omics data and greatly improves our understanding of pathogenic mechanisms in cancer.

Publications and Conferences

MECHANISMS OF MALIGNANT TRANSFORMATION IN *TP53* WILD-TYPE BURKITT LYMPHOMA BY INTEGRATION OF MOLECULAR AND FUNCTIONAL GENOMICS

Jennifer Huellein[1], Mikolaj Slabicki[1], Maciej Rosolowski[2], René Scholtysik[5], Alexander Jethwa[1], Marina Lukas[1], Katarzyna Tomska[1], Hanne Helferich[4], Reiner Siebert[3], Ralf Küppers[5], Michael Hummel[6], Wolfram Klapper[7], Stephan Stilgenbauer[4], Markus Löffler[2], Markus Kreuz[2], Lorenz Trümper[8], Christof von Kalle[1] , and Thorsten Zenz[1, 9]

[1]Department of Translational Oncology, NCT and DKFZ, Heidelberg, Germany; [2] Institute for Medical Informatics, Statistic and Epidemiology, Leipzig, Germany; [3] Department of Human Genetics, Christian-Albrechts University Kiel & University Hospital Schleswig-Holstein, Kiel, Germany; [4] Department of Internal Medicine III, University of Ulm, Germany; [5] Institute of Cell Biology (Cancer Research), University of Duisburg-Essen, Medical School, Essen, Germany; [6] Institute of Pathology, Charité–University Medicine Berlin, Berlin, Germany; [7] Department of Pathology, Hematopathology Section and Lymph Node Registry, University Hospital Schleswig-Holstein, Campus Kiel, Christian-Albrechts-University Kiel, Kiel, Germany; [8] Department of Hematology and Medical Oncology, Göttingen University Medical Center, Göttingen, Germany
[9] Department of Medicine V, Heidelberg University Medical Center, Heidelberg, Germany

13th International Conference On Malignant Lymphoma, June 2015, Lugano, Switzerland

ANALYSIS OF MECHANISMS OF MALIGNANT TRANSFORMATION IN *TP53* WILD-TYPE BURKITT LYMPHOMA BY INTEGRATION OF MOLECULAR AND FUNCTIONAL GENOMICS DATA

Jennifer Huellein[1], Mikolaj Slabicki[1], Maciej Rosolowski[2], René Scholtysik[5], Alexander Jethwa[1], Marina Lukas[1], Katarzyna Tomska[1], Hanne Helferich[4], Reiner Siebert[3], Ralf Küppers[5], Michael Hummel[6], Wolfram Klapper[7], Stephan Stilgenbauer[4], Markus Löffler[2], Markus Kreuz[2], Lorenz Trümper[8], Christof von Kalle[1] , and Thorsten Zenz[1, 9]

[1]Department of Translational Oncology, NCT and DKFZ, Heidelberg, Germany; [2] Institute for Medical Informatics, Statistic and Epidemiology, Leipzig, Germany; [3] Department of Human Genetics, Christian-Albrechts University Kiel & University Hospital Schleswig-Holstein, Kiel, Germany; [4] Department of Internal Medicine III, University of Ulm, Germany; [5] Institute of Cell Biology (Cancer Research), University of Duisburg-Essen, Medical School, Essen, Germany; [6] Institute of Pathology, Charité–University Medicine Berlin, Berlin, Germany; [7] Department of Pathology, Hematopathology Section and Lymph Node Registry, University Hospital Schleswig-Holstein, Campus Kiel, Christian-Albrechts-University Kiel, Kiel, Germany; [8] Department of Hematology and Medical Oncology, Göttingen University Medical Center, Göttingen, Germany
[9] Department of Medicine V, Heidelberg University Medical Center, Heidelberg, Germany

20th Congress of the European Hematology Association, June 2015, Vienna, Germany

Mechanisms of malignant transformation in *TP53* wild-type Burkitt´s lymphoma

Jennifer Huellein[1], Mikolaj Slabicki[1], Alexander Jethwa[1], Marina Lukas[1], Kartazyna Tomska[1], Maciej Rosolowski[3], Markus Kreuz[3], Christof von Kalle[1] and Thorsten Zenz[1,2]

[1]Department of Translational Oncology, NCT and DKFZ, Heidelberg, Germany
[2]Department for Medicine V, Heidelberg University Medical Center, Heidelberg, Germany
[3] Institute for Medical Informatics, Statistic and Epidemiology, Leipzig, Germany

DKFZ PhD Retreat, July 2014, Weil der Stadt

Mechanisms of malignant transformation in Burkitt´s lymphoma without *TP53* aberrations

Jennifer Huellein[1], Mikolaj Slabicki[1], Alexander Jethwa[1], Marina Lukas[1], Kartazyna Tomska[1], Maciej Rosolowski[3], Markus Kreuz[3], Christof von Kalle[1] and Thorsten Zenz[1,2]

[1]Department of Translational Oncology, NCT and DKFZ, Heidelberg, Germany
[2]Department for Medicine V, Heidelberg University Medical Center, Heidelberg, Germany
[3]Institute for Medical Informatics, Statistics and Epidemiology, Leipzig, Germany

DKFZ PhD Student Poster Presentation, December 2014, Heidelberg, Germany

References

1 Bassing, C. H., Swat, W. & Alt, F. W. The mechanism and regulation of chromosomal V(D)J recombination. *Cell* **109 Suppl**, S45-55 (2002).

2 Stavnezer, J., Guikema, J. E. & Schrader, C. E. Mechanism and regulation of class switch recombination. *Annual review of immunology* **26**, 261-292, doi:10.1146/annurev.immunol.26.021607.090248 (2008).

3 Mani, R. S. & Chinnaiyan, A. M. Triggers for genomic rearrangements: insights into genomic, cellular and environmental influences. *Nat Rev Genet* **11**, 819-829, doi:10.1038/nrg2883 (2010).

4 Klein, U. & Dalla-Favera, R. Germinal centres: role in B-cell physiology and malignancy. *Nat Rev Immunol* **8**, 22-33, doi:10.1038/nri2217 (2008).

5 Basso, K. & Dalla-Favera, R. Germinal centres and B cell lymphomagenesis. *Nat Rev Immunol* **15**, 172-184, doi:10.1038/nri3814 (2015).

6 MacLennan, I. C. Germinal centers. *Annual review of immunology* **12**, 117-139, doi:10.1146/annurev.iy.12.040194.001001 (1994).

7 Hu, B. T., Lee, S. C., Marin, E., Ryan, D. H. & Insel, R. A. Telomerase is up-regulated in human germinal center B cells in vivo and can be re-expressed in memory B cells activated in vitro. *Journal of immunology* **159**, 1068-1071 (1997).

8 Hanahan, D. & Weinberg, R. A. Hallmarks of cancer: the next generation. *Cell* **144**, 646-674, doi:10.1016/j.cell.2011.02.013 (2011).

9 Victora, G. D. *et al.* Identification of human germinal center light and dark zone cells and their relationship to human B-cell lymphomas. *Blood* **120**, 2240-2248, doi:10.1182/blood-2012-03-415380 (2012).

10 Kuppers, R., Klein, U., Hansmann, M. L. & Rajewsky, K. Cellular origin of human B-cell lymphomas. *N Engl J Med* **341**, 1520-1529, doi:10.1056/NEJM199911113412007 (1999).

11 Lenz, G. & Staudt, L. M. Aggressive lymphomas. *N Engl J Med* **362**, 1417-1429, doi:10.1056/NEJMra0807082 (2010).

12 Kuppers, R. & Dalla-Favera, R. Mechanisms of chromosomal translocations in B cell lymphomas. *Oncogene* **20**, 5580-5594, doi:10.1038/sj.onc.1204640 (2001).

13 Tsujimoto, Y., Gorham, J., Cossman, J., Jaffe, E. & Croce, C. M. The t(14;18) chromosome translocations involved in B-cell neoplasms result from mistakes in VDJ joining. *Science* **229**, 1390-1393 (1985).

14 de Boer, C. J. *et al.* Multiple breakpoints within the BCL-1 locus in B-cell lymphoma: rearrangements of the cyclin D1 gene. *Cancer Res* **53**, 4148-4152 (1993).

15 Dalla-Favera, R. *et al.* Human c-myc onc gene is located on the region of chromosome 8 that is translocated in Burkitt lymphoma cells. *Proceedings of the National Academy of Sciences of the United States of America* **79**, 7824-7827 (1982).

16 Ladanyi, M., Offit, K., Jhanwar, S. C., Filippa, D. A. & Chaganti, R. S. MYC rearrangement and translocations involving band 8q24 in diffuse large cell lymphomas. *Blood* **77**, 1057-1063 (1991).

17 Phan, R. T. & Dalla-Favera, R. The BCL6 proto-oncogene suppresses p53 expression in germinal-centre B cells. *Nature* **432**, 635-639, doi:10.1038/nature03147 (2004).

18 Pasqualucci, L. *et al.* Hypermutation of multiple proto-oncogenes in B-cell diffuse large-cell lymphomas. *Nature* **412**, 341-346, doi:10.1038/35085588 (2001).

19 Swerdlow, S. H. C., E.; Harris, N.L.; Jaffe, E.S.; Pileri, S.A.; Stein, H.; Thiele, J.; Vardiman, J.W. WHO Classification of Tumours of Haematopoietic and Lymphoid Tissues. *IARC Press* (2008).

20 Ziegler, J. L. *et al.* Outbreak of Burkitt's-like lymphoma in homosexual men. *Lancet* **2**, 631-633 (1982).

21 Jaffe, E. S. The 2008 WHO classification of lymphomas: implications for clinical practice and translational research. *Hematology / the Education Program of the American Society of Hematology. American Society of Hematology. Education Program*, 523-531, doi:10.1182/asheducation-2009.1.523 (2009).

22 Burkitt, D. A sarcoma involving the jaws in African children. *Br J Surg* **46**, 218-223 (1958).

23 Burchenal, J. H. Geographic chemotherapy--Burkitt's tumor as a stalking horse for leukemia: presidential address. *Cancer Res* **26**, 2393-2405 (1966).

24 Epstein, M. A., Achong, B. G. & Barr, Y. M. Virus Particles in Cultured Lymphoblasts from Burkitt's Lymphoma. *Lancet* **1**, 702-703 (1964).

25 Facer, C. A. & Playfair, J. H. Malaria, Epstein-Barr virus, and the genesis of lymphomas. *Adv Cancer Res* **53**, 33-72 (1989).

26 Breen, E. C. *et al.* The development of AIDS-associated Burkitt's/small noncleaved cell lymphoma is preceded by elevated serum levels of interleukin 6. *Clin Immunol* **92**, 293-299, doi:10.1006/clim.1999.4760 (1999).

27 Zech, L., Haglund, U., Nilsson, K. & Klein, G. Characteristic chromosomal abnormalities in biopsies and lymphoid-cell lines from patients with Burkitt and non-Burkitt lymphomas. *Int J Cancer* **17**, 47-56 (1976).

28 Linch, D. C. Burkitt lymphoma in adults. *British journal of haematology* **156**, 693-703, doi:10.1111/j.1365-2141.2011.08877.x (2012).

29 Magrath, I. Epidemiology: clues to the pathogenesis of Burkitt lymphoma. *British journal of haematology* **156**, 744-756, doi:10.1111/j.1365-2141.2011.09013.x (2012).

30 Hesseling, P., Molyneux, E., Kamiza, S., Israels, T. & Broadhead, R. Endemic Burkitt lymphoma: a 28-day treatment schedule with cyclophosphamide and intrathecal methotrexate. *Annals of tropical paediatrics* **29**, 29-34, doi:10.1179/146532809X402006 (2009).

31 Mbulaiteye, S. M., Biggar, R. J., Bhatia, K., Linet, M. S. & Devesa, S. S. Sporadic childhood Burkitt lymphoma incidence in the United States during 1992-2005. *Pediatr Blood Cancer* **53**, 366-370, doi:10.1002/pbc.22047 (2009).

32 Miles, R. R., Arnold, S. & Cairo, M. S. Risk factors and treatment of childhood and adolescent Burkitt lymphoma/leukaemia. *British journal of haematology* **156**, 730-743, doi:10.1111/j.1365-2141.2011.09024.x (2012).

33 Salaverria, I. *et al.* Chromosomal alterations detected by comparative genomic hybridization in subgroups of gene expression-defined Burkitt's lymphoma. *Haematologica* **93**, 1327-1334, doi:10.3324/haematol.13071 (2008).

34 Molyneux, E. M. *et al.* Burkitt's lymphoma. *Lancet* **379**, 1234-1244, doi:10.1016/S0140-6736(11)61177-X (2012).

35 Patte, C. *et al.* The Societe Francaise d'Oncologie Pediatrique LMB89 protocol: highly effective multiagent chemotherapy tailored to the tumor burden and initial response in 561 unselected children with B-cell lymphomas and L3 leukemia. *Blood* **97**, 3370-3379 (2001).

36 Patte, C. *et al.* High survival rate in advanced-stage B-cell lymphomas and leukemias without CNS involvement with a short intensive polychemotherapy: results from the French Pediatric Oncology Society of a randomized trial of 216 children. *Journal of clinical oncology : official journal of the American Society of Clinical Oncology* **9**, 123-132 (1991).

37 Divine, M. *et al.* Burkitt lymphoma in adults: a prospective study of 72 patients treated with an adapted pediatric LMB protocol. *Ann Oncol* **16**, 1928-1935, doi:10.1093/annonc/mdi403 (2005).

38 Thomas, D. A. *et al.* Chemoimmunotherapy with hyper-CVAD plus rituximab for the treatment of adult Burkitt and Burkitt-type lymphoma or acute lymphoblastic leukemia. *Cancer* **106**, 1569-1580, doi:10.1002/cncr.21776 (2006).

39 Murphy, S. B. Classification, staging and end results of treatment of childhood non-Hodgkin's lymphomas: dissimilarities from lymphomas in adults. *Seminars in oncology* **7**, 332-339 (1980).

40 Murphy, S. B., Fairclough, D. L., Hutchison, R. E. & Berard, C. W. Non-Hodgkin's lymphomas of childhood: an analysis of the histology, staging, and response to treatment of 338 cases at a single institution. *Journal of clinical oncology : official journal of the American Society of Clinical Oncology* **7**, 186-193 (1989).

41 Lones, M. A. *et al.* Mature B-cell lymphoma/leukemia in children and adolescents: intergroup pathologist consensus with the revised European-American Lymphoma Classification. *Ann Oncol* **11**, 47-51 (2000).

42 Dave, S. S. *et al.* Molecular diagnosis of Burkitt's lymphoma. *N Engl J Med* **354**, 2431-2442, doi:10.1056/NEJMoa055759 (2006).

43 Hummel, M. *et al.* A biologic definition of Burkitt's lymphoma from transcriptional and genomic profiling. *N Engl J Med* **354**, 2419-2430, doi:10.1056/NEJMoa055351 (2006).

44 Schmitz, R. *et al.* Burkitt lymphoma pathogenesis and therapeutic targets from structural and functional genomics. *Nature* **490**, 116-120, doi:10.1038/nature11378 (2012).

45 Poirel, H. A. *et al.* Specific cytogenetic abnormalities are associated with a significantly inferior outcome in children and adolescents with mature B-cell non-Hodgkin's lymphoma: results of the FAB/LMB 96 international study. *Leukemia* **23**, 323-331, doi:10.1038/leu.2008.312 (2009).

46 Nelson, M. *et al.* An increased frequency of 13q deletions detected by fluorescence in situ hybridization and its impact on survival in children and adolescents with Burkitt lymphoma: results from the Children's Oncology Group study CCG-5961. *British journal of haematology* **148**, 600-610, doi:10.1111/j.1365-2141.2009.07967.x (2010).

47 Toujani, S. *et al.* High resolution genome-wide analysis of chromosomal alterations in Burkitt's lymphoma. *PloS one* **4**, e7089, doi:10.1371/journal.pone.0007089 (2009).

48 Davidsson, J. *et al.* Tiling resolution array comparative genomic hybridization, expression and methylation analyses of dup(1q) in Burkitt lymphomas and pediatric high hyperdiploid acute lymphoblastic leukemias reveal clustered near-centromeric breakpoints and overexpression of genes in 1q22-32.3. *Human molecular genetics* **16**, 2215-2225, doi:10.1093/hmg/ddm173 (2007).

49 Scholtysik, R. *et al.* Detection of genomic aberrations in molecularly defined Burkitt's lymphoma by array-based, high resolution, single nucleotide polymorphism analysis. *Haematologica* **95**, 2047-2055, doi:10.3324/haematol.2010.026831 (2010).

50 Schiffman, J. D. *et al.* Genome wide copy number analysis of paediatric Burkitt lymphoma using formalin-fixed tissues reveals a subset with gain of chromosome 13q and corresponding miRNA over expression. *British journal of haematology* **155**, 477-486, doi:10.1111/j.1365-2141.2011.08883.x (2011).

51 Lundin, C. *et al.* Submicroscopic genomic imbalances in Burkitt lymphomas/leukemias: association with age and further evidence that 8q24/MYC translocations are not sufficient for leukemogenesis. *Genes, chromosomes & cancer* **52**, 370-377, doi:10.1002/gcc.22034 (2013).

52 Onciu, M. *et al.* Secondary chromosomal abnormalities predict outcome in pediatric and adult high-stage Burkitt lymphoma. *Cancer* **107**, 1084-1092, doi:10.1002/cncr.22089 (2006).

53 Havelange, V. *et al.* Patterns of genomic aberrations suggest that Burkitt lymphomas with complex karyotype are distinct from other aggressive B-cell lymphomas with MYC rearrangement. *Genes, chromosomes & cancer* **52**, 81-92, doi:10.1002/gcc.22008 (2013).

54 Karpova, M. B. *et al.* Combined spectral karyotyping, comparative genomic hybridization, and in vitro apoptyping of a panel of Burkitt's lymphoma-derived B cell lines reveals an unexpected complexity of chromosomal aberrations and a recurrence

of specific abnormalities in chemoresistant cell lines. *International journal of oncology* **28**, 605-617 (2006).

55 Maria Murga Penas, E. *et al.* Comprehensive cytogenetic and molecular cytogenetic analysis of 44 Burkitt lymphoma cell lines: secondary chromosomal changes characterization, karyotypic evolution, and comparison with primary samples. *Genes, chromosomes & cancer* **53**, 497-515, doi:10.1002/gcc.22161 (2014).

56 O'Donnell, K. A., Wentzel, E. A., Zeller, K. I., Dang, C. V. & Mendell, J. T. c-Myc-regulated microRNAs modulate E2F1 expression. *Nature* **435**, 839-843, doi:10.1038/nature03677 (2005).

57 Mu, P. *et al.* Genetic dissection of the miR-17~92 cluster of microRNAs in Myc-induced B-cell lymphomas. *Genes & development* **23**, 2806-2811, doi:10.1101/gad.1872909 (2009).

58 Xiao, C. *et al.* Lymphoproliferative disease and autoimmunity in mice with increased miR-17-92 expression in lymphocytes. *Nat Immunol* **9**, 405-414, doi:10.1038/ni1575 (2008).

59 Tagawa, H., Karube, K., Tsuzuki, S., Ohshima, K. & Seto, M. Synergistic action of the microRNA-17 polycistron and Myc in aggressive cancer development. *Cancer Sci* **98**, 1482-1490, doi:10.1111/j.1349-7006.2007.00531.x (2007).

60 Volinia, S. *et al.* A microRNA expression signature of human solid tumors defines cancer gene targets. *Proceedings of the National Academy of Sciences of the United States of America* **103**, 2257-2261, doi:10.1073/pnas.0510565103 (2006).

61 Beroukhim, R. *et al.* The landscape of somatic copy-number alteration across human cancers. *Nature* **463**, 899-905, doi:10.1038/nature08822 (2010).

62 Klein, U. *et al.* Transcriptional analysis of the B cell germinal center reaction. *Proceedings of the National Academy of Sciences of the United States of America* **100**, 2639-2644, doi:10.1073/pnas.0437996100 (2003).

63 Calado, D. P. *et al.* The cell-cycle regulator c-Myc is essential for the formation and maintenance of germinal centers. *Nat Immunol* **13**, 1092-1100, doi:10.1038/ni.2418 (2012).

64 Dominguez-Sola, D. *et al.* The proto-oncogene MYC is required for selection in the germinal center and cyclic reentry. *Nat Immunol* **13**, 1083-1091, doi:10.1038/ni.2428 (2012).

65 Hemann, M. T. *et al.* Evasion of the p53 tumour surveillance network by tumour-derived MYC mutants. *Nature* **436**, 807-811, doi:10.1038/nature03845 (2005).

66 Bahram, F., von der Lehr, N., Cetinkaya, C. & Larsson, L. G. c-Myc hot spot mutations in lymphomas result in inefficient ubiquitination and decreased proteasome-mediated turnover. *Blood* **95**, 2104-2110 (2000).

67 Richter, J. *et al.* Recurrent mutation of the ID3 gene in Burkitt lymphoma identified by integrated genome, exome and transcriptome sequencing. *Nature genetics*, doi:10.1038/ng.2469 (2012).

68 Love, C. *et al.* The genetic landscape of mutations in Burkitt lymphoma. *Nature genetics*, doi:10.1038/ng.2468 (2012).

69 Fenaux, P. *et al.* Mutations of the p53 gene in B-cell lymphoblastic acute leukemia: a report on 60 cases. *Leukemia* **6**, 42-46 (1992).

70 Vennstrom, B., Sheiness, D., Zabielski, J. & Bishop, J. M. Isolation and characterization of c-myc, a cellular homolog of the oncogene (v-myc) of avian myelocytomatosis virus strain 29. *Journal of virology* **42**, 773-779 (1982).

71 Eilers, M. & Eisenman, R. N. Myc's broad reach. *Genes & development* **22**, 2755-2766, doi:10.1101/gad.1712408 (2008).

72 Meyer, N. & Penn, L. Z. Reflecting on 25 years with MYC. *Nature reviews. Cancer* **8**, 976-990, doi:10.1038/nrc2231 (2008).

73 Dang, C. V. MYC on the path to cancer. *Cell* **149**, 22-35, doi:10.1016/j.cell.2012.03.003 (2012).

74 Coller, H. A. *et al.* Expression analysis with oligonucleotide microarrays reveals that MYC regulates genes involved in growth, cell cycle, signaling, and adhesion. *Proceedings of the National Academy of Sciences of the United States of America* **97**, 3260-3265 (2000).

75 Adams, J. M. *et al.* The c-myc oncogene driven by immunoglobulin enhancers induces lymphoid malignancy in transgenic mice. *Nature* **318**, 533-538 (1985).

76 Sander, S. *et al.* Synergy between PI3K signaling and MYC in Burkitt lymphomagenesis. *Cancer cell* **22**, 167-179, doi:10.1016/j.ccr.2012.06.012 (2012).

77 Kuttler, F. *et al.* c-myc box II mutations in Burkitt's lymphoma-derived alleles reduce cell-transformation activity and lower response to broad apoptotic stimuli. *Oncogene* **20**, 6084-6094, doi:10.1038/sj.onc.1204827 (2001).

78 Gregory, M. A. & Hann, S. R. c-Myc proteolysis by the ubiquitin-proteasome pathway: stabilization of c-Myc in Burkitt's lymphoma cells. *Molecular and cellular biology* **20**, 2423-2435 (2000).

79 Sears, R. *et al.* Multiple Ras-dependent phosphorylation pathways regulate Myc protein stability. *Genes & development* **14**, 2501-2514 (2000).

80 Pelengaris, S., Khan, M. & Evan, G. c-MYC: more than just a matter of life and death. *Nature reviews. Cancer* **2**, 764-776, doi:10.1038/nrc904 (2002).

81 Lane, D. P. Cancer. p53, guardian of the genome. *Nature* **358**, 15-16, doi:10.1038/358015a0 (1992).

82 Momand, J., Zambetti, G. P., Olson, D. C., George, D. & Levine, A. J. The mdm-2 oncogene product forms a complex with the p53 protein and inhibits p53-mediated transactivation. *Cell* **69**, 1237-1245 (1992).

83 Honda, R., Tanaka, H. & Yasuda, H. Oncoprotein MDM2 is a ubiquitin ligase E3 for tumor suppressor p53. *FEBS letters* **420**, 25-27 (1997).

84 Shvarts, A. *et al.* Isolation and identification of the human homolog of a new p53-binding protein, Mdmx. *Genomics* **43**, 34-42, doi:10.1006/geno.1997.4775 (1997).

85 Eischen, C. M., Weber, J. D., Roussel, M. F., Sherr, C. J. & Cleveland, J. L. Disruption of the ARF-Mdm2-p53 tumor suppressor pathway in Myc-induced lymphomagenesis. *Genes & development* **13**, 2658-2669 (1999).

86 Sherr, C. J. The INK4a/ARF network in tumour suppression. *Nature reviews. Molecular cell biology* **2**, 731-737, doi:10.1038/35096061 (2001).

87 Gaidano, G. *et al.* p53 mutations in human lymphoid malignancies: association with Burkitt lymphoma and chronic lymphocytic leukemia. *Proceedings of the National Academy of Sciences of the United States of America* **88**, 5413-5417 (1991).

88 Bhatia, K. G., Gutierrez, M. I., Huppi, K., Siwarski, D. & Magrath, I. T. The pattern of p53 mutations in Burkitt's lymphoma differs from that of solid tumors. *Cancer Res* **52**, 4273-4276 (1992).

89 Soussi, T. & Jonveaux, P. p53 gene alterations in human hematological malignancies: a review. *Nouv Rev Fr Hematol* **33**, 477-480 (1991).

90 Farrell, P. J., Allan, G. J., Shanahan, F., Vousden, K. H. & Crook, T. p53 is frequently mutated in Burkitt's lymphoma cell lines. *The EMBO journal* **10**, 2879-2887 (1991).

91 Wiman, K. G., Magnusson, K. P., Ramqvist, T. & Klein, G. Mutant p53 detected in a majority of Burkitt lymphoma cell lines by monoclonal antibody PAb240. *Oncogene* **6**, 1633-1639 (1991).

92 O'Connor, P. M. *et al.* Role of the p53 tumor suppressor gene in cell cycle arrest and radiosensitivity of Burkitt's lymphoma cell lines. *Cancer Res* **53**, 4776-4780 (1993).

93 Vousden, K. H., Crook, T. & Farrell, P. J. Biological activities of p53 mutants in Burkitt's lymphoma cells. *J Gen Virol* **74 (Pt 5)**, 803-810 (1993).

94 Fan, S. *et al.* p53 gene mutations are associated with decreased sensitivity of human lymphoma cells to DNA damaging agents. *Cancer Res* **54**, 5824-5830 (1994).

95 Schmitt, C. A., McCurrach, M. E., de Stanchina, E., Wallace-Brodeur, R. R. & Lowe, S. W. INK4a/ARF mutations accelerate lymphomagenesis and promote chemoresistance by disabling p53. *Genes & development* **13**, 2670-2677 (1999).

96 Klangby, U. *et al.* p16/INK4a and p15/INK4b gene methylation and absence of p16/INK4a mRNA and protein expression in Burkitt's lymphoma. *Blood* **91**, 1680-1687 (1998).

97 Baur, A. S. *et al.* Frequent methylation silencing of p15(INK4b) (MTS2) and p16(INK4a) (MTS1) in B-cell and T-cell lymphomas. *Blood* **94**, 1773-1781 (1999).

98 Lindstrom, M. S., Klangby, U. & Wiman, K. G. p14ARF homozygous deletion or MDM2 overexpression in Burkitt lymphoma lines carrying wild type p53. *Oncogene* **20**, 2171-2177, doi:10.1038/sj.onc.1204303 (2001).

99 Moffat, J. & Sabatini, D. M. Building mammalian signalling pathways with RNAi screens. *Nature reviews. Molecular cell biology* **7**, 177-187, doi:10.1038/nrm1860 (2006).

100 Shalem, O., Sanjana, N. E. & Zhang, F. High-throughput functional genomics using CRISPR-Cas9. *Nat Rev Genet* **16**, 299-311, doi:10.1038/nrg3899 (2015).

101 Hannon, G. J. RNA interference. *Nature* **418**, 244-251, doi:10.1038/418244a (2002).

102 Sharp, P. A. RNAi and double-strand RNA. *Genes & development* **13**, 139-141 (1999).

103 Fire, A. *et al.* Potent and specific genetic interference by double-stranded RNA in Caenorhabditis elegans. *Nature* **391**, 806-811, doi:10.1038/35888 (1998).

104 Martinez, J., Patkaniowska, A., Urlaub, H., Luhrmann, R. & Tuschl, T. Single-stranded antisense siRNAs guide target RNA cleavage in RNAi. *Cell* **110**, 563-574 (2002).

105 Hutvagner, G. & Zamore, P. D. A microRNA in a multiple-turnover RNAi enzyme complex. *Science* **297**, 2056-2060, doi:10.1126/science.1073827 (2002).

106 Elbashir, S. M., Harborth, J., Weber, K. & Tuschl, T. Analysis of gene function in somatic mammalian cells using small interfering RNAs. *Methods* **26**, 199-213, doi:10.1016/S1046-2023(02)00023-3 (2002).

107 Brummelkamp, T. R., Bernards, R. & Agami, R. A system for stable expression of short interfering RNAs in mammalian cells. *Science* **296**, 550-553, doi:10.1126/science.1068999 (2002).

108 Paddison, P. J., Caudy, A. A., Bernstein, E., Hannon, G. J. & Conklin, D. S. Short hairpin RNAs (shRNAs) induce sequence-specific silencing in mammalian cells. *Genes & development* **16**, 948-958, doi:10.1101/gad.981002 (2002).

109 Stewart, S. A. *et al.* Lentivirus-delivered stable gene silencing by RNAi in primary cells. *RNA* **9**, 493-501 (2003).

110 Moffat, J. *et al.* A lentiviral RNAi library for human and mouse genes applied to an arrayed viral high-content screen. *Cell* **124**, 1283-1298, doi:10.1016/j.cell.2006.01.040 (2006).

111 Root, D. E., Hacohen, N., Hahn, W. C., Lander, E. S. & Sabatini, D. M. Genome-scale loss-of-function screening with a lentiviral RNAi library. *Nat Methods* **3**, 715-719, doi:10.1038/nmeth924 (2006).

112 Cowley, G. S. *et al.* Parallel genome-scale loss of function screens in 216 cancer cell lines for the identification of context-specific genetic dependencies. *Scientific data* **1**, 140035, doi:10.1038/sdata.2014.35 (2014).

113 Cheung, H. W. *et al.* Systematic investigation of genetic vulnerabilities across cancer cell lines reveals lineage-specific dependencies in ovarian cancer. *Proceedings of the National Academy of Sciences of the United States of America* **108**, 12372-12377, doi:10.1073/pnas.1109363108 (2011).

114 Fellmann, C. & Lowe, S. W. Stable RNA interference rules for silencing. *Nature cell biology* **16**, 10-18, doi:10.1038/ncb2895 (2014).

115 Hart, T., Brown, K. R., Sircoulomb, F., Rottapel, R. & Moffat, J. Measuring error rates in genomic perturbation screens: gold standards for human functional genomics. *Molecular systems biology* **10**, 733, doi:10.15252/msb.20145216 (2014).

116 Hsu, P. D., Lander, E. S. & Zhang, F. Development and applications of CRISPR-Cas9 for genome engineering. *Cell* **157**, 1262-1278, doi:10.1016/j.cell.2014.05.010 (2014).
117 Mojica, F. J., Diez-Villasenor, C., Garcia-Martinez, J. & Soria, E. Intervening sequences of regularly spaced prokaryotic repeats derive from foreign genetic elements. *Journal of molecular evolution* **60**, 174-182, doi:10.1007/s00239-004-0046-3 (2005).
118 Pourcel, C., Salvignol, G. & Vergnaud, G. CRISPR elements in Yersinia pestis acquire new repeats by preferential uptake of bacteriophage DNA, and provide additional tools for evolutionary studies. *Microbiology* **151**, 653-663, doi:10.1099/mic.0.27437-0 (2005).
119 Barrangou, R. *et al.* CRISPR provides acquired resistance against viruses in prokaryotes. *Science* **315**, 1709-1712, doi:10.1126/science.1138140 (2007).
120 Cong, L. *et al.* Multiplex genome engineering using CRISPR/Cas systems. *Science* **339**, 819-823, doi:10.1126/science.1231143 (2013).
121 Mali, P. *et al.* RNA-guided human genome engineering via Cas9. *Science* **339**, 823-826, doi:10.1126/science.1232033 (2013).
122 Capecchi, M. R. Altering the genome by homologous recombination. *Science* **244**, 1288-1292 (1989).
123 Wen, W. S., Yuan, Z. M., Ma, S. J., Xu, J. & Yuan, D. T. CRISPR-Cas9 systems: versatile cancer modelling platforms and promising therapeutic strategies. *Int J Cancer* **138**, 1328-1336, doi:10.1002/ijc.29626 (2016).
124 Bibikova, M., Golic, M., Golic, K. G. & Carroll, D. Targeted chromosomal cleavage and mutagenesis in Drosophila using zinc-finger nucleases. *Genetics* **161**, 1169-1175 (2002).
125 Jinek, M. *et al.* A programmable dual-RNA-guided DNA endonuclease in adaptive bacterial immunity. *Science* **337**, 816-821, doi:10.1126/science.1225829 (2012).
126 Wang, T. *et al.* Identification and characterization of essential genes in the human genome. *Science*, doi:10.1126/science.aac7041 (2015).
127 Shalem, O. *et al.* Genome-scale CRISPR-Cas9 knockout screening in human cells. *Science* **343**, 84-87, doi:10.1126/science.1247005 (2014).
128 Rosolowski, M. *et al.* Massive transcriptional perturbation in subgroups of diffuse large B-cell lymphomas. *PloS one* **8**, e76287, doi:10.1371/journal.pone.0076287 (2013).
129 Schwaenen, C. *et al.* Automated array-based genomic profiling in chronic lymphocytic leukemia: development of a clinical tool and discovery of recurrent genomic alterations. *Proceedings of the National Academy of Sciences of the United States of America* **101**, 1039-1044, doi:10.1073/pnas.0304717101 (2004).
130 Fiegler, H. *et al.* DNA microarrays for comparative genomic hybridization based on DOP-PCR amplification of BAC and PAC clones. *Genes, chromosomes & cancer* **36**, 361-374, doi:10.1002/gcc.10155 (2003).
131 Dai, Z. *et al.* shRNA-seq data analysis with edgeR. *F1000Res* **3**, 95, doi:10.12688/f1000research.3928.1 (2014).
132 Jihye, K. & Aik, C. T. BiNGS!SL-seq: A Bioinformatics Pipeline for the Analysis and Interpretation of Deep Sequencing Genome-Wide Synthetic Lethal Screen. *Next Generation Microarray Bioinformatics: Methods and Protocols* **802**, 389-398, doi:10.1007/978–1-61779–400–1_26 (2012).
133 Klijn, C. *et al.* A comprehensive transcriptional portrait of human cancer cell lines. *Nat Biotechnol* **33**, 306-312, doi:10.1038/nbt.3080 (2015).
134 Bieging, K. T., Amick, A. C. & Longnecker, R. Epstein-Barr virus LMP2A bypasses p53 inactivation in a MYC model of lymphomagenesis. *Proceedings of the National Academy of Sciences of the United States of America* **106**, 17945-17950, doi:10.1073/pnas.0907994106 (2009).
135 Saha, A. *et al.* Epstein-Barr virus nuclear antigen 3C augments Mdm2-mediated p53 ubiquitination and degradation by deubiquitinating Mdm2. *Journal of virology* **83**, 4652-4669, doi:10.1128/JVI.02408-08 (2009).

136 Ngo, V. N. *et al.* Oncogenically active MYD88 mutations in human lymphoma. *Nature* **470**, 115-119, doi:10.1038/nature09671 (2011).
137 Lau, L. M., Nugent, J. K., Zhao, X. & Irwin, M. S. HDM2 antagonist Nutlin-3 disrupts p73-HDM2 binding and enhances p73 function. *Oncogene* **27**, 997-1003, doi:10.1038/sj.onc.1210707 (2008).
138 Boerma, E. G., Siebert, R., Kluin, P. M. & Baudis, M. Translocations involving 8q24 in Burkitt lymphoma and other malignant lymphomas: a historical review of cytogenetics in the light of todays knowledge. *Leukemia* **23**, 225-234, doi:10.1038/leu.2008.281 (2009).
139 Aukema, S. M. *et al.* Sequential karyotyping in Burkitt lymphoma reveals a linear clonal evolution with increase in karyotype complexity and a high frequency of recurrent secondary aberrations. *British journal of haematology*, doi:10.1111/bjh.13501 (2015).
140 Kim, T. M. *et al.* Clinical implication of recurrent copy number alterations in hepatocellular carcinoma and putative oncogenes in recurrent gains on 1q. *Int J Cancer* **123**, 2808-2815, doi:10.1002/ijc.23901 (2008).
141 Skawran, B. *et al.* Gene expression profiling in hepatocellular carcinoma: upregulation of genes in amplified chromosome regions. *Modern pathology : an official journal of the United States and Canadian Academy of Pathology, Inc* **21**, 505-516, doi:10.1038/modpathol.3800998 (2008).
142 Orsetti, B. *et al.* Genetic profiling of chromosome 1 in breast cancer: mapping of regions of gains and losses and identification of candidate genes on 1q. *British journal of cancer* **95**, 1439-1447, doi:10.1038/sj.bjc.6603433 (2006).
143 Muthuswami, M. *et al.* Breast tumors with elevated expression of 1q candidate genes confer poor clinical outcome and sensitivity to Ras/PI3K inhibition. *PloS one* **8**, e77553, doi:10.1371/journal.pone.0077553 (2013).
144 Micci, F. *et al.* Genomic profile of ovarian carcinomas. *BMC cancer* **14**, 315, doi:10.1186/1471-2407-14-315 (2014).
145 Sawyer, J. R. The prognostic significance of cytogenetics and molecular profiling in multiple myeloma. *Cancer genetics* **204**, 3-12, doi:10.1016/j.cancergencyto.2010.11.002 (2011).
146 Hanamura, I. *et al.* Frequent gain of chromosome band 1q21 in plasma-cell dyscrasias detected by fluorescence in situ hybridization: incidence increases from MGUS to relapsed myeloma and is related to prognosis and disease progression following tandem stem-cell transplantation. *Blood* **108**, 1724-1732, doi:10.1182/blood-2006-03-009910 (2006).
147 Johansson, B., Mertens, F. & Mitelman, F. Cytogenetic evolution patterns in non-Hodgkin's lymphoma. *Blood* **86**, 3905-3914 (1995).
148 Flaherty, K. T. *et al.* Inhibition of mutated, activated BRAF in metastatic melanoma. *N Engl J Med* **363**, 809-819, doi:10.1056/NEJMoa1002011 (2010).
149 Solit, D. B. & Rosen, N. Resistance to BRAF inhibition in melanomas. *N Engl J Med* **364**, 772-774, doi:10.1056/NEJMcibr1013704 (2011).
150 Lin, L. *et al.* The Hippo effector YAP promotes resistance to RAF- and MEK-targeted cancer therapies. *Nature genetics*, doi:10.1038/ng.3218 (2015).
151 Scholl, C. *et al.* Synthetic lethal interaction between oncogenic KRAS dependency and STK33 suppression in human cancer cells. *Cell* **137**, 821-834, doi:10.1016/j.cell.2009.03.017 (2009).
152 McCleland, M. L. *et al.* Lactate dehydrogenase B is required for the growth of KRAS-dependent lung adenocarcinomas. *Clinical cancer research : an official journal of the American Association for Cancer Research* **19**, 773-784, doi:10.1158/1078-0432.CCR-12-2638 (2013).
153 Werner, K. *et al.* Simultaneous gene silencing of KRAS and anti-apoptotic genes as a multitarget therapy. *Oncotarget*, doi:10.18632/oncotarget.6766 (2015).

154 Helming, K. C. *et al.* ARID1B is a specific vulnerability in ARID1A-mutant cancers. *Nature medicine* **20**, 251-254, doi:10.1038/nm.3480 (2014).
155 Levine, A. J. & Oren, M. The first 30 years of p53: growing ever more complex. *Nature reviews. Cancer* **9**, 749-758, doi:10.1038/nrc2723 (2009).
156 Olivier, M., Hollstein, M. & Hainaut, P. TP53 mutations in human cancers: origins, consequences, and clinical use. *Cold Spring Harbor perspectives in biology* **2**, a001008, doi:10.1101/cshperspect.a001008 (2010).
157 Muller, P. A. & Vousden, K. H. p53 mutations in cancer. *Nature cell biology* **15**, 2-8, doi:10.1038/ncb2641 (2013).
158 Cerami, E. *et al.* The cBio cancer genomics portal: an open platform for exploring multidimensional cancer genomics data. *Cancer discovery* **2**, 401-404, doi:10.1158/2159-8290.CD-12-0095 (2012).
159 Gao, J. *et al.* Integrative analysis of complex cancer genomics and clinical profiles using the cBioPortal. *Science signaling* **6**, pl1, doi:10.1126/scisignal.2004088 (2013).
160 Shvarts, A. *et al.* MDMX: a novel p53-binding protein with some functional properties of MDM2. *The EMBO journal* **15**, 5349-5357 (1996).
161 Kawai, H., Wiederschain, D. & Yuan, Z. M. Critical contribution of the MDM2 acidic domain to p53 ubiquitination. *Molecular and cellular biology* **23**, 4939-4947 (2003).
162 Linke, K. *et al.* Structure of the MDM2/MDMX RING domain heterodimer reveals dimerization is required for their ubiquitylation in trans. *Cell death and differentiation* **15**, 841-848, doi:10.1038/sj.cdd.4402309 (2008).
163 Tanimura, S. *et al.* MDM2 interacts with MDMX through their RING finger domains. *FEBS letters* **447**, 5-9 (1999).
164 Finch, R. A. *et al.* mdmx is a negative regulator of p53 activity in vivo. *Cancer Res* **62**, 3221-3225 (2002).
165 Parant, J. *et al.* Rescue of embryonic lethality in Mdm4-null mice by loss of Trp53 suggests a nonoverlapping pathway with MDM2 to regulate p53. *Nature genetics* **29**, 92-95, doi:10.1038/ng714 (2001).
166 Migliorini, D. *et al.* Mdm4 (Mdmx) regulates p53-induced growth arrest and neuronal cell death during early embryonic mouse development. *Molecular and cellular biology* **22**, 5527-5538 (2002).
167 Huang, L. *et al.* The p53 inhibitors MDM2/MDMX complex is required for control of p53 activity in vivo. *Proceedings of the National Academy of Sciences of the United States of America* **108**, 12001-12006, doi:10.1073/pnas.1102309108 (2011).
168 Pant, V., Xiong, S., Iwakuma, T., Quintas-Cardama, A. & Lozano, G. Heterodimerization of Mdm2 and Mdm4 is critical for regulating p53 activity during embryogenesis but dispensable for p53 and Mdm2 stability. *Proceedings of the National Academy of Sciences of the United States of America* **108**, 11995-12000, doi:10.1073/pnas.1102241108 (2011).
169 Sharp, D. A., Kratowicz, S. A., Sank, M. J. & George, D. L. Stabilization of the MDM2 oncoprotein by interaction with the structurally related MDMX protein. *The Journal of biological chemistry* **274**, 38189-38196 (1999).
170 Gu, J. *et al.* Mutual dependence of MDM2 and MDMX in their functional inactivation of p53. *The Journal of biological chemistry* **277**, 19251-19254, doi:10.1074/jbc.C200150200 (2002).
171 Pan, Y. & Chen, J. MDM2 promotes ubiquitination and degradation of MDMX. *Molecular and cellular biology* **23**, 5113-5121 (2003).
172 Meulmeester, E., Pereg, Y., Shiloh, Y. & Jochemsen, A. G. ATM-mediated phosphorylations inhibit Mdmx/Mdm2 stabilization by HAUSP in favor of p53 activation. *Cell cycle* **4**, 1166-1170 (2005).
173 Wade, M., Li, Y. C. & Wahl, G. M. MDM2, MDMX and p53 in oncogenesis and cancer therapy. *Nature reviews. Cancer* **13**, 83-96, doi:10.1038/nrc3430 (2013).

174 Riemenschneider, M. J. *et al.* Amplification and overexpression of the MDM4 (MDMX) gene from 1q32 in a subset of malignant gliomas without TP53 mutation or MDM2 amplification. *Cancer Res* **59**, 6091-6096 (1999).

175 Cancer Genome Atlas Research, N. Comprehensive genomic characterization defines human glioblastoma genes and core pathways. *Nature* **455**, 1061-1068, doi:10.1038/nature07385 (2008).

176 Danovi, D. *et al.* Amplification of Mdmx (or Mdm4) directly contributes to tumor formation by inhibiting p53 tumor suppressor activity. *Molecular and cellular biology* **24**, 5835-5843, doi:10.1128/MCB.24.13.5835-5843.2004 (2004).

177 Meric-Bernstam, F. *et al.* Concordance of genomic alterations between primary and recurrent breast cancer. *Molecular cancer therapeutics* **13**, 1382-1389, doi:10.1158/1535-7163.MCT-13-0482 (2014).

178 Eirew, P. *et al.* Dynamics of genomic clones in breast cancer patient xenografts at single-cell resolution. *Nature* **518**, 422-426, doi:10.1038/nature13952 (2015).

179 Bartel, F. *et al.* Significance of HDMX-S (or MDM4) mRNA splice variant overexpression and HDMX gene amplification on primary soft tissue sarcoma prognosis. *Int J Cancer* **117**, 469-475, doi:10.1002/ijc.21206 (2005).

180 Ito, M. *et al.* Comprehensive mapping of p53 pathway alterations reveals an apparent role for both SNP309 and MDM2 amplification in sarcomagenesis. *Clinical cancer research : an official journal of the American Association for Cancer Research* **17**, 416-426, doi:10.1158/1078-0432.CCR-10-2050 (2011).

181 Laurie, N. A. *et al.* Inactivation of the p53 pathway in retinoblastoma. *Nature* **444**, 61-66, doi:10.1038/nature05194 (2006).

182 Leventaki, V. *et al.* TP53 pathway analysis in paediatric Burkitt lymphoma reveals increased MDM4 expression as the only TP53 pathway abnormality detected in a subset of cases. *British journal of haematology* **158**, 763-771, doi:10.1111/j.1365-2141.2012.09243.x (2012).

183 Miller, K. R., Kelley, K., Tuttle, R. & Berberich, S. J. HdmX overexpression inhibits oncogene induced cellular senescence. *Cell cycle* **9**, 3376-3382, doi:10.4161/cc.9.16.12779 (2010).

184 Lenos, K. *et al.* Oncogenic functions of hMDMX in in vitro transformation of primary human fibroblasts and embryonic retinoblasts. *Mol Cancer* **10**, 111, doi:10.1186/1476-4598-10-111 (2011).

185 Pellegrino, R. *et al.* EEF1A2 inactivates p53 by way of PI3K/AKT/mTOR-dependent stabilization of MDM4 in hepatocellular carcinoma. *Hepatology* **59**, 1886-1899, doi:10.1002/hep.26954 (2014).

186 Vassilev, L. T. *et al.* In vivo activation of the p53 pathway by small-molecule antagonists of MDM2. *Science* **303**, 844-848, doi:10.1126/science.1092472 (2004).

187 Barbieri, E. *et al.* MDM2 inhibition sensitizes neuroblastoma to chemotherapy-induced apoptotic cell death. *Molecular cancer therapeutics* **5**, 2358-2365, doi:10.1158/1535-7163.MCT-06-0305 (2006).

188 Tovar, C. *et al.* Small-molecule MDM2 antagonists reveal aberrant p53 signaling in cancer: implications for therapy. *Proceedings of the National Academy of Sciences of the United States of America* **103**, 1888-1893, doi:10.1073/pnas.0507493103 (2006).

189 Sullivan, K. D. *et al.* ATM and MET kinases are synthetic lethal with nongenotoxic activation of p53. *Nat Chem Biol* **8**, 646-654, doi:10.1038/nchembio.965 (2012).

190 Vu, B. T. & Vassilev, L. Small-molecule inhibitors of the p53-MDM2 interaction. *Current topics in microbiology and immunology* **348**, 151-172, doi:10.1007/82_2010_110 (2011).

191 de Lange, J. *et al.* Synergistic growth inhibition based on small-molecule p53 activation as treatment for intraocular melanoma. *Oncogene* **31**, 1105-1116, doi:10.1038/onc.2011.309 (2012).

192 Coll-Mulet, L. *et al.* MDM2 antagonists activate p53 and synergize with genotoxic drugs in B-cell chronic lymphocytic leukemia cells. *Blood* **107**, 4109-4114, doi:10.1182/blood-2005-08-3273 (2006).
193 Cheok, C. F., Dey, A. & Lane, D. P. Cyclin-dependent kinase inhibitors sensitize tumor cells to nutlin-induced apoptosis: a potent drug combination. *Mol Cancer Res* **5**, 1133-1145, doi:10.1158/1541-7786.MCR-07-0161 (2007).
194 Bottger, V. *et al.* Comparative study of the p53-mdm2 and p53-MDMX interfaces. *Oncogene* **18**, 189-199, doi:10.1038/sj.onc.1202281 (1999).
195 Patton, J. T. *et al.* Levels of HdmX expression dictate the sensitivity of normal and transformed cells to Nutlin-3. *Cancer Res* **66**, 3169-3176, doi:10.1158/0008-5472.CAN-05-3832 (2006).
196 Wade, M., Wong, E. T., Tang, M., Stommel, J. M. & Wahl, G. M. Hdmx modulates the outcome of p53 activation in human tumor cells. *The Journal of biological chemistry* **281**, 33036-33044, doi:10.1074/jbc.M605405200 (2006).
197 Reed, D. *et al.* Identification and characterization of the first small molecule inhibitor of MDMX. *The Journal of biological chemistry* **285**, 10786-10796, doi:10.1074/jbc.M109.056747 (2010).
198 Bista, M. *et al.* On the mechanism of action of SJ-172550 in inhibiting the interaction of MDM4 and p53. *PloS one* **7**, e37518, doi:10.1371/journal.pone.0037518 (2012).
199 Zhan, C. & Lu, W. Peptide activators of the p53 tumor suppressor. *Current pharmaceutical design* **17**, 603-609 (2011).
200 Walensky, L. D. & Bird, G. H. Hydrocarbon-stapled peptides: principles, practice, and progress. *Journal of medicinal chemistry* **57**, 6275-6288, doi:10.1021/jm4011675 (2014).
201 Bernal, F. *et al.* A stapled p53 helix overcomes HDMX-mediated suppression of p53. *Cancer cell* **18**, 411-422, doi:10.1016/j.ccr.2010.10.024 (2010).
202 Gembarska, A. *et al.* MDM4 is a key therapeutic target in cutaneous melanoma. *Nature medicine*, doi:10.1038/nm.2863 (2012).
203 de Lange, J. *et al.* High levels of Hdmx promote cell growth in a subset of uveal melanomas. *Am J Cancer Res* **2**, 492-507 (2012).
204 Gyuris, J., Golemis, E., Chertkov, H. & Brent, R. Cdi1, a human G1 and S phase protein phosphatase that associates with Cdk2. *Cell* **75**, 791-803 (1993).
205 Hannon, G. J., Casso, D. & Beach, D. KAP: a dual specificity phosphatase that interacts with cyclin-dependent kinases. *Proceedings of the National Academy of Sciences of the United States of America* **91**, 1731-1735 (1994).
206 Poon, R. Y. & Hunter, T. Dephosphorylation of Cdk2 Thr160 by the cyclin-dependent kinase-interacting phosphatase KAP in the absence of cyclin. *Science* **270**, 90-93 (1995).
207 Nalepa, G. *et al.* The tumor suppressor CDKN3 controls mitosis. *The Journal of cell biology* **201**, 997-1012, doi:10.1083/jcb.201205125 (2013).
208 Liu, X. & Winey, M. The MPS1 family of protein kinases. *Annual review of biochemistry* **81**, 561-585, doi:10.1146/annurev-biochem-061611-090435 (2012).
209 Srinivas, V., Kitagawa, M., Wong, J., Liao, P. J. & Lee, S. H. The Tumor Suppressor Cdkn3 Is Required for Maintaining the Proper Number of Centrosomes by Regulating the Centrosomal Stability of Mps1. *Cell reports* **13**, 1569-1577, doi:10.1016/j.celrep.2015.10.039 (2015).
210 Lee, S. W., Reimer, C. L., Fang, L., Iruela-Arispe, M. L. & Aaronson, S. A. Overexpression of kinase-associated phosphatase (KAP) in breast and prostate cancer and inhibition of the transformed phenotype by antisense KAP expression. *Molecular and cellular biology* **20**, 1723-1732 (2000).
211 Barron, E. V. *et al.* CDKN3 mRNA as a Biomarker for Survival and Therapeutic Target in Cervical Cancer. *PloS one* **10**, e0137397, doi:10.1371/journal.pone.0137397 (2015).
212 Lin, W. R., Lai, M. W. & Yeh, C. T. Cyclin-dependent kinase-associated protein phosphatase is overexpressed in alcohol-related hepatocellular carcinoma and

influences xenograft tumor growth. *Oncology reports* **29**, 903-910, doi:10.3892/or.2012.2208 (2013).

213 Lai, M. W., Chen, T. C., Pang, S. T. & Yeh, C. T. Overexpression of cyclin-dependent kinase-associated protein phosphatase enhances cell proliferation in renal cancer cells. *Urologic oncology* **30**, 871-878, doi:10.1016/j.urolonc.2010.09.010 (2012).

214 Xing, C. *et al.* Cyclin-dependent kinase inhibitor 3 is overexpressed in hepatocellular carcinoma and promotes tumor cell proliferation. *Biochemical and biophysical research communications* **420**, 29-35, doi:10.1016/j.bbrc.2012.02.107 (2012).

215 Pita, J. M., Banito, A., Cavaco, B. M. & Leite, V. Gene expression profiling associated with the progression to poorly differentiated thyroid carcinomas. *British journal of cancer* **101**, 1782-1791, doi:10.1038/sj.bjc.6605340 (2009).

216 Li, T., Xue, H., Guo, Y. & Guo, K. CDKN3 is an independent prognostic factor and promotes ovarian carcinoma cell proliferation in ovarian cancer. *Oncology reports* **31**, 1825-1831, doi:10.3892/or.2014.3045 (2014).

217 Fan, C. *et al.* Overexpression of major CDKN3 transcripts is associated with poor survival in lung adenocarcinoma. *British journal of cancer* **113**, 1735-1743, doi:10.1038/bjc.2015.378 (2015).

218 Baldi, A. *et al.* Apoptosis induced by piroxicam plus cisplatin combined treatment is triggered by p21 in mesothelioma. *PloS one* **6**, e23569, doi:10.1371/journal.pone.0023569 (2011).

219 Galaktionov, K. *et al.* CDC25 phosphatases as potential human oncogenes. *Science* **269**, 1575-1577 (1995).

220 Galaktionov, K., Chen, X. & Beach, D. Cdc25 cell-cycle phosphatase as a target of c-myc. *Nature* **382**, 511-517, doi:10.1038/382511a0 (1996).

221 Saha, P., Eichbaum, Q., Silberman, E. D., Mayer, B. J. & Dutta, A. p21CIP1 and Cdc25A: competition between an inhibitor and an activator of cyclin-dependent kinases. *Molecular and cellular biology* **17**, 4338-4345 (1997).

222 Mailand, N. *et al.* Rapid destruction of human Cdc25A in response to DNA damage. *Science* **288**, 1425-1429 (2000).

223 Guo, S. L. *et al.* Akt-p53-miR-365-cyclin D1/cdc25A axis contributes to gastric tumorigenesis induced by PTEN deficiency. *Nature communications* **4**, 2544, doi:10.1038/ncomms3544 (2013).

224 Nutt, S. L., Morrison, A. M., Dorfler, P., Rolink, A. & Busslinger, M. Identification of BSAP (Pax-5) target genes in early B-cell development by loss- and gain-of-function experiments. *The EMBO journal* **17**, 2319-2333, doi:10.1093/emboj/17.8.2319 (1998).

225 Adams, B. *et al.* Pax-5 encodes the transcription factor BSAP and is expressed in B lymphocytes, the developing CNS, and adult testis. *Genes & development* **6**, 1589-1607 (1992).

226 Busslinger, M., Klix, N., Pfeffer, P., Graninger, P. G. & Kozmik, Z. Deregulation of PAX-5 by translocation of the Emu enhancer of the IgH locus adjacent to two alternative PAX-5 promoters in a diffuse large-cell lymphoma. *Proceedings of the National Academy of Sciences of the United States of America* **93**, 6129-6134 (1996).

227 Bousquet, M. *et al.* A novel PAX5-ELN fusion protein identified in B-cell acute lymphoblastic leukemia acts as a dominant negative on wild-type PAX5. *Blood* **109**, 3417-3423, doi:10.1182/blood-2006-05-025221 (2007).

228 Imoto, N. *et al.* BLNK is a selective target of repression by PAX5-PML in the differentiation block that leads to the development of acute lymphoblastic leukemia. *The Journal of biological chemistry*, doi:10.1074/jbc.M115.637835 (2015).

229 Laudet, V., Hanni, C., Stehelin, D. & Duterque-Coquillaud, M. Molecular phylogeny of the ETS gene family. *Oncogene* **18**, 1351-1359, doi:10.1038/sj.onc.1202444 (1999).

230 Schutte, J., Moignard, V. & Gottgens, B. Establishing the stem cell state: insights from regulatory network analysis of blood stem cell development. *Wiley interdisciplinary reviews. Systems biology and medicine* **4**, 285-295, doi:10.1002/wsbm.1163 (2012).

231 Wilson, N. K. *et al.* Combinatorial transcriptional control in blood stem/progenitor cells: genome-wide analysis of ten major transcriptional regulators. *Cell stem cell* **7**, 532-544, doi:10.1016/j.stem.2010.07.016 (2010).

232 Ben-David, Y., Giddens, E. B. & Bernstein, A. Identification and mapping of a common proviral integration site Fli-1 in erythroleukemia cells induced by Friend murine leukemia virus. *Proceedings of the National Academy of Sciences of the United States of America* **87**, 1332-1336 (1990).

233 Zhang, L. *et al.* An immunological renal disease in transgenic mice that overexpress Fli-1, a member of the ets family of transcription factor genes. *Molecular and cellular biology* **15**, 6961-6970 (1995).

234 Delattre, O. *et al.* Gene fusion with an ETS DNA-binding domain caused by chromosome translocation in human tumours. *Nature* **359**, 162-165, doi:10.1038/359162a0 (1992).

235 Li, Y. J. *et al.* Drug-mediated inhibition of Fli-1 for the treatment of leukemia. *Blood cancer journal* **2**, e54, doi:10.1038/bcj.2011.52 (2012).

236 Ladenstein, R. *et al.* Primary disseminated multifocal Ewing sarcoma: results of the Euro-EWING 99 trial. *Journal of clinical oncology : official journal of the American Society of Clinical Oncology* **28**, 3284-3291, doi:10.1200/JCO.2009.22.9864 (2010).

237 Bhatia, S. *et al.* Therapy-related myelodysplasia and acute myeloid leukemia after Ewing sarcoma and primitive neuroectodermal tumor of bone: A report from the Children's Oncology Group. *Blood* **109**, 46-51, doi:10.1182/blood-2006-01-023101 (2007).

Declaration

Hiermit erkläre ich, dass ich die vorliegende Arbeit selbständig angefertigt habe. Es wurden nur die in der Arbeit ausdrücklich benannten Quellen und Hilfsmittel benutzt. Wörtlich oder sinngemäß übernommenes Gedankengut habe ich als solches kenntlich gemacht.

Ich erkläre außerdem, dass diese Arbeit weder in dieser noch in einer anderen Form anderweitig als Dissertation oder Prüfungsarbeit verwendet oder einer anderen Fakultät als Dissertation vorgelegt wurde.

Frankfurt am Main, _____ _____

Ort, Datum Unterschrift

Acknowledgement

I herewith would like to thank all the people who contributed to this work in any way and who supported me during the course of this work.

An dieser Stelle möchte ich allen danken, die zum Gelingen dieser Arbeit in irgendeiner Weise beigetragen haben.

Ich möchte mich bei Professor Thorsten Zenz für die Breitstellung dieses interessanten Themas bedanken, für das entgegengebrachte Vertrauen und die Förderung meiner selbstständigen wissenschaftlichen Leistungen. Außerdem möchte ich mich bedanken für die Möglichkeit, meine Arbeit auf internationalen Konferenzen zu präsentieren, und für die Unterstützung und Diskussionen während der Anfertigung von wissenschaftlichen Publikationen und von meiner Doktorarbeit.

Den Mitgliedern meines Thesis Advisory Committees, Professor Christof von Kalle, Professor Rodewald und Professor Küppers, möchte ich herzlich danken für die Beurteilung des Fortschritts meiner Doktorarbeit und die vielen nützlichen Kommentare, die mein Projekt vorangebracht haben. Professor von Kalle möchte ich außerdem danken für die finanzielle Unterstützung meines Projektes. Ich danke allen Prüfern im Voraus für ihre Bereitschaft, an der Prüfungskommission teilzunnehmen und meine Arbeit zu bewerten: Professor Christof von Kalle (Erstgutachter), Professor Wiemann (Zweitgutachter), Professor Frank Lyko (Vorsitz) und Dr. Michael Milsom.

Meinem Kollegen Dr. Mikołaj Slabicki möchte ich für die Motivation und jahrelange Unterstützung danken, vor allem für die zahlreichen Diskussionen, die wissenschaftliche Anleitung, die Überprüfung meiner Doktorarbeit sowie die Fortführung offener Experimente.

Ich möchte mich bei allen Kollaborateuren für ihren Beitrag zu meinem Projekt bedanken. Bei Dr. Maciej Rosolowski und Dr. Markus Kreuz bedanke ich mich für die hervorragenden bioinformatischen Analysen und die gute Zusammenarbeit. Professor Ulrich Keller, Dr. Stefan Habringer und Jolanta Slawska danke ich für die Durchführung der *in vivo* Experimente. Vielen Dank auch an Professor Anna Jauch, Professor Henri-Jacques Delecluse, Dr. Heiko Trautmann, Dr. Christiane Pott, Dr. Elodie Caboux für Bereitstellung und Charackterisierung der Zelllinien. Dr. Agnes Hotz-Wagenblatt möchte ich danken für die Analyse von überlappenden shRNA Regionen.

Ich danke allen Mitgliedern des MMML Konsortiums für die Bereitstellung der Daten aus Primärmaterial.

Natürlich danke ich allen Kollegen aus dem Labor und Büro. Allen voran möchte ich Dr. Carolin Blume danken, für Diskussionen, Ratschläge und für die Motivation. Ich bin froh darüber, dass wir einen Teil des Weges gemeinsam gehen konnten. Tatjana Walther danke ich für die

Organisation im Labor, technische Unterstützung und eine großartige Laboratmosphäre. Genauso danke ich Carolin Muley und Lena Wagner für Unterstüzung bei den Laborversuchen. Dr. Leopold Sellner, Dr. Sascha Dietrich, Alexander Jethwa, Marina Lukas, Katarzyna Tomska Kwang Seok Lee, Dr. Bian Wu, Xiyang Liu danke ich für Diskussionen und eine gute Zusammenarbeit. Marina Lukas und Katarzyna Tomska danke ich außerdem für die Bereitstellung der Compound Screening Daten. Ich danke auch allen weiteren Mitgliedern der G100 Abteilung, die mich in den letzten Jahren begleitet haben, vor allem Dr. Eva-Maria Hartinger, Dr. Felix Oppel, Dr. Klara Gießler und Dr. Taronish Dubash für ihre Unterstützung und Freundschaft. Professor Hanno Glimm, Dr. Claudia Ball, Sylvia Fessler und der restlichen AG Glimm danke ich für die Unterstützung vor allem zu Beginn meines Projektes während des Aufbaus unserer neuen Arbeitsgruppe.

Ich bedanke mich bei der Genomics and Proteomics Core Facility des DKFZ für die professionelle Dienstleistung, vor allem Dr. Stephan Wolf und Frau Sabine Schmidt für Beratung bei der Sequenzierung der shRNA libraries sowie Herrn Oliver Heil und Dr. Melanie Bewerunge-Hudler für die Auswertung der Genexpressionsdaten in Zelllinien.

Ein ganz großer Dank geht an meinen Ehemann und besten Freund, Andreas, für die bedingungslose Unterstützung, für deine Geduld und für die erholsamen Auszeiten. Ich freue mich auf jeden gemeinsamen Moment mit dir.

Ein ganz lieber Dank geht auch an meinen Vater, der immer an mich geglaubt hat und mir die Freiräume gegeben hat, meinen Interessen zu folgen. Ich bedanke mich bei meinen Geschwistern und allen Freunden dafür, dass ihr mich auf meinem Lebensweg begleitet.

Diese Arbeit widme ich meiner Mutter, die diesen Moment leider nicht miterleben kann.